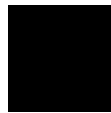


kassel
university



press

**Modelling, Simulation, and Performance Analysis of a Hybrid
Power System for Mobile Medical Clinic**

David arap Cheruiyot Cherus

Die vorliegende Arbeit wurde vom Fachbereich Elektrotechnik / Informatik der Universität Kassel als Dissertation zur Erlangung des akademischen Grades eines Doktors der Ingenieurwissenschaften (Dr.-Ing.) angenommen.

Erster Gutachter: Prof. Dr.-Ing. Jürgen Schmid
Zweiter Gutachter: Prof. Dr.-Ing. Werner Kleinkauf

Tag der mündlichen Prüfung

29. Juni 2004

Bibliografische Information Der Deutschen Bibliothek
Die Deutsche Bibliothek verzeichnet diese Publikation in der Deutschen
Nationalbibliografie; detaillierte bibliografische Daten sind im Internet über
<http://dnb.ddb.de> abrufbar

Zugl.: Kassel, Univ., Diss. 2004
ISBN 3-89958-079-6

© 2004, kassel university press GmbH, Kassel
www.upress.uni-kassel.de

Umschlaggestaltung: 5 Büro für Gestaltung, Kassel
Druck und Verarbeitung: Unidruckerei der Universität Kassel
Printed in Germany

ABSTRACT

The described study involves the modelling and dynamic simulation of a mobile hybrid power system intended to supply medical equipment on-board an omnibus. It comprises a high-output (retrofitted) alternator, a variable-speed diesel generator set, a photovoltaic (PV) generator mounted on the roof of the vehicle, a flooded lead-acid battery system, power conditioning and control electronics. As an initial step in the system design and analysis, a simulation study was undertaken. This is done at the system-level and implemented in MATLAB/SIMULINK simulation environment. The individual component models used may be physical, analytical, or empirical and are of interdisciplinary nature. The model parameters are derived from manufacturer's performance data sheets or measurements obtained from literature. Environmental influences such as ambient temperature, latitude and altitude on component performances are incorporated where necessary in the simulation models. Component dimensions are initially selected based on rule-of-thumb methods and then simulation is used to confirm or modify them. Using this simulation model, it is possible to carry out virtual experiments that give graphical (oscilloscope-like) results that mimic experimental tests. In this way, visualization of system dynamical behaviour by means of current, voltage and power plots over a chosen time range, for example, a daily cycle is then possible. By the same means, component functional behaviour such as the charging characteristics (algorithms) of charge controllers can be simulated. Finally, control strategy, in particular, dispatch strategy, can be optimised in order to minimize diesel fuel consumption and maximize battery cycle life.

KURZFASSUNG

Diese Studie beinhaltet die Modellbildung und die dynamische Simulation eines hybriden Energieversorgungssystems zur Versorgung medizinischen Geräte. Die Anlage ist in einem Omnibus installiert, der als mobile Klinik genutzt wird. Die Energieversorgung beinhaltet einen nachgerüsteten Kfz-generator, einen Dieselmotorsatz mit variable-Drehzahl, einen Photovoltaischen Generator (PV), der auf dem Dach des Busses angebracht ist, ein Bleibatteriesystem und die Energieaufbereitung und Steuerelektronik. Als ersten Schritt zum Systemdesign und zur Systemanalyse wurde eine Simulationsstudie durchgeführt. Die Simulation erfolgt auf Systemebene und wird in eine MATLAB/SIMULINK Simulationsumgebung implementiert. Für die einzelnen Komponenten werden physikalische, analytische, oder empirische Modelle verwandt. Modellparameter sind von den Leistungsblättern der Hersteller oder Literaturangabe abgeleitet. Die Umgebungseinflüsse auf die Komponentenleistungen wie Umgebungstemperatur, Breitengrad und Höhe über Normal-Null werden, falls notwendig, in der Simulation berücksichtigt. Die Komponentendimensionierung basiert auf Erfahrungswerten und wird durch die Simulation festgelegt. Mit dieser Simulation ist es möglich, virtuelle Experimente durchzuführen, die ähnliche Resultate liefern wie experimentelle Tests. Auf diese Art ist eine Visualisierung des dynamischen Verhaltens des Systems mittels der Strom-, Spannungs- und Leistungsverläufe in einem gewählten Zeitstrahmen wie zum Beispiel täglichem Zyklus möglich. Mit den gleichen Mitteln können Komponentenverhalten wie die Lade-Algorithmen eines Ladereglers simuliert werden. Schließlich können Regelungsstrategie und Energiemanagement optimiert werden, um den Dieselmotorkraftstoffverbrauch herabzusetzen und die Batterielebensdauer zu maximieren.

Acknowledgements

First of all, I would like to express my sincere gratitude to a number of persons at the Institut für Solare Energieversorgungstechnik (ISET) associated with the University of Kassel for their invaluable assistance during the course of my work. I would particularly like to thank my supervisor Prof. Dr. -Ing. Jürgen Schmid for his invaluable assistance throughout the course of this work. I will surely miss the very friendly environment both at the Institute (ISET) and at his department at the University (Department of Efficient Energy Conversion). The very multi-disciplinary research group made up of very diverse nationalities working under his supervision, made the group discussions very lively. Full appreciation also goes to Prof. Dr.-Ing. Werner Kleinkauf who agreed to be my second supervisor, and under whom I also took an exciting course in Power Electronics. My very special thanks go to Ms Claudia Erdt who assisted me on very many occasions. I cannot thank her enough. I would also like to mention Ms Nandi Vergara Gómez, Ms Doris Schmidt, and Mr Uwe Krenzel at ISET.

Secondly, I would like to sincerely thank the members of the Division of Energy Conversion and Control Engineering especially the Head of Division Mr Peter Caselitz for allowing me to use the battery simulation software (the ISET-LAB battery model developed by him and others at ISET) in my work, and the helpful discussions which contributed a lot to the success of this work. My appreciation also goes to following persons: Dr. R. Juchem (former ISET staff), Bahram Panahandeh and Christof Bröker for their help on various aspects of modelling and simulation, Dr. D. Lehmkuhl for suggestions on the thesis, Christian Langer and Jochen Giebhardt for making sure my computer had all the necessary software installed.

The financial support from German Foreign Student Exchange Programme (DAAD) is gratefully appreciated

Finally, I would like to thank my family and parents, for their support during this time.

TABLE OF CONTENTS

1	INTRODUCTION	1
1.1	Motivation	1
1.2	Mobile hybrid power systems	2
1.3	Software simulators	3
1.4	Objectives of study	4
1.5	Outline of the thesis	4
2	VEHICLE-BASED (MOBILE) HYBRID POWER SYSTEMS	5
2.1	On-board auxiliary power generation	6
2.2	DC power sources	7
2.2.1	DC alternators	7
2.2.2	DC genset	19
2.2.3	PV generator	20
2.2.4	Lead-acid battery	21
2.3	AC power sources	21
2.4	Variable-speed operation in diesel gensets	23
3	CASE STUDY: HYBRID POWER SYSTEM FOR MOBILE MEDICAL CLINIC ..	25
3.1	System Description	25
3.2	Load characteristics (profile)	27
3.3	Component sizing	29
3.3.1	Alternator	29
3.3.2	Battery bank	30
3.3.3	Genset	32
3.3.4	PV generator	32
3.3.5	Inverter	32
3.4	Operation and Control	33
3.4.1	Diesel genset and load management	34
3.4.2	Battery management	34

4	MODELLING AND SIMULATION	37
4.1	Dynamic modelling and simulation	37
4.2	MATLAB/SIMULINK Modelling Environment	39
4.3	Forward-facing and backward-facing calculation	39
4.4	Simulation models	41
4.4.1	Alternator model	42
4.4.2	Diesel DC Genset Model	43
4.4.3	Inverter model.....	48
4.4.4	ISET-LAB battery model	48
4.4.5	Charge controller model	49
4.4.6	System controller model	50
4.4.7	Photovoltaic (PV) Generator Performance Model.....	51
5	SIMULATION RESULTS AND DISCUSSIONS	63
5.1	Power flow simulations	65
5.2	Diesel and Load management.....	70
5.2.1	Control set-points.....	70
5.3	Battery management	71
5.3.1	Battery charge/discharge cycle.....	71
5.3.2	IUU controller functional behaviour.....	72
5.3.3	Battery temperature	74
6	CONCLUSIONS AND RECOMMENDATIONS	77
6.1	Outlook and future work.....	78
7	REFERENCES	79
8	APPENDICES	83
8.1	Appendix A: Vehicle Engine driven Alternators.....	83
8.2	Appendix B: Inverter Efficiency Curve.....	84
8.3	Appendix C: Relationship between battery measured parameters.....	84
8.4	Appendix D: The Sandia I-V curve Translation Procedure	86

8.5 **Appendix E: Genset Rating and De-rating** 88

TABLE OF FIGURES

Figure 2-1: Block diagram of vehicle-based hybrid power system	7
Figure 2-2: A wound rotor synchronous machine alternator	9
Figure 2-3: Performance curve for a 3kW/28V DC alternator	11
Figure 2-4: Brushless wound rotor DC alternator.....	13
Figure 2-5: Performance curves for dual stator DC alternator	14
Figure 2-6: Dual stator wound rotor DC alternator with thyristor switches	15
Figure 2-7: Dual stator wound rotor DC alternator topology with MOSFET switch ..	15
Figure 2-8: Permanent magnet DC alternator with controlled bridge rectifier	17
Figure 2-9: Permanent magnet hybrid homopolar (PMHH) DC alternator	18
Figure 2-10: Configuration for a variable-speed DC generator set	19
Figure 2-11: Configuration for a variable-speed AC generator set.....	22
Figure 3-1: A hybrid power system concept for a mobile medical clinic.....	26
Figure 3-2: Map of western Kenya showing area of operation.....	26
Figure 3-3: Estimated load profile with refrigerator at 100% duty cycle	29
Figure 3-4: Block diagram of a system controller.....	34
Figure 3-5: IU ₀ U charging algorithm in 'Alpha' voltage regulator	35
Figure 4-1: Block-oriented (causal) modelling scheme	37
Figure 4-2: Forward-facing calculation in MATLAB/SIMULINK.....	40
Figure 4-3: Backward-facing calculation in MATLAB/SIMULINK	41
Figure 4-4: DC Alternator performance curve	42
Figure 4-5: Block-diagram of alternator model in Simulink.....	43
Figure 4-6: Synthetic engine and alternator speed profiles.....	43
Figure 4-7 : Diesel DC genset performance model in Simulink.....	44
Figure 4-8: Estimated operating line in a variable-speed diesel genset.....	45
Figure 4-9: Engine speed as a function of output power.....	46
Figure 4-10: Linearized fuel consumption as a function of output power	47
Figure 4-11: Estimated specific fuel consumption curve.....	47
Figure 4-12: 24V/900W Inverter Efficiency Curve.....	48
Figure 4-13 : Block diagram for ISET-LAB battery model in Simulink.....	49
Figure 4-14: User-interface for the 'Alpha' IUU charge controller.....	50
Figure 4-15: System controller user-interface	51
Figure 4-16: Equivalent circuit of a PV generator model	52
Figure 4-17: Simulated PV cell temperature	59

Figure 4-18: Simulated IV characteristics for the PV array at STC temperature	60
Figure 4-19: Simulated IV characteristics using calculated cell temperature	60
Figure 4-20: Simulated IV characteristics for different ambient temperatures.....	61
Figure 4-21: User-interface for the PV array model	62
Figure 5-1: Synthetic engine speed profiles.....	63
Figure 5-2: Synthetic monthly mean daily irradiance profile.....	65
Figure 5-3: Speed profiles for round trip between Eldoret and Nakuru.....	66
Figure 5-4 : Power flow simulation for operation without genset.....	66
Figure 5-5: Power flow simulation for operation with genset	67
Figure 5-6: Power flow simulation for system with larger array size	68
Figure 5-7: Power flow simulation for 50% duty cycle operation of refrigerator	69
Figure 5-8 : Effect on simulated SOC profile by changing control set-points	71
Figure 5-9: Simulated battery charge/discharge cycle	72
Figure 5-10: Simulated IUU charging characteristics.....	73
Figure 5-11: Two interruptions in the charging at the absorption phase	74
Figure 5-12: Simulated battery temperature and synthetic ambient temperature	75
Figure 8-1: Belt-drive mounting arrangement for 3kW DC alternator.....	83
Figure 8-2: User-interface for initialisation of ISET-LAB model.....	85
Figure 8-3: User-interface for ISET-LAB model for battery dimensions	86

1 INTRODUCTION

1.1 Motivation

The concept of mobile medical clinic has been proposed to serve homeless street people, who rarely get access to medical attention from public health institutions in Kenya due to socio-economic factors. For a number of years, there has been a concerted effort by some organizations to re-locate them, in particular the children, to rehabilitation centres some distance away from the town centres to prevent them from engaging in urban criminal activities. A number of essential services such as medical services, educational and entertainment activities are required at the site, but the main problem is that there is lack of grid power in some of these sites. Other than this particular case, a mobile medical clinic could also be used in remote areas of Kenya where no health facilities exist. For instance, local health centres may extend their services to the rural communities, e.g. immunization programmes, primary health care, general health screening, and treatment of minor injuries, etc.

Provision of electrical power on-board or from vehicles to run auxiliary equipment is increasingly becoming important in vehicles used for medical/emergency/rescue operations, or other similar vehicular applications such as fire-fighting, recreation (RVs), television and broadcasting, construction and maintenance, etc. Mobile electric power systems are designed to provide power temporarily at non-fixed locations, for periods ranging from a few hours to a couple of days, in particular where utility power is normally unavailable, or where utility power is disrupted by man-made or natural disasters or extreme weather conditions such as fire outbreaks, floods, earthquakes, volcanic eruptions, storms, hurricanes and drought. In a country like Kenya, where power disruption due to malfunctions on the utility grid or as a result of power rationing are very common experiences, a mobile power system is a practical solution.

This work is motivated by emerging mobile power concepts with a trend towards increasing use of standard AC power on-board vehicles. For example, electric vehicles (EVs) and hybrid electric vehicles (HEVs), which normally draw power from the grid are now being designed with a bi-directional power grid interface to provide mobile AC power when not on the road. This is a feature employed in the so-called

'vehicle-to-grid' power system concept, whereby the EV or HEV plays the role of distributed generation (DG) by feeding back power to the grid [Kempton, et al, 2001/Lipman, 2002]. Such vehicles can function as power sources while parked by sourcing power from the battery storage (usually dedicated to supplying the traction motors) to run auxiliary equipment. DaimlerChrysler, for instance, is reported to have plans for producing a hybrid pick-up truck with 20kW of on-site (stationary) generation capacity targeted to contractors for providing power at construction work sites [Brooks, 2001]. In a related concept, mobile power may be obtained from a vehicle engine coupled to an electrical machine whose output is connected to a power electronic converter so as to create the standard AC power of 120/240V at 50/60Hz. The system configuration is essentially similar to that of a variable-speed generator set, whereby the vehicle engine takes the place of a genset engine. The power electronic converter module could also simultaneously provide a 14V or 28V DC output for battery recharging and/or supplying DC loads. A commercial device sold by the trademark name of AuraGen[®] is one example of this concept [Morinigo et al, 1998]. It employs a compact pancake shaped induction machine that is coupled to the engine using belts and pulleys just like a conventional vehicle alternator.

1.2 Mobile hybrid power systems

A common mobile hybrid power system (MHPS) concept, consists of the following components:

- A diesel genset,
- A photovoltaic (PV) generator
- A storage battery bank

These are housed in a 'cargo container', usually carried on the back of a truck or in a trailer towed along to the site of application. In such a system, the vehicle functions primarily as a carrier for the power supply unit and does not play a role in the electrical power generation. However, if it is known that the vehicle is frequently being driven over long distances before it arrives at the site where the power supply is needed, then the electrical power generation capability of the vehicle alternator may be exploited. Such an alternator acts as an opportunity battery charging source, and is often an extra (retrofitted) high-power version with the capability to generate a high charging current typically in the range of 100 – 250A at usual automotive DC

voltage bus (i.e., 12, 24, or 36¹V system). It can thus recharge a large auxiliary battery bank in a relatively short time depending on the battery charge acceptance and its size. This represents a more cost effective solution in comparison to the use of grid-fed battery charger rectifiers considering such a high current regime (100 – 250A).

1.3 Software simulators

It is generally agreed that experimental test platforms are time consuming and costly if different configurations, component dimensions, and control (dispatch) parameters have to be examined before an optimum design is arrived at. Computer simulation is a time saving and cost-effective method that can be used for system design, performance analysis, optimisation, and control strategy before an experimental platform is set up. In this way, the behaviour of real systems can be relatively accurately predicted and modified accordingly before implementation. In this regard, system dynamic behaviour is of particular interest.

PV hybrid system software simulators on the market are designed with different goals in mind, and have various limitations for solving certain problems. Simulation programs generally fall into two broad groups, namely: logistical (or static) and dynamic models [Baring-Gould et al., 1996]. Logistical simulators are used primarily for long-term system performance predictions, economical analysis and component sizing, etc. Examples are, for instance, Hybrid2, PVS and PVSYT, which are generally considered suitable for system dimensioning and economic calculations for PV systems over a long-term period, usually annually [Turcotte, 2001]. Dynamical system simulators give a closer look at system operation and enables study of power management and control strategies. They are able to mimic real system behaviour, but require special simulation environments to do this.

Software simulators may also be classified according to the degree of details of the models. In this connection, there are the so-called network and block-oriented simulators. Examples of network simulators are SIMPLORER[®] from Ansoft Corporation and SABER[®] from Saber Corporation. An example of block-oriented simulator is the widely used MATLAB/SIMULINK program from Math Works

¹ 42V bus system (36V nominal battery voltage) is expected to be the future standard bus voltage

Incorporated. It is particularly considered suitable for dynamic system simulation and is used here.

1.4 Objectives of study

A simulation study was undertaken at the 'Institut für Solare Energieversorgungstechnik' (ISET) associated with the University of Kassel, Germany. Its aim was the system design and performance analysis through computer modelling and simulation prior to practical realization. Specifically, the objectives may be stated as follows:

- Visualization and analysis of the system dynamic behaviour using current, voltage, and power flow traces over medium-term duration (daily cycle).
- The creation of a simulation model into which detailed manufacturer's performance data can be entered in order to accurately predict the performance of the MHPS made up of specified components, that can, in principle, be subjected to experimental validation.
- Undertake sensitivity analyses of the effect of changes in the system component dimensions, environmental conditions, and control (in particular dispatch) parameters of the hybrid power system.

1.5 Outline of the thesis

Chapter 1 gives an introduction to the concept of mobile hybrid power system, the need for simulation software tools, and objectives of study. **Chapter 2** gives a more detailed description of the concept of vehicular-based hybrid electric power systems, the on-board electrical system architecture and trends in electrical machine designs for use as vehicle alternators, and a discussion on on-board DC and AC power systems. **Chapter 3** discusses a mobile medical clinic as a case study, describes the nature of the load and its estimated profile, and some aspects of operation and control. **Chapter 4** deals with modelling and simulation using Matlab/Simulink, and discusses individual component models. **Chapter 5** presents the simulation results and discussion. In **Chapter 6**, we draw the conclusions. References are given in **Chapter 7**, and indices in **Chapter 8**.

2 VEHICLE-BASED (MOBILE) HYBRID POWER SYSTEMS

Basically power generation and energy storage components used in stationary (residential) applications may also be used for mobile applications. However, their specifications and requirements may often differ. For instance, component physical parameters mainly volume and weight (used to define power and energy densities) are much more relevant to mobile than stationary applications. In this regard, the following characteristic features and constraints in mobile applications that do not normally play any role in stationary applications are noted below:

- The PV array size is constrained by the area available on the roof of the bus
- The battery bank and the auxiliary diesel genset are constrained by both volume and weight that can be accommodated on-board
- Use of power electronic components in an automotive environment (especially under-the-hood) demand stringent cooling arrangements and are sometimes difficult to integrate in the confined space
- Sometimes the mounting of extra components, for example, the second alternator or extra batteries as retrofits are unforeseen in some vehicle platforms and may sometimes invalidate vehicle insurance policies or call for re-negotiation of the contract
- Safe electrical distribution of standard AC-voltage (240V) may be an issue in vehicular application, although experiences from related applications such as marine (boats, ships, etc) may be transferable to road vehicles

In designing vehicle-based power systems, new developments in vehicular electrical networks such as the trend towards change to 42V DC-bus (36V battery) system appearing in some pioneer vehicles (a concept expected to be the future standard) cannot be over-looked as this is anticipated to lead to new standard DC voltage ratings of some peripheral components [Miller et al, 1998 / Kassakian et al, 1996]. For instance, inverters for mobile application, which have traditionally been rated for 12 or 24V to match standard battery blocks, will consequently be rated for 36V.

In the following sections, a review of the vehicular on-board auxiliary power system architecture, alternator technology options, and on-board DC- and AC power

generation systems are discussed. Some selected circuit topologies are included only for illustration without any intent on detailed circuit analysis – which is beyond the scope of study. The subjects of interest are associated costs and conversion efficiencies.

2.1 On-board auxiliary power generation

Vehicles that carry on-board auxiliary electrical equipment (e.g. compressor motor driven refrigerators, computers, power tools, or medical equipment) need extra (auxiliary) power sources. A typical class of vehicles that possess this type of electrical system architecture are, for example, tour buses, motor homes, heavy-duty long-haul trucks, ambulances and recreational vehicles. Their electrical systems may be separated into two distinct circuits as follows:

- Standard automotive circuit
- Auxiliary power circuit

A standard automotive network used in all conventional road vehicles, consists of the standard alternator and starter battery plus all automotive loads and systems e.g. headlamps and indicators, heating, ventilation and air-conditioning (HVAC), etc. This circuit is not relevant to the current work and is beyond the scope of study.

An auxiliary power system specifically designed to supply non-automotive loads may have a similar configuration to the standard automotive circuit but typically uses a 'high-power' alternator rated at ~3 kW or higher and a larger deep-cycle on-board (a.k.a. 'service' or 'auxiliary') battery bank as opposed to the shallow-cycle starter battery as shown in **Figure 2-1** below. For cases where power from a vehicle at standstill (with engine switched off) is required, or, where the load demand exceeds about 3kW such that it cannot be covered by renewable energy sources and/or battery storage alone, a small internal combustion (IC) engine genset is included. Such gensets, commonly called Auxiliary Power Units (APUs), are typically available with ratings in the range of 3 – 10KW, and may be designed to have an AC and/or DC power output. Generally, a vehicular APU may be a scaled down IC engine genset, a micro-gas turbine, or a fuel cell generator, etc. A large on-board deep-cycle

battery bank acting as a 'buffer', is often included to take care of peak- and/or transient loads, or allow genset 'off' periods to minimize fuel consumption.

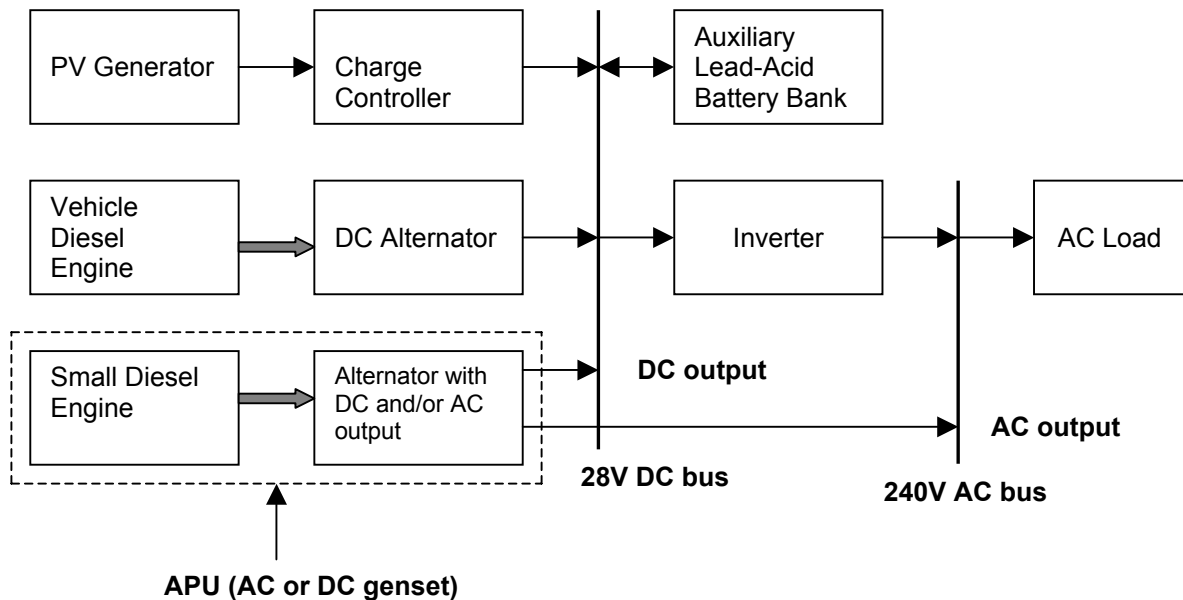


Figure 2-1: Block diagram of vehicle-based hybrid power system

2.2 DC power sources

In the vehicular-based mobile hybrid power system described above, the generated DC power is used to recharge the auxiliary battery bank and supply inverter and/or DC loads and is obtained from:

- Vehicle engine driven DC alternator
- Genset engine driven DC alternator
- PV-generator
- Lead-acid battery

In the following sections, these DC power sources are individually discussed.

2.2.1 DC alternators

Electrical machine technologies employed in the new generation of vehicle alternators, particularly the 42V-based bus systems, are similar or identical to those used in DC gensets. In a DC genset, the engine operates at a variable-speed similar

to that of a variable-speed AC genset. The reason for this is twofold. Firstly, the standard nominal voltages (usually 12 and 24V) in both fields of application are common (DC gensets are also available with 36 and 48V DC output options). Secondly, the prime movers, which are IC engines in both cases, have a variable-speed character with comparable operating speed range (~700 – 3000rpm for large diesel vehicle engines like those of buses and trucks, and ~1000 – 3600rpm for variable speed genset diesel engines). In view of these similarities, the discussion on DC alternators in the next section is in general, valid for both areas of application.

A number of electrical machine technologies can be used in DC alternators, namely: induction (asynchronous) machines (IM or AM), permanent magnet synchronous machines (PMSM), wound rotor synchronous machines (SM), and switched-reluctance machines (SRM).

The PMSM is generally considered to have higher efficiency, low maintenance due to its brushless design, and high power density. However, it has the disadvantage of being more expensive due to the high cost of magnets. Also, power electronic converters are needed for output voltage regulation although a hybrid topology such as the permanent magnet hybrid homopolar (PMHH) require a minimum of power electronics.

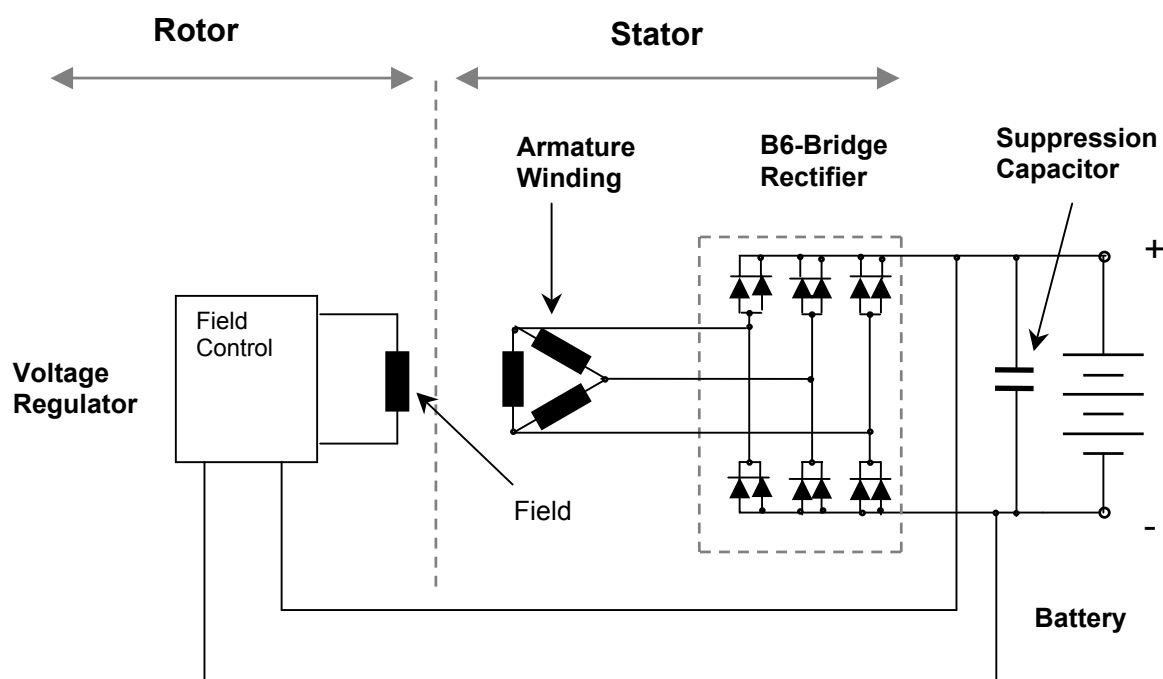
The wound rotor SM is considered to be cheaper, has a simpler circuit design that allows easier voltage regulation, but is less efficient, has low power density, and need higher maintenance when the brush-type design (cheaper solution) is used.

The IM (or AM) is generally cheaper, but need power electronic converters (with bi-directional power flow capability) in combination with a battery source and/or large capacitors when used in stand-alone (non-grid fed) application. It is currently one of the candidate machines employed in the integrated starter-generator (ISG) application. Due to the low power density of the conventional squirrel cage-rotor design for the induction machine, alternative machine (rotor) designs that are compact enough to be integrated under-the-bonnet (under-the-hood) in vehicular application are needed.

A quick review of the machine electrical circuit topologies highlights the strengths and weaknesses of the various options for those specialized in the art, however, the main focus of this work is the system-level analysis which is associated with power flow and conversion efficiencies.

Wound rotor SM alternator

The operating principle of the wound rotor SM alternator, considered a standard design, is well documented in automotive electrical systems-oriented literature, for example in [Bosch, 2000]. The alternator produces usually a 3-phase (sometimes multi-phase such as 6-phase, etc) AC output voltage that is converted to DC voltage having a slight ripple by a 6- (or more) diode bridge rectifier. The ripple is further smoothed by the battery, and sometimes by a voltage suppression capacitor, connected in parallel with it. The three phases are connected in either star or delta connection and these windings are wound on the stator. The star connection allows the commencement of power generation at much lower alternator speeds in comparison to the delta connection, which, on the other hand, gives a higher power output at high alternator speeds.



[Source: Mastervolt GmbH]

Figure 2-2: A wound rotor synchronous machine alternator

Figure 2-2 shows a conventional wound rotor synchronous machine alternator. This circuit is widely used in what is commonly known as a 'claw-pole' rotor alternator (or Lundell machine). However, rotor design variations with shapes other than the traditional claw-shape are also possible. The alternator rotor is coupled to the engine (crankshaft) by means of belts and pulleys as shown in the picture in **Figure 8-1** in **Appendix A**.

Performance curve

The voltage generated by the alternator increases along with alternator speed and the excitation current. Theoretically, for a fully excited alternator unconnected to the battery or load, the unregulated voltage would increase linearly with alternator speed, that is, $v = k f$, for low- to medium speeds (typically < 6000 rpm) where v is the voltage, f is the frequency, and k is a constant, called machine constant as shown in **Figure 2-3**. At high speeds, however, a point of saturation is reached whereby the voltage increase is very small for large speed increase due to losses (iron core, copper, and frictional losses). The alternator does not produce any current until the open circuit voltage, $V_{d(oc)}$ at the terminals of the rectifier is greater than the battery open circuit voltage $V_{batt(oc)}$ and this occurs at an alternator rotor speed denoted by n_0 in **Figure 2-3**. The output current is low at engine idling speeds ~700rpm corresponding to alternator rotor speed, $n_{idle} = 1800 - 2100$ rpm when a transmission ratio of about 3:1 is assumed. However, it increases tremendously and then levels off to almost maximum charging rate as soon as the vehicle attains cruising speed, which is normally in the range of 1300 – 2500 rpm for an omnibus or heavy-duty trucks.

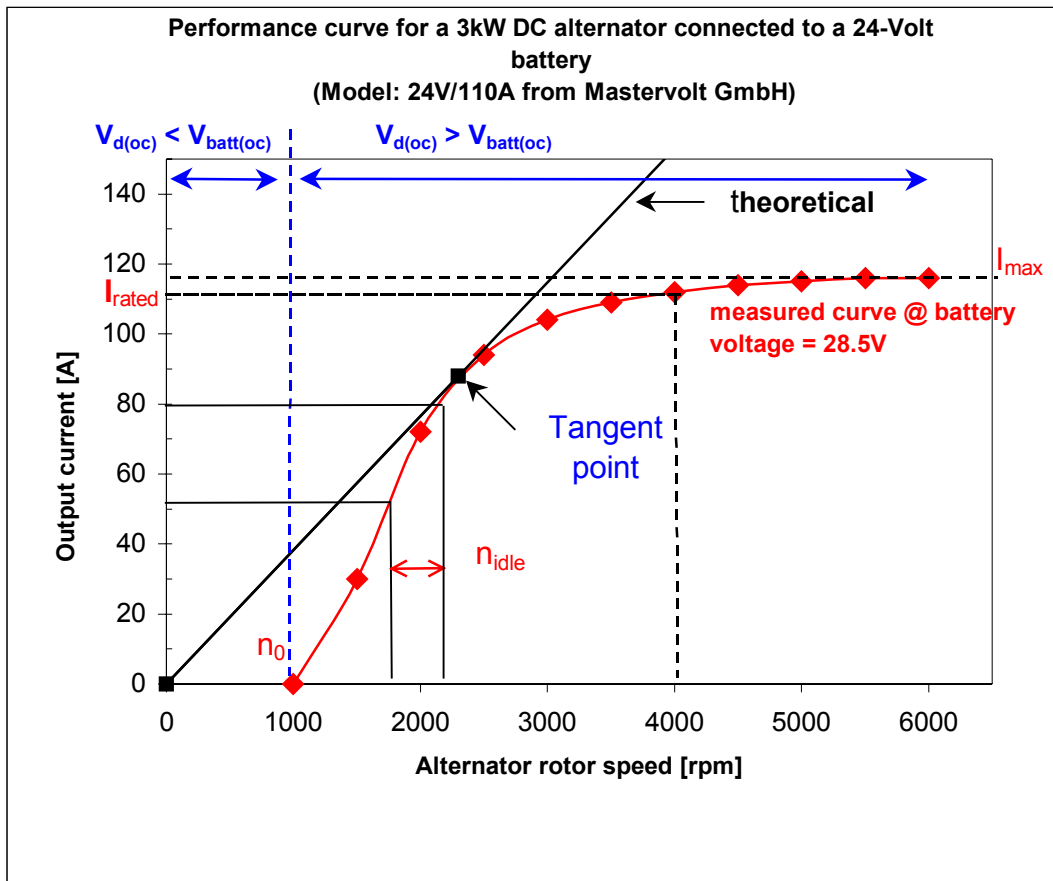


Figure 2-3: Performance curve for a 3kW/28V DC alternator

The alternator terminal voltage is clamped at a value set to about 28V for a 24V battery system. A fine adjustment to this voltage value is needed for different operating temperatures and different battery types. Controlling the amount of excitation current can regulate the alternator voltage. This is done by switching on/off the current flowing through the field winding by means of a power transistor switch driven by a pulse-width-modulated (PWM) signal. A microprocessor (μP) may be used to provide the control signals. The μP enables intelligent control in which desired battery charging characteristics (algorithms) can be easily implemented.

The mechanical-to-electrical conversion efficiency of common serially produced 14 and 28V Lundell machine alternators (including integrated rectifiers) varies in the range of 40 – 70% (or 50% average efficiency) over the engine operating speed typically $\sim 700 - 6000\text{rpm}$ (corresponding to alternator speed range of $\sim 2000 - 15,000\text{rpm}$) for small vehicles with electrical loads ranging from 1.2 – 1.5kW [Miller et al, 1998]. For heavy-duty vehicles, the engine operating speeds are lower being

roughly in the range ~700 – 3000rpm (corresponding to alternator speed range of ~2000 – 6000rpm) with maximum electrical loads about 2 – 3kW. The alternators used in the latter case are mainly rated at 24V. For the same alternator topology as above, the efficiency would vary in the range of 60 –70% (or 65% average efficiency).

The Lundell machine uses slip rings and brushes that necessitate occasional maintenance. However, despite this relatively low performance of the Lundell machine, the system was for many years the best compromise between efficiency and cost [Miller et al, 1998 / Kassakian et al, 1996]. The practical maximum rating limit for a (claw-pole) Lundell alternator technology is generally considered to be approximately 3KW (~200A at 14V, or ~100A at 28V). Increasing the nominal bus voltage from 14V to 42V in a Lundell machine, would reduce the losses on the diode rectifiers by a factor of 3, however, overall conversion efficiency improvement is not much. The new trend to replace mechanical and hydraulic components with electromechanical actuators in vehicles, and the increasing use of auxiliary equipment on-board, will probably phase out the Lundell machine.

Brushless wound rotor SM alternator

A brushless version of a wound rotor synchronous machine as shown in **Figure 2-4** below has the advantage of requiring less maintenance and hence has a longer lifespan, but has the disadvantage of having a more complex circuit topology that translates to a high component count and therefore high cost. There is no notable efficiency advantage of this circuit topology over the brush-type Lundell machine counterpart apart from the elimination of brush-slip ring related losses.

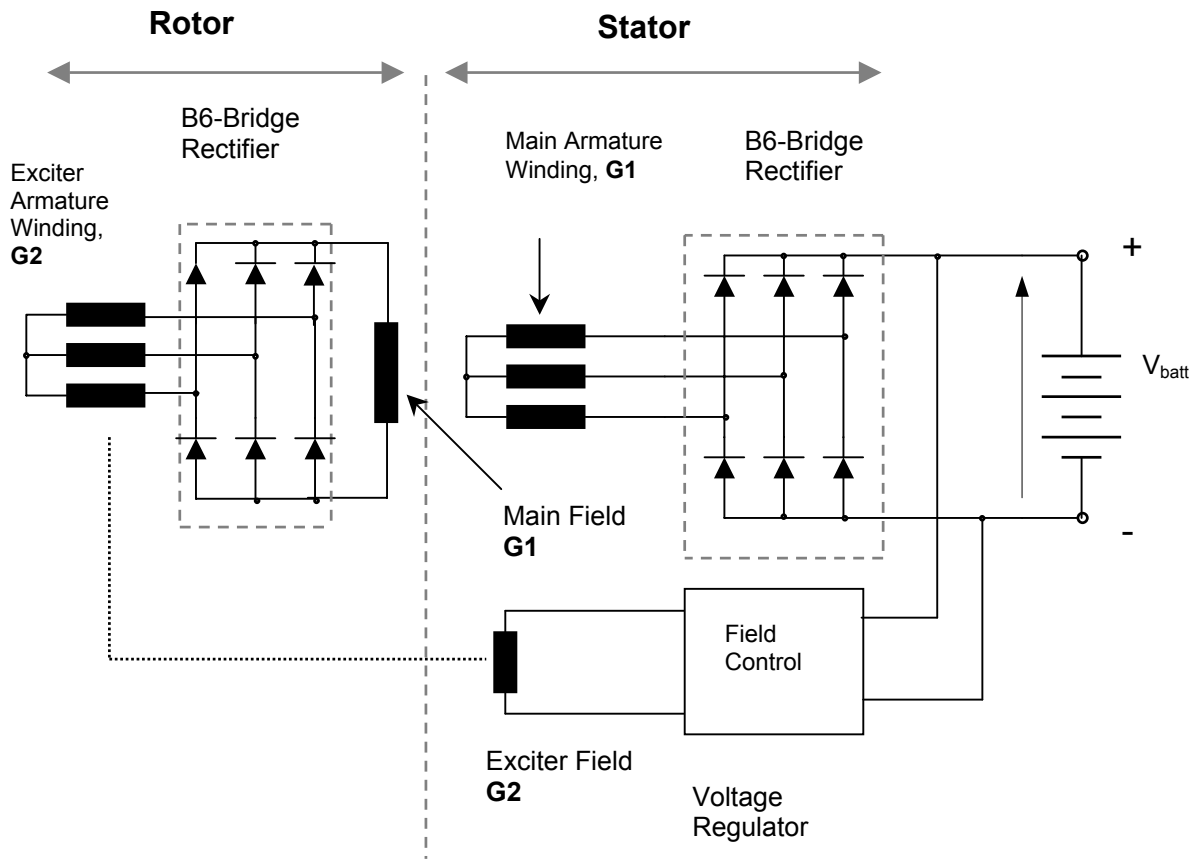


Figure 2-4: Brushless wound rotor DC alternator

Dual stator wound rotor SM alternator

A slight modification of the existing, established alternator technology is the use of dual stator windings [Hofmann, 2001]. Two identical, galvanically insulated stator winding systems are connected either in series or in parallel by means of power switches (e.g. Thyristors or MOSFETs) that are controlled to be either ON (triggered) or OFF (blocking) at low or high alternator rotor speed, respectively. At low speeds, the alternator minimum speed for power generation (n_0) for the series-connection is lower by a factor of 2 in comparison to the parallel connection case, that is, $n_{0, \text{series}} = \frac{1}{2} \cdot n_{0, \text{parallel}}$, while at high speeds the maximum output current (or power) for the parallel connected stators is twice that of the series connection, that is, $I_{d\text{max}, \text{parallel}} = 2 \cdot I_{d\text{max}, \text{series}}$ (or $P_{\text{max}, \text{parallel}} = 2 \cdot P_{\text{max}, \text{series}}$). The performance curve for the dual stator alternator is shown in **Figure 2-5**. By carefully choosing the transition (change-over)

point, the magnetic circuit is thus exploited well over a wide speed range. The power output can therefore be doubled compared to a single stator winding system for a fixed number of turns. Hofmann has discussed in detail the operation of dual stator alternators designed for the new 42V system by reviewing a number of patents adopted by some leading alternator manufacturers. Two such circuit topologies employed in two commercial alternators are shown in **Figure 2-6** and **Figure 2-7**, respectively [Hofmann, 2001]. Results on the 42V series-parallel dual stator alternator show that at maximum load, the efficiency varies between 65 and slightly over 75% for an alternator speed range of ~1000 – 10,000rpm; where 75% or more corresponds to near idle speed while at higher speeds it is about 65%.

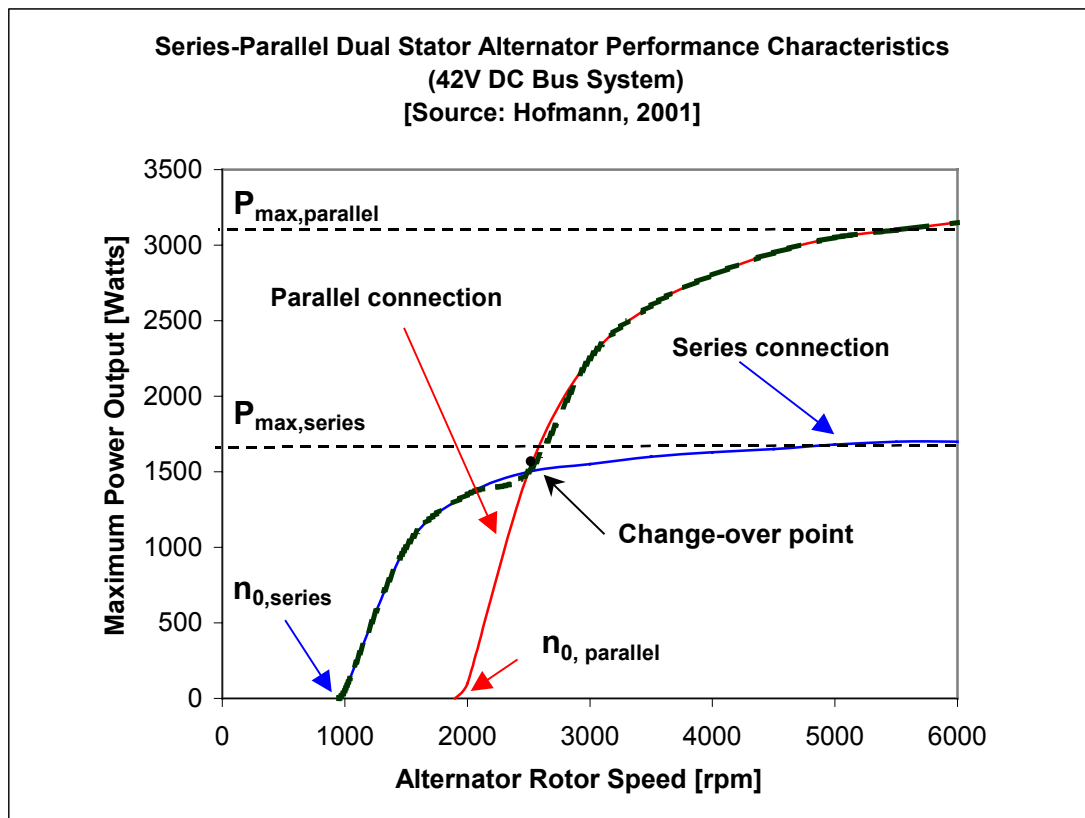


Figure 2-5: Performance curves for dual stator DC alternator

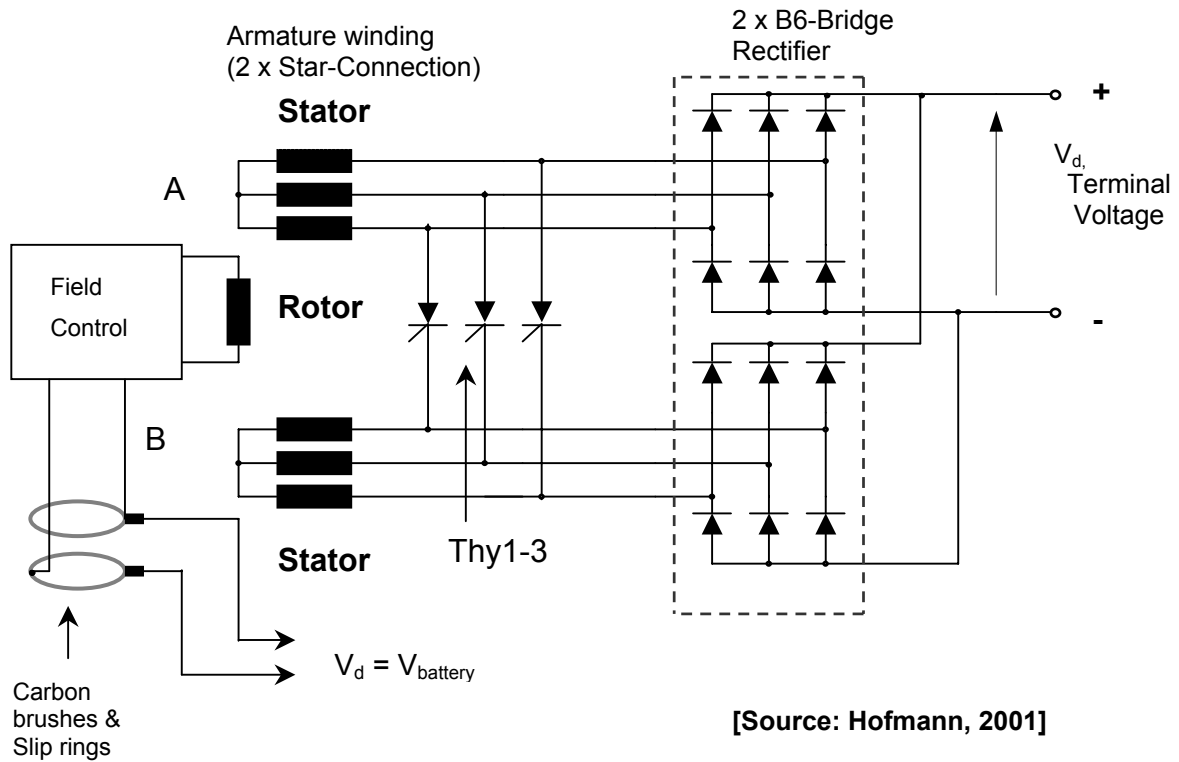


Figure 2-6: Dual stator wound rotor DC alternator topology with thyristor switches

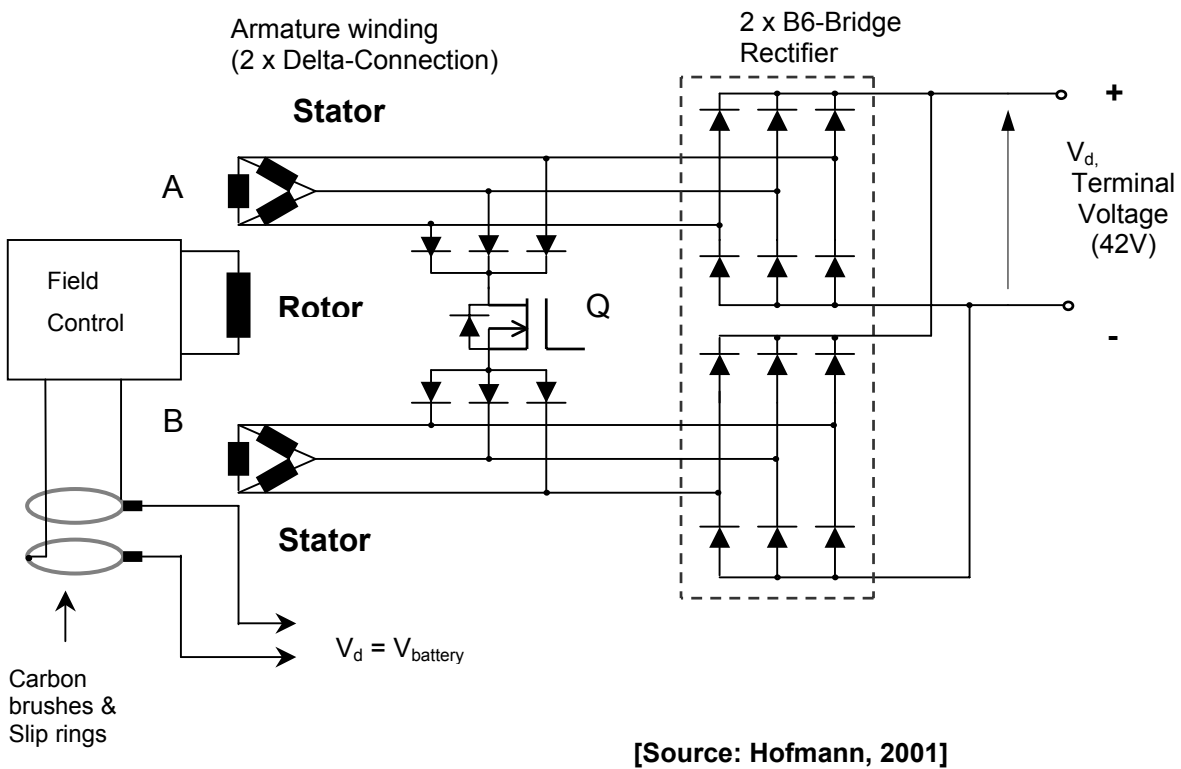


Figure 2-7: Dual stator wound rotor DC alternator topology with MOSFET switch

PM alternators

Permanent magnet machines are increasingly being employed as DC alternators. An electrical machine design option claimed to offer efficiencies in the range (70 – 84%) over the operating speed range (2000 – 6500rpm) based on measurements from a laboratory prototype employing a permanent magnet synchronous machine (PMSM) and a thyristor (silicon controlled rectifier, SCR) bridge for output voltage regulation as shown in **Figure 2-8**, has been reported [Malakondaiah et al, 2000]. In this design, however, the author notes that several technical issues related to cost, cooling and packaging of electronics, EMI/RFI, reliability and durability had not been completely solved by the time the report was published. The use of active rectifier bridges, particularly thyristors, comes with high costs for the controller and also requires stringent cooling arrangements, in particular liquid-cooling. For topologies with uncontrolled (diode) rectifiers, air-cooling is more often adequate. The conventional designs that employ a DC/DC converter stage (e.g. Buck, Boost, or Buck/Boost converter) after the uncontrolled rectifier (diode) bridge as means of voltage regulation may not be very attractive because of the high cost of extra power components (inductors, capacitors and power switches) needed, which besides are a source of EMI/RFI problems, difficult to integrate into the alternator casing, and again need large heat sinks. Furthermore, the magnets have an upper operating temperature limit of about 100°C. Generally, liquid-cooling is a rule rather than an exception for PM machines making their thermal management designs more complex than those of air-cooled machines. For instance, a path for coolant (normally water/ethylene/glycol) flow, an external pump, and air-fluid heat exchanger are needed [Goldie, 2002].

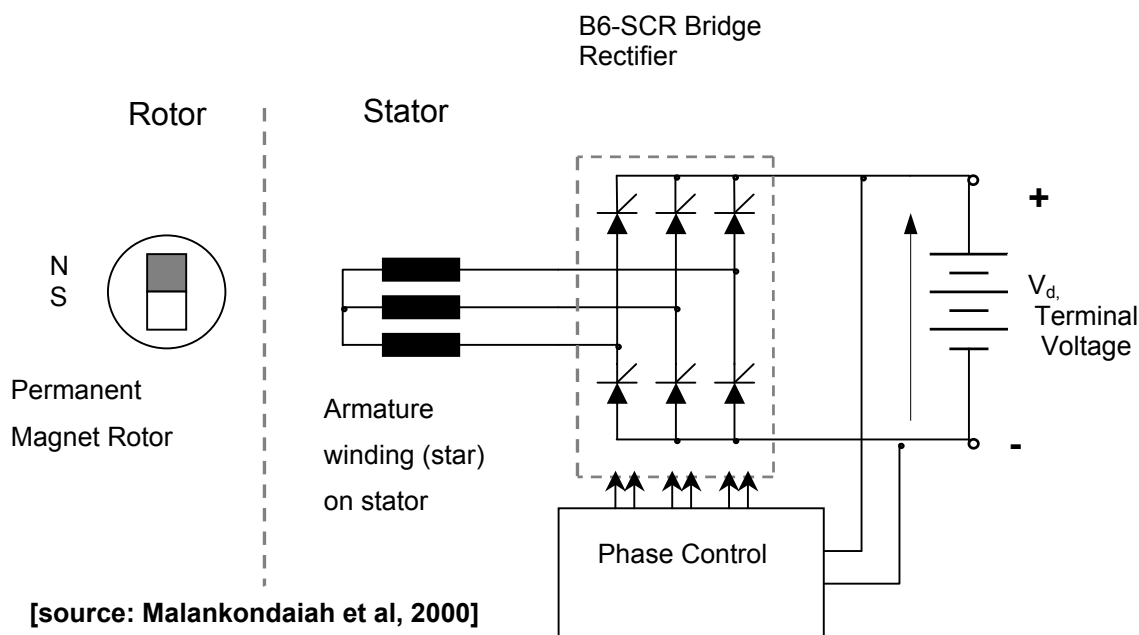


Figure 2-8: Permanent magnet DC alternator topology with controlled bridge rectifier

An attractive alternative to using active (also called switched mode rectifier or SMR) bridge for output voltage regulation when permanent magnet technology is employed, is to use the so-called permanent magnet hybrid homopolar (PMHH) machine in which a PM rotor is combined with a stationary field winding located on the stator. The advantages of having the field winding in the stator is the elimination of slip rings and greatly simplified rotor construction. **Figure 2-9** shows a PMHH machine topology claimed to have peak efficiencies in the range of 70 – 85%. The homopolar magnetic flux is superposed on to the PM flux, in order to provide active control of the terminal voltage of the alternator [Goldie, 2002]. The field control has three modes of operation: boost, buck, and ‘off’. In the boost mode, a forward polarity is applied to the field winding and its magnetic field supplements the PM field since they are in the same direction thus increasing the voltage output. In the buck mode, a reverse polarity is applied to the field coil and its field opposes the PM field thereby decreasing the voltage output. During the transition from forward to reverse polarity or vice versa no voltage or near ‘zero’ voltage is applied to the winding and this is the ‘off’ mode (also called decay mode).

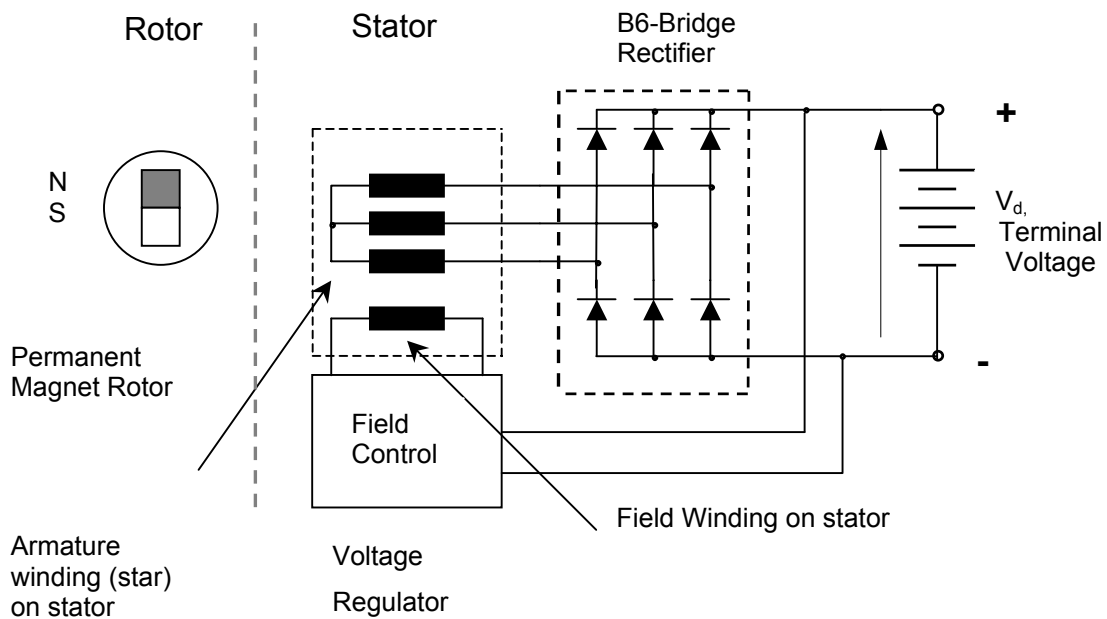


Figure 2-9: Permanent magnet hybrid homopolar (PMHH) DC alternator

The various alternator technology efficiency comparisons are summarized in **Table 2-1** below from which it can be seen that the PMHH offers the highest efficiency. However, the choice of technology and/or circuit topology option to use is normally a question of a compromise between efficiency, cost, circuit simplicity and maintenance.

Table 2-1: Different alternator technology efficiency comparisons

Electrical Machine	Peak Efficiency at max. Load over Operating Speed Range [%]
Wound rotor synchronous machine (Lundell i.e. Claw-Pole rotor or similar designs)	40 – 70 (small alternator) 60 – 70 (large alternator)
Dual Stator synchronous machine (Claw-Pole)	65 – 75
Induction (Asynchronous) machine	70 – 80
PMSM with controlled or switched mode rectifier (SMR)	70 – 85
PM hybrid homopolar (PMHH)	75 – 85

2.2.2 DC genset

The use of a DC genset is driven by the fact that inverter AC power has become a preferred choice for powering loads sensitive to voltage and frequency changes. The DC generator set comprises a variable-speed diesel engine coupled to an alternator that is specifically configured to directly connect to a battery bank (more often acting as a buffer). An external DC/AC inverter is employed when AC power is desired. Some of the known DC genset manufacturers are, for example, Polar Power Incorporated (USA) and Fischer Panda (Germany). The alternators used in most of the DC gensets are based on PM technology due to their high efficiency and power density using either conventional PMSM with DC/DC converter or PMHH technology. DC gensets, though relatively new, are already becoming popular in marine and remote land applications because of their ability to quickly recharge batteries due to their high DC current output capability compared to grid connected or conventional AC genset powered battery charger rectifiers. This configuration is shown in **Figure 2-10** below.

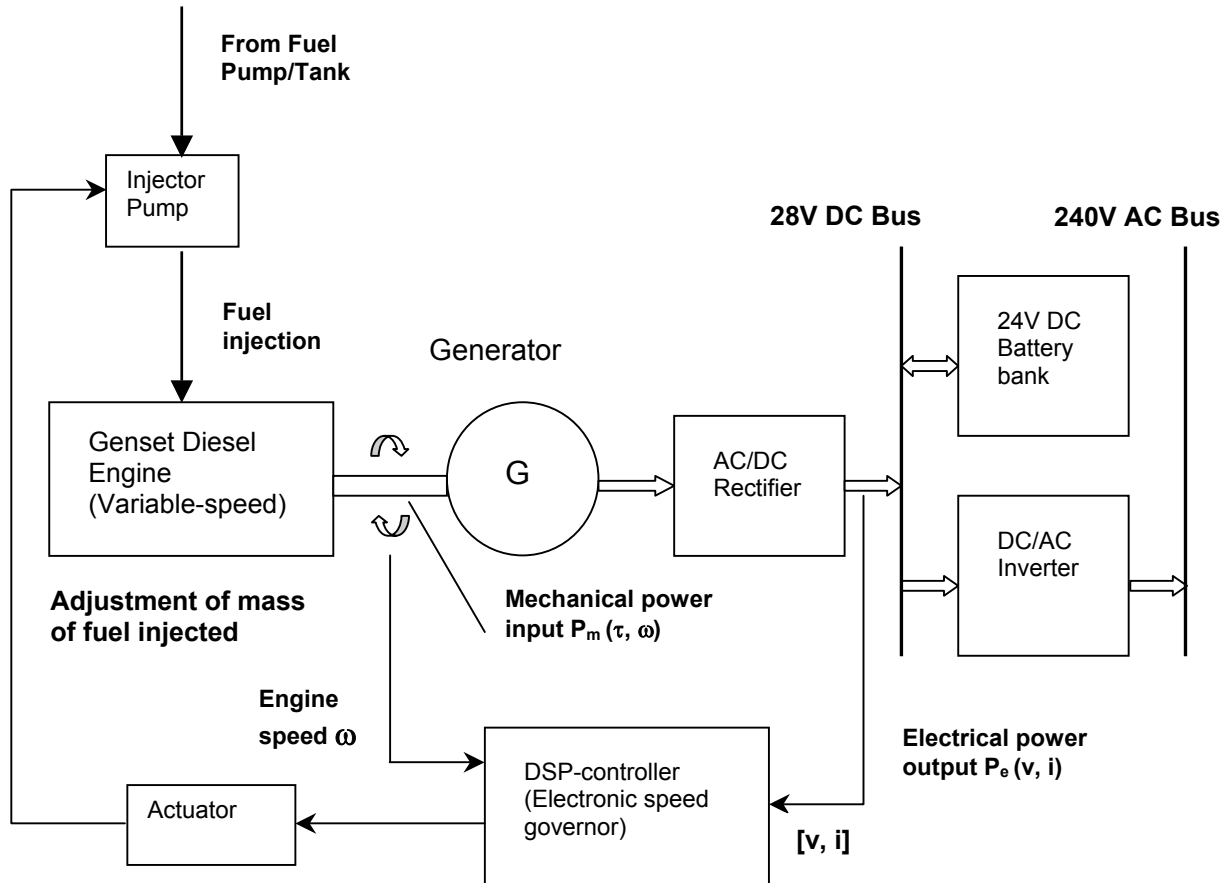


Figure 2-10: Configuration for a variable-speed DC generator set

The conversion of DC power into AC represents an extra power conversion step. However the efficiency of a good PM alternator together with rectifier (75 – 85%) and an inverter (90 – 94%) is comparable to the efficiency of a good synchronous or induction machine AC genset (70 – 80%). The major source of inefficiency in a DC generator/inverter combination system is in the battery charge/discharge cycle. A battery is only about 80% (and even sometimes as low as 40%) efficient depending on the age of the battery and charge cycle method.

2.2.3 PV generator

The DC genset with inverter and battery provides a system that allows simple integration of DC power sources such as a PV generator on the 28V DC bus. Solar Photovoltaic (PV) generators are considered to be suitable for mobile application due to their portability and modularity. They can economically recharge the batteries or directly power loads whenever the sun shines. However, their high dependence on sunny weather conditions makes them on their own unreliable for critical loads.

The number of modules that could possibly be mounted on vehicle's roof is limited by mainly two factors: the available surface area and initial cost. An omnibus with a length of about 12 metres presents a mounting area on the roof of about 25m². For mono-crystalline silicon modules that have the highest power density of about 100 – 120 W/m² at peak power conditions, this means a maximum PV array rating of about 2.5kW. However, the rule-of-thumb has shown that the optimal array size also depends on the size of the battery bank. If there is an option of connecting other power sources, the PV array and battery dimensions can be scaled down.

When combined with a PV generator, the DC genset provides the bulk charge to the batteries probably during the night, evenings or early in the morning. The PV array would provide the finishing charge in the afternoon. Such an arrangement would save fuel and engine maintenance. The PV array also keeps the batteries charged when the system is not supplying power during the day so that the genset run time is reduced.

2.2.4 Lead-acid battery

An auxiliary lead-acid battery provides means of energy storage of the generated power that is not consumed directly and should be designed for deep-cycle service. It also acts as a power source when other sources are 'off' or unavailable. A traction-type battery is considered an ideal choice although other types such as semi-traction or solar batteries may be used as alternatives. Most typical solar batteries are of the so-called stationary battery constructions that have very thick plates. Unlike the SLI or traction batteries, they are not suitable for high-charging rates provided by vehicle alternators (output currents ~100A or more). If they are to be employed, then unreasonably large battery bank sizes may be reckoned with since large electrode surface area would be needed. It is a recommended practice not to discharge flooded (wet) Lead acid batteries below 80% (or 50% for optimum performance) in order to achieve long life [Linden, 1995]. For maintenance-free (also called Sealed or Valve Regulated Lead Acid, that is, SLA or VRLA) the limit is strictly 50% of depth of discharge (DOD). To observe this rule, however, the system should have a means of estimating the battery state of charge [Berndt, 1993].

Battery technology influences charge efficiency, charge acceptance, cycle life, lifetime amp-hour recovery, periodic maintenance requirements, safety and other physical considerations. A larger alternator output will reduce engine run-time to charge the system provided that the battery bank has an adequate charge acceptance rate. The charge acceptance rate is proportional to battery bank size and is influenced by battery technology. Rapid charging of a battery bank must take into account battery temperature in managing charge voltage. Purpose built alternator regulators and battery chargers are available that take temperature into account.

2.3 AC power sources

AC power is obtained by means of a DC/AC converter (inverter) that may take any of the following forms:

- A separate piece of equipment externally connected to the battery and/or DC genset
- An integral part of a portable variable-speed AC genset

- An integral part of a power electronic converter module also called Electronic Control Unit (ECU) attached to an alternator driven by the vehicle engine

The AC generator set is made up of a variable-speed diesel engine coupled to an AC machine and a power electronic converter module that includes a rectifier, an inverter, and a bi-directional DC/DC converter stage as shown in **Figure 2-11**. A prototype having this configuration is described in detail in [Tolbert, et al 2001]. In the report by Tolbert et al, the diesel genset engine is adjusted to operate in the 2000 – 3000 RPM speed range. A permanent magnet (PM) alternator generates a corresponding output voltage in the range 350 – 450V DC that forms the intermediate circuit (or DC link) voltage. Power electronics costs are reduced as the result of higher voltage allowing for low current.

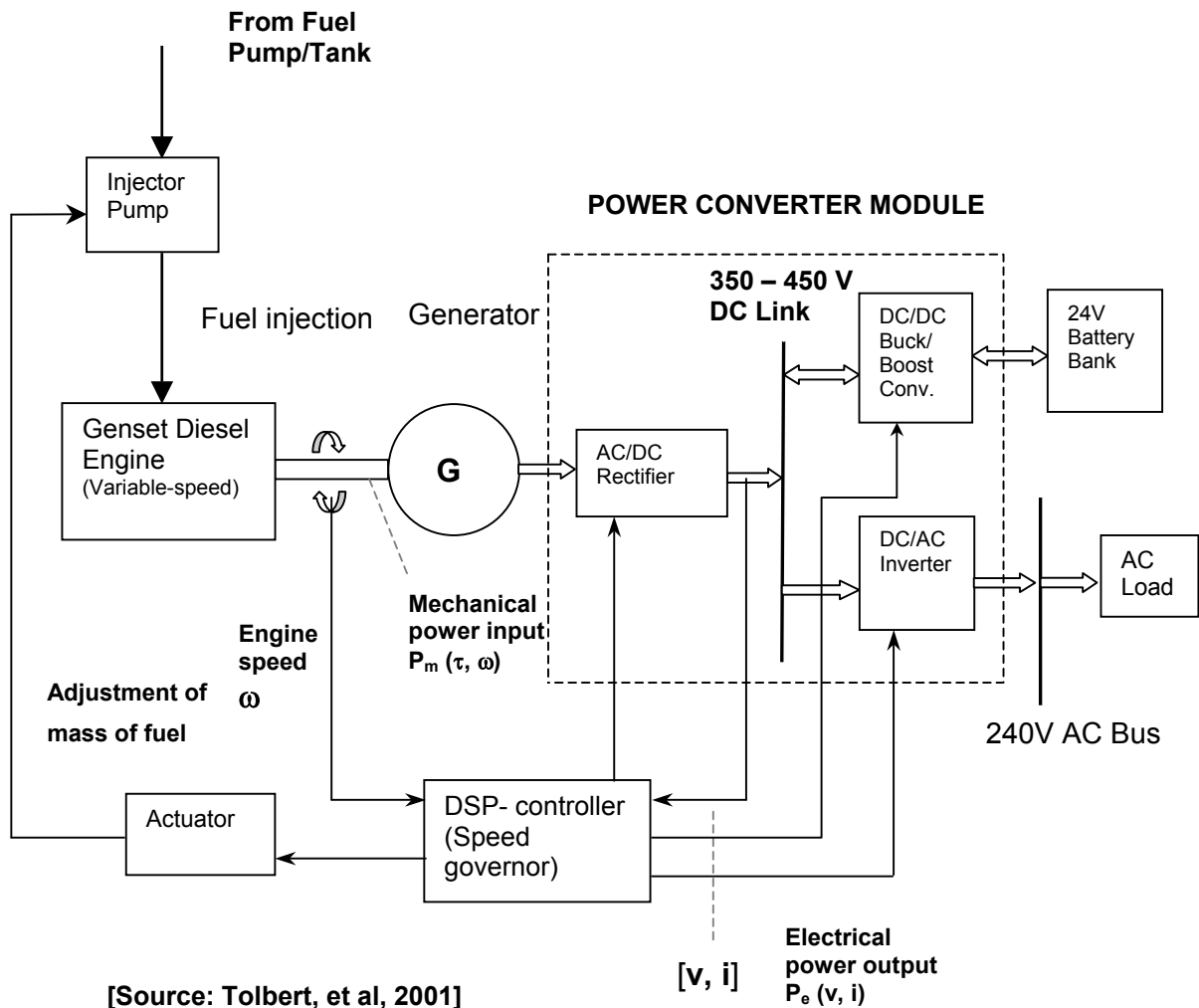


Figure 2-11: Configuration for a variable-speed AC generator set

2.4 Variable-speed operation in diesel gensets

The variable-speed diesel generator uses power electronic converters to provide the proper voltage and frequency of the generated power while allowing the diesel engine's speed to vary in proportion to the electrical load. Common generator sets (gensets) operate on fixed-speed whereby the ICE is governed to run at a constant speed typically 1500 or 3000 RPM for a 50Hz system, and 1800 or 3600 RPM for a 60Hz system. The concern over using an AC generator is being able to maintain proper engine speed. There are two major causes of a genset failing to maintain constant frequency and voltage:

- The engine can develop mechanical problem in the fuel injection control system (or carburetion in the case of spark ignition (SI) engines)
- Engine operation at non-steady state or transient conditions such as during power surges resulting from start-up of inverter- or motor driven equipment
- Engine operation at non-constant load-size conditions (a change from light to heavy load causes voltage/frequency droop)

The majority of small portable generators are prone to this problem, and are therefore only suitable for devices that can tolerate a wide swing in voltage and frequency such as lights, power tools, heaters etc. They are unsuitable for frequency sensitive equipment e.g. compressor motors for refrigerators, computers, medical equipment, etc. The load transient problem can be eliminated by using a battery bank (acting as a buffer) that is connected at the DC bus, either directly as in the DC genset configuration, or via a bi-directional DC/DC converter to the intermediate DC link as in the AC genset configuration. If the engine develops a problem causing a change in its speed there is no effect on the battery, nor the inverter and appliances. Deviation from ideal operation in the fuel injection control mechanism in a variable-speed engine is not a very serious issue and this reduces need for the regular maintenance such as frequency re-calibration common in fixed-speed generators, which mainly use mechanical speed governors.

A conventional approach to tackle the frequency problem in fixed-speed gensets, is to heavily oversize them in relation to the prevalent load conditions since large engines have high inertia and hence can ride through these transient conditions with

little change in frequency. However, this approach is counter-productive in many ways:

- Over-sizing is a waste of resources since it leads to high capital cost and high fuel consumption
- Genset weight is not minimized which is an important requirement in a mobile application
- Operation on very light loads relative to the maximum rating is destructive to the engine in the long run

The last point is explained as follows: operation at an average load lower than 30% of genset capacity would lead unnecessarily to high fuel consumption in relation to power output, engine oil dilution, carbon build-up or wet-stacking, cylinder glazing and reduced engine life [Andriulli et al, 2001]. "Wet-stacking" is a condition in which excessive or unburned fuel deposits build up in the engine and occurs primarily when diesel engines are run on low or unloaded conditions, or operated at low temperatures before the engine has had time to warm up. Likewise, automotive engines would experience the same problem when run at idle speed for long durations.

Load-adaptive variable-speed technology enables right sizing of the genset for the application. It adapts to any load and runs its engine at the most economical speed for the instantaneous load. By combining a variable-speed engine with a battery energy storage system, a much smaller, less expensive engine with a wide speed range (such as small diesel engines used in automotive application), which moreover are less noisy, have optimal fuel efficiency, and lower emissions, may be used [Andriulli et al, 2001].

3 CASE STUDY: HYBRID POWER SYSTEM FOR MOBILE MEDICAL CLINIC

3.1 System Description

As a case study, a hybrid power system for a mobile medical clinic application is considered. In this system, a 12-metre long bus is fitted with on-board medical equipment as illustrated in **Figure 3-1**. The mobile medical clinic is a project proposed by an organisation called “Bindura Children’s Home” operating in Kenya (Africa) and sponsored by a religious group. Its goal is to rehabilitate street children and other homeless people.

The Organization currently manages three children’s homes situated in different locations that are several kilometres apart: one in Eldoret Town (serving as the headquarters), another at a village 30 km away from Eldoret Town, and a third one on the outskirts of Nakuru Town (some 150 km away from Eldoret).

Pick-ups, vans, buses and trucks are ideal candidate vehicle platforms for mounting electric power system components due to the available space they offer. The MHPS comprises:

- A retrofitted high-power (second) alternator
- A variable-speed diesel generator set (as an Auxiliary Power Unit or APU)
- A PV generator mounted on the roof of the bus, and
- An auxiliary lead-acid battery bank (electrically isolated from the starter battery)

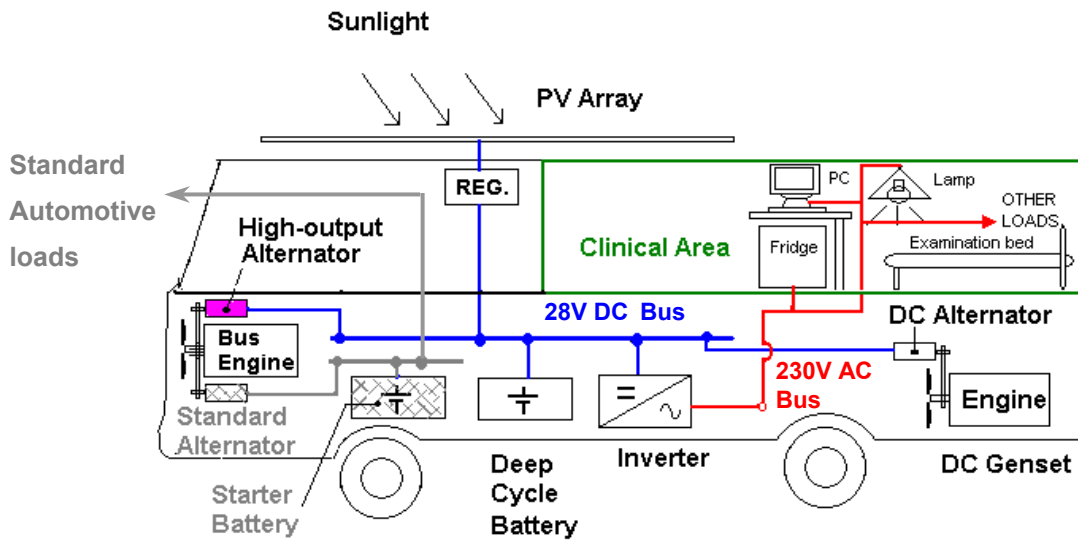


Figure 3-1: A hybrid power system concept for a mobile medical clinic

The area of operation is practically on the Equator as indicated on the map in **Figure 3-2** below. The bus is expected to make frequent trips between the towns Eldoret and Nakuru.



Figure 3-2: Map of western Kenya showing area of operation

3.2 Load characteristics (profile)

A typical list of on-board medical equipment is provided in **Table 3-1** below.

Equipment	Rated power [W]	Quantity	Estimated Usage Frequency per day	Sub-total power [W]	Estimated Run time [h]	Energy Consumed per day [Wh]
Medical Refrigerator/ Freezer	200	1	Continuous	200	24 (100% duty-cycle)	4800
Room Lights	11	4	1	44	5	220
Microscope (12V halogen lamp)	30	2	6	60	1.0	60
Ultrasound	100	1	5	100	1	100
Power saw (for cutting plaster)	125	1	3	125	0.24	30
Electrocardiograph (ECG)	100	1	3	100	0.6	60
Autoclave	1100	1	3	1100	0.75	825
Centrifuge	30	3	3	90	0.25	22.5
Incubator	30	3	1	90	24	2160
Personal Computer	100	1	1	100	5	500
	Same-time total power (W) →			1999 (≈2000)	Total Energy →	8778

Additional miscellaneous loads such as hot plates and electric kettles that may be needed for warming meals or boiling water, respectively, have not been included in the analysis although they may occasionally be part of the load. Non-electrical heating sources such as gas burners that use bottled gas may be used as alternatives, however, not on-board due to the danger of catching fire because of the close proximity of inflammable vehicle fuel (diesel). They may be temporarily set up at the site of operation in some tent or other similar structure at a safe distance away from the vehicle.

The requirement of a medical refrigerator for storing critical vaccines or blood is absolutely critical; therefore the required power source must be ideally 100% reliable. In the so-called 'cold chain', all vaccines must be maintained at a temperature

between 0°C and +8°C during the transport between one point and the next. Therefore all transportation links must be able to protect vaccines from heat, sunlight, and extreme cold. Refrigerators for medical application are commercially available with both DC (12- or 24 Volt) and standard AC (240 Volt) power requirements. To avoid inverter power losses, the DC-type refrigerator is often preferred for solar photovoltaic application. An example, is the variable-speed compressors driven by permanent magnet brushless DC motor e.g. the Danfoss® compressor from Danfoss Compressors GmbH. It is claimed that every start-up of the Danfoss® compressor takes place at low-speed (soft start): meaning relatively lower start-up power surge in comparison to similarly sized fixed-speed compressor motor [Danfoss Website Information, 2003]. After start up, the speed of the compressor will be ramped up and adapted to the load or available solar power. The software algorithm adapts the capacity of the compressor to the actual thermal load of the system or available solar power [Bergeron, 2001]. However, reliable DC refrigerators use expensive compressors and are not readily available on the Kenyan market, a conventional standard 230V AC version has been considered in the analysis.

From the list, the following observations on the load characteristics are noted:

- Most of the equipment have power ratings not exceeding 200 W (with the exception of the autoclave which is rated at 1100 W)
- The medical refrigerator has the highest energy consumption (4.8 Kilowatthours for an assumed duty cycle of 100% or 2.4 kWh for 50% duty cycle)
- Long (or continuously) running loads are primarily the refrigerator and incubator

From **Table 3-1** above, the maximum same-time load power is estimated to be 2.0 kW. The medical operation is assumed to take about 5 hours, and the time of operation selected to fall at mid-day hours e.g. from 10.00 – 15.00 hrs so as to coincide with period near or at maximum solar irradiance. In the early morning and late afternoon hours, it is assumed that the only significant load is a medical refrigerator with peak power consumption of 200 W. Refrigerator compressors do not necessarily run continuously for 24-hours and may have total run times of only 8 – 12 hours per day [meaning operation at 30 – 50% duty cycle]. This depends on the ambient temperature, number of door openings, cabinet insulating materials, and whether the freezer is included, etc [Bergeron, 2001]. A 50 and 100% duty cycle

operation is considered in the analysis. The latter is a very conservative assumption, but one that should give a slightly over-dimensioned system necessary to ensure system reliability. Thus the simplified load profile used in the analysis is as shown in **Figure 3-3**.

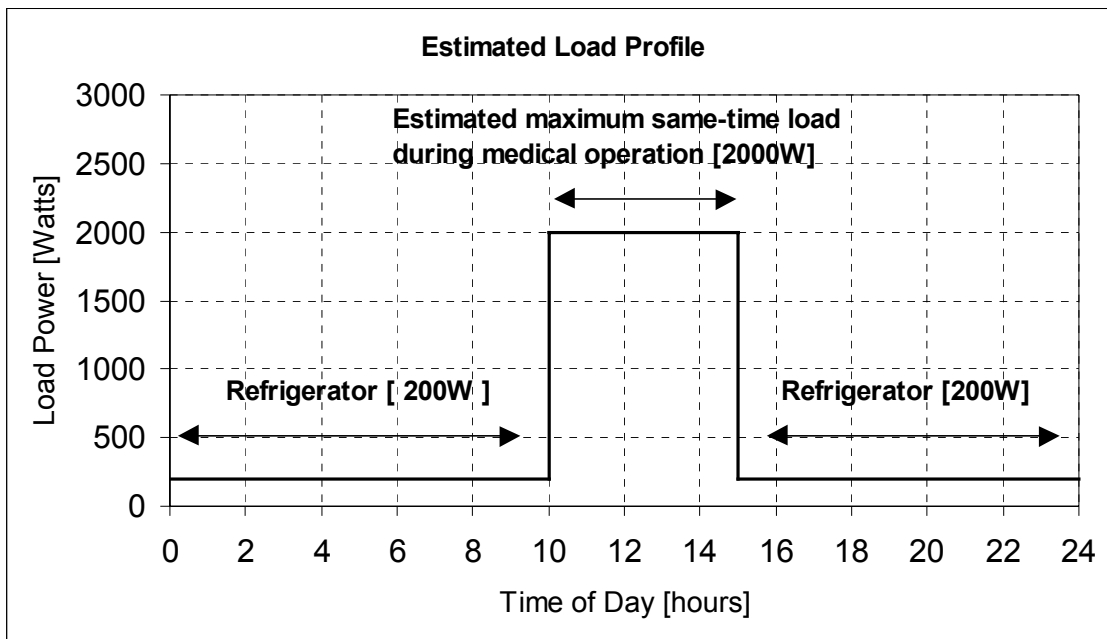


Figure 3-3: Estimated load profile with refrigerator at 100% duty cycle

3.3 Component sizing

The criteria for component sizing generally depend on several factors which may be interdependent e.g. energy source and load characteristics, commercially available component ratings, system operation and control, and component capital and operating costs, etc [Patel, 2001 / Seeling, 1997]. Component dimensions are initially selected based on rule-of-thumb methods and then simulation is used to confirm or modify them. This is done by correctly identifying the key variables, and then repeatedly running the simulation, adjusting the variables manually to converge on an acceptable sizing.

3.3.1 Alternator

The alternator sizes commercially available for vehicular auxiliary power application have current ratings typically in the range of 100 – 250A for 24V battery systems. A 24V/110A model from Mastervolt GmbH was commercially available and was

selected for the analysis. The current rating usually has an impact on the size of battery bank to be employed. The rule-of-thumb for the dimensioning of the alternator and battery bank is that the alternator output equals 20 – 25% of the battery capacity. For a 110-Amp alternator considered for this work, a corresponding minimum battery capacity rating of 440 - 550Ah would be required. If other charging sources are also present e.g. a PV generator, the total charging current (alternator plus PV) is first determined, and then appropriate battery capacity is calculated using the same rule. In this particular case, however, the PV generator current contribution was considered less significant in comparison to the alternator charging current and was therefore not included in the calculation.

3.3.2 Battery bank

There is no definite guide to choosing battery size and operating strategies for a hybrid system. Some of the factors that make up the design criteria (or rules-of-thumb) generally depend on the nature of sources and loads [Turcotte et al, 2002]. These are, for example:

1. Load energy consumption analysis
2. Allowed depth of discharge (DOD)
3. Number of days of autonomy
4. System efficiencies or losses (e.g. battery, wiring, and power conversion)
5. Operating temperature
6. Allowed maximum battery weight
7. Recommended charging rate (or battery charge acceptance rate)

In view of these factors, the following criteria are investigated in the search for an optimum battery bank size:

Criterion 1: Energy consumption analysis formula

By relating factors (1 – 5), a rule-of-thumb battery sizing formula based on energy consumption can be expressed as [Schmid, 1999]:

$$C_B = \frac{L \cdot T_A}{DOD \cdot D_T \cdot \eta_C \cdot \eta_W \cdot \eta_B} \quad (3.1)$$

where: C_B = battery capacity [kWh]

L = daily mean energy consumption [kWh/d]

T_A = number of autonomy days [d]

DOD = maximum depth of discharge [decimal]

D_T = derate for temperature [decimal]

η_C = efficiency of power conversion [decimal]

η_W = efficiency of wiring [decimal]

η_B = efficiency of battery [decimal]

If the following are assumed for the system: $L = 8.778$ kWh/d, $T_A = 1$, DOD = 0.6, $D_T = 1.0$, $\eta_C = 0.9$, $\eta_W = 0.95$, $\eta_B = 0.8$, then $C_B = 21.4$ kWh (or **891 Ah** for a 24V system). This pre-sizing value is typical of residential PV/Battery only system. A hybrid system that includes a diesel genset and a vehicle DC alternator can do with a smaller battery bank size.

Criterion 2: Maximum allowable weight

In mobile application, there is battery weight limitation. A battery weight of 500kg is considered the upper weight limit for this system. By considering an energy density of 30 Wh/kg for lead-acid battery at 20-hour discharge rate rating, the corresponding maximum battery capacity would be 30 Wh/kg x 500kg = 15kWh (or **625 Ah** for a 24 V battery system).

Criterion 3: Battery charging rate

Battery charging using DC alternators is characterized by high charging rates (due to alternator's high output current) and hence battery charge acceptance must be considered. The battery charge acceptance is the maximum rate at which a battery bank can be recharged [Linden, 1995]. It is determined by capacity, battery type, and state of charge. Experience has shown that it is best to cycle lead-acid batteries between 50% and 80 – 90% of full charge whenever possible [Barley et al, 1995]. Under these conditions, three types of lead-acid batteries, namely: flooded, gelled, and absorbed glass mat (AGM) batteries have been shown to have acceptance rates equal to 25%, 40%, and 100% of their total 20-hour Amp-Hour rating (i.e. C/4, C/2.5, and 1C), respectively. Hence, for the flooded lead-acid battery, the recommended battery capacity size (in Ah) should at least be 4 times the alternator current rating. As such, an 110 A alternator requires a minimum battery capacity of **440 Ah**.

Optimum battery size determination

In this application, we can ignore the use of energy consumption analysis (**Criterion 1**) and use only the maximum allowable battery weight (**Criterion 2**) and the charge acceptance rate (**Criterion 3**) sizing criteria. These two factors alone determine the minimum and maximum battery bank size. An optimum battery size would lie between these two limits, that is, $(440 + 625)/2 = 532.5$ Ah. A commercially available standard value is, for instance, **550Ah**.

3.3.3 Genset

A genset with a maximum electrical prime power rating of ~10kW at maximum speed was selected. Altitude de-rating is included in the analysis. Under variable speed operation, the power output varies in the range 4 – 10kW.

3.3.4 PV generator

From experience, the relation between storage capacity [kWh] and peakpower [kW_p] of the PV array is more or less 10:1 in a PV/Battery only system [Kininger, 2003]. In cases where the global radiation at the site is nearly constant throughout the year, this value will be lower than 10:1. For the selected battery size (24V/550Ah or 13.2kWh), the calculated PV generator size is 1.32KW_p. In a hybrid system, a smaller PV generator size may be selected. An initial guess was to select a PV generator size of 550W_p. Depending on the available resources for purchasing the PV modules, we can increase the PV generator size upto or slightly less than the value based on the above rule. In this regard, we have also considered the performance of a 1100W_p in the simulation study.

3.3.5 Inverter

Inverter size is selected to handle the peak load. In this system, a 3kW inverter would be required to cover all possible load combinations. Considering the general shape of the inverter efficiency curve, there is a region of low efficiency operation when the connected load is less than about 10% of the inverter rating. Therefore, a 3kW unit would operate at low efficiency when the only connected load is a refrigerator rated

at 200W, that is, only 6.7% of inverter rating. From the load list, it is evident that most of the equipment has individual power ratings below 200W. Other than the refrigerator whose time of use can be predicted, the time of use for rest of the equipment cannot be 100% predicted. This makes it somewhat difficult to find the optimum rating for the inverter. Therefore, it is proposed to have two inverter units: a 3kW unit to take care of the peak load (indicated as 2kW in the load profile in **Figure 3-3**), and another rated at 900W for periods of low power consumption, especially when only the refrigerator and/or a few of the low power equipment are in use.

A summary of the main system component dimensions are listed below:

Component	Rating
High output DC alternator	24V / 110A, Maximum Power ~3kW)
Lead acid Battery bank	24V, Capacity rating @ C ₂₀ = 550Ah
Variable-speed diesel genset	Peak output range 4 – 10kW
PV generator	Peak power range 500 – 1100W
Inverter(s)	24V, 2 x rated at 900W & 3000W

3.4 Operation and Control

Optimal operation of the MHPS requires complex control strategies implemented by means of a system controller. There are three important aspects of operation and control that such a controller is required to perform, are:

- Load management
- Battery management
- Diesel generator management

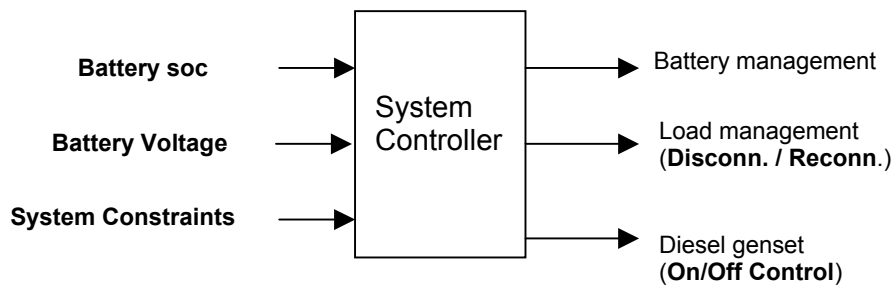


Figure 3-4: Block diagram of a system controller

3.4.1 Diesel genset and load management

One of the design issues in such systems is dispatch strategy: the aspect of control strategy that pertains to the sources and destinations of energy flows. In systems with both batteries and diesel genset(s), dispatch strategy impacts long-term fuel usage as well as battery life [Barley, 1996]. In this system, a non-predictive (or non-forecasting) system controller because it is easy to implement in a real system controller is considered. The decision when to disconnect or reconnect the load (that is, loss of load acceptability) and when to turn on/off the diesel genset is based on battery state of charge. The system constraints are minimum and maximum battery SOC control set points needed to activate the relays for load disconnect/reconnect and diesel genset on/off control, minimum battery voltage, diesel minimum run time, and times when diesel genset must not be allowed to run.

3.4.2 Battery management

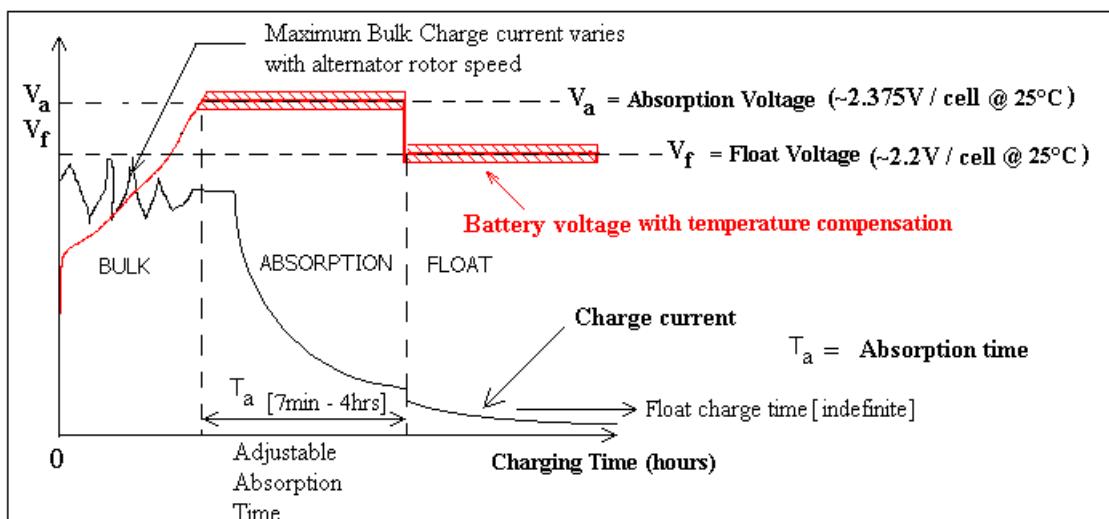
Battery management generally concerns avoidance of the following detrimental effects that shorten service life:

- Sulphating due to frequent deep discharges
- Corrosion due to high battery temperature conditions
- Loss of water due to frequent overcharge conditions

This involves the use of proper charging characteristics (or algorithms). Most regulators charging algorithms are based on real-time measurement of battery voltage, current, time, and operating temperature. The 3-stage (bulk, absorption, and

float stages also called IUU) charge algorithm is commonly used method for charging most lead-acid batteries. There are a number of variations of the 3-stage algorithm. For instance, in the IU_oU version, the alternator is allowed to output its maximum possible current until the recommended charge voltage (about 2.375V per cell for flooded batteries at 25°C) is reached, the voltage is then held constant for a set time, or until the charging current drops to a certain percentage of the maximum alternator current, after which the voltage is lowered to float voltage (about 2.2V per cell at 25°C) which may be held indefinitely as long as the charging source is connected. The criteria for transition to the float voltage differs among regulator designs, and further depends on whether the battery is flooded, absorbed glass mat (AGM), or gel type.

We have considered an IU_oU version used in a commercial voltage regulator for DC alternator application with brand name 'Alpha' from Mastervolt GmbH as shown in **Figure 3-4**. The transition from absorption to float voltage is by means of a timer. The subscript 'o' indicates that the absorption time is automatically terminated. The voltage set points are temperature compensated. If during the absorption stage, the voltage drops by more than 0.5V for 5 or more minutes, the timer resets and starts timing afresh if the voltage recovers back to the absorption value, otherwise the cycle reverts to the bulk charge stage. The same is true for the float stage.



[Source: Sketch based on 'Alpha' Regulator Manual description from Mastervolt GmbH]

Figure 3-5: IU_oU charging algorithm in 'Alpha' voltage regulator

4 MODELLING AND SIMULATION

4.1 Dynamic modelling and simulation

Special modelling languages have been developed to facilitate modelling and simulation. There are two broad language categories in this domain: causal and non-causal modelling.

Causal (or block-oriented) languages are most popular and examples are Simulink from Math Works Incorporated and Ptolemy II from University of California at Berkeley. Arrows and blocks represent the simulation model, where the arrows represent data flow, and the blocks the system. Mathematically, such a block diagram corresponds to a system of ordinary differential equations (ODEs) in explicit form. In such an ODE, the causality, that is, the cause-and-effect relationship is explicit: "known" quantities (inputs and state variables) are used to define „unknown" quantities (outputs and state derivatives); hence the name causal modelling. In causal modelling, the equations that represent the physics of the system must be written so that the direction of signal flow, the causality, is explicit.

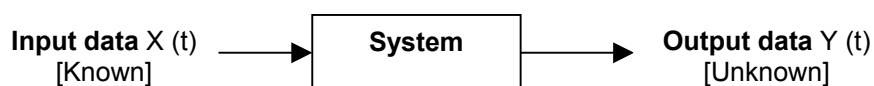


Figure 4-1: Block-oriented (causal) modelling scheme

The second class of language is the non-causal (or object-oriented) in which the model focuses on the interconnection of the components of the system being modelled, from which causality is then inferred. Examples include Modelica and Dymola which both use Modelica syntax [Tiller, 2001 / Brück et al, 2002 / Richert et al, 2003].

Generally, simulation models can be built in many different ways depending on the objectives of a particular problem to be solved. Major factors to consider while building models are:

- The step-time response of individual component models, which is also an indication of the level of abstraction (or detail) of a system
- Time-range of interest (or the length of simulation run e.g. over several seconds, minutes, hours, days, etc)
- Assumptions to be made e.g. influence of environmental factors such as ambient temperature, altitude, atmospheric pressure, etc

In this study, our focus is on the simulation of power flows and control (dispatch) in a hybrid power system. The time range of interest considered is in the order of a few seconds to several hours, which we define as 'medium-term' behaviour. Within this definition, a simulation run of 24-hours or daily cycle is considered adequate for system analysis in this particular case. The following assumptions are made:

- Sub-second component behaviour (that is, events lasting < 1 second) is not taken into account.
- The accuracy of the simulation depends on MATLAB Ordinary Differential Equation (ODE) solver functions selected, whose performances are further assumed to be optimised. This is done by selecting suitable simulation parameters before running the simulation.

The implications of the first assumption are that the following rapidly changing physical quantities are not modelled:

- The instantaneous magnitude of the current and voltage (sinusoidal variation) on the 240V AC / 50Hz bus (value changes over a period of 20ms)
- Dynamics of the power switches in power converters e.g. the Pulse-Width-Modulation (PWM) behaviour
- Transients e.g. during the start-up of inverters or electric motor driven loads

The simulation therefore reduces to a system-level problem, whereby only the macroscopic dynamic behaviour of the components is considered (that is, internal circuit details are irrelevant). This approach helps to achieve reasonable simulation

times, which is always a problem with dynamical simulations. Consequently, power electronic systems such as inverters, DC/DC converters, rectifiers, etc are simply characterized by their measured performance data, which is normally in the form of efficiency curves. Models for the PV modules and batteries are taken from manufacturers data and reputed existing literature sources.

4.2 MATLAB/SIMULINK Modelling Environment

Modelling and Simulation of the power system has been done in the MATLAB/SIMULINK simulation environment. This simulation package is widely used in academia and industry for modelling and simulating dynamical systems. For modelling, SIMULINK provides a graphical user interface (GUI) for building models as block diagrams. One can build models using top-down and bottom-up approaches. One can view the system at a high level, then double-click on the blocks to go down through the levels to see increasing levels of model details.

4.3 Forward-facing and backward-facing calculation

The actual simulation calculation is performed using a combination of “forward-facing” and “backward-facing” modelling approaches. In the forward-facing approach, the power flows from the energy source(s) to the energy sink (forward direction) and can be tracked downstream beginning with the known input parameters. The data flows from left to right, often through a controller. For instance, the battery may need to be charged and discharged within certain voltage limits. By means of appropriate controls, e.g. using logic switches or relays, the power flow from the energy source to sink can be regulated. The forward-looking approach allows more accurate representation of the system dynamics and control strategy, an important consideration in optimising the complex power systems and energy storage system interactions [Wipke et al, 1999]. **Figure 4-2** shows a block-diagram representation of this approach.

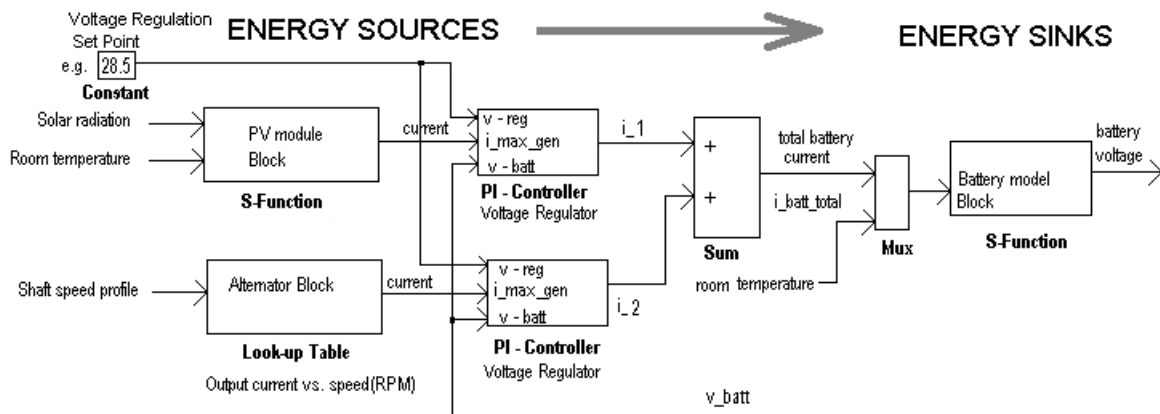


Figure 4-2: Forward-facing calculation in MATLAB/SIMULINK

In the backward-facing approach, the output (e.g. power demand or load profile) is known initially but the input (e.g. power available from energy source) has to be computed. Power system simulators using a backward-facing approach answer the question “How must each component perform, assuming the power source met the requested power?” Component by component, this calculation approach carries backwards from the load (sink) to the power source until the electrical energy use that would be necessary to meet the power requested is met. It can happen that the load power request cannot be delivered by the source. This results in non-convergence of the solution causing the simulation to stop or ‘crash’. The weakness of the backward-facing approach comes from the assumption that the power request will be met, which is a valid assumption in the case when the energy source is the grid (normally considered an infinite energy source). Another weakness is the use of efficiency/loss maps (e.g. the inverter efficiency curves), which are obtained from steady-state testing conditions where dynamic effects are not considered. However, the explicit nature of the efficiency/loss calculation allows very simple iteration routines to be used with relatively large steps on the order of 1 second. Thus simulations using backward approach tend to execute quickly. In the **Figure 4-3** below, the arrows show power flowing in the opposite direction to the reality and therefore the current is assigned a negative sign for better interpretation of the simulated results e.g. the inverter DC-side current (I_{dc_inv}).

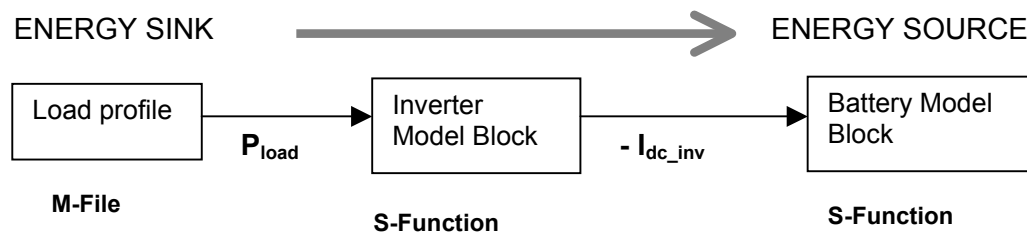


Figure 4-3: Backward-facing calculation in MATLAB/SIMULINK

The two modelling approaches above can be combined to form the forward/backward facing calculation. In the current simulation model, this would represent the effects of component interaction (i.e. power sources/load/inverter/battery). For example, this may be interpreted as battery charge/discharge process or equivalently power generation/consumption process.

Similar modelling approaches have been employed in Electric and Hybrid Electric Vehicle simulators, e.g. the ADVISOR developed by the National Renewable Energy Laboratory, USA, which is a software package also based on MATLAB/SIMULINK used to analyse energy use and emissions in conventional and hybrid electric vehicles [Wipke et al, 1999].

4.4 Simulation models

System-level simulators often use empirical models that are based on measurements supplied by component manufacturers or extracted from measurements obtained from literature sources. These are modelled in Simulink as Look-up tables. Other component models are physical or analytical in nature and are modelled by mathematical functions. Still others may be a hybrid between empirical and physical models and may even include control functions. These can be modelled as system functions (or S-functions). Hence, the Simulink blocks can be Look-up tables, mathematical functions, or S-functions, etc. Some Simulink in-built blocks or libraries are very slow to execute and so when they are used, the simulations run very slowly. The S-functions used in the simulation can be written and compiled using the

Microsoft Visual C++ programming environment, which allows run time improvements.

4.4.1 Alternator model

The vehicle alternator performance curve is modelled as a look-up table [see **Figure 4-4** and **Figure 4-5**] that represents the maximum output current versus alternator speed measured at a constant voltage typically about 28.5V for a 24V alternator. When a room temperature of 25°C is assumed, the DC alternator operating temperature between 80 – 90°C are normal when the vehicle is in cruising speed [Bosch, 2000]. The performance curve can shift with change in alternator operating temperature and/or terminal (battery) voltage but this is ignored in the simulation. The simulation input profile for the alternator model block for a particular scenario in which an omnibus engine [Type: SCANIA diesel engine DS-9] with an operating speed range 1300 – 2200 rpm is driven on a highway for 2.5 hours is as shown in **Figure 4-6**.

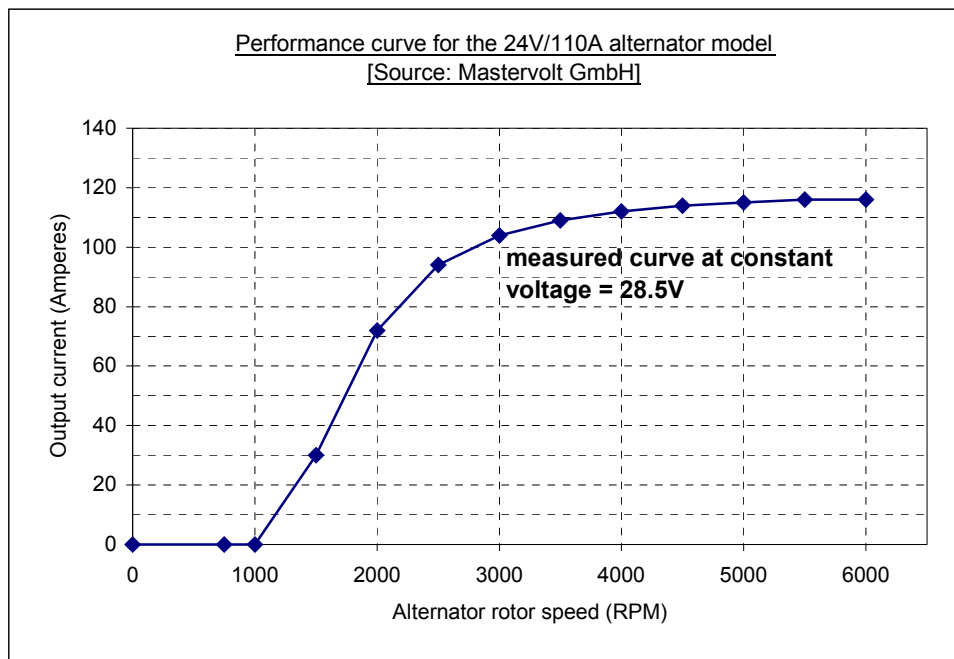


Figure 4-4: DC Alternator performance curve

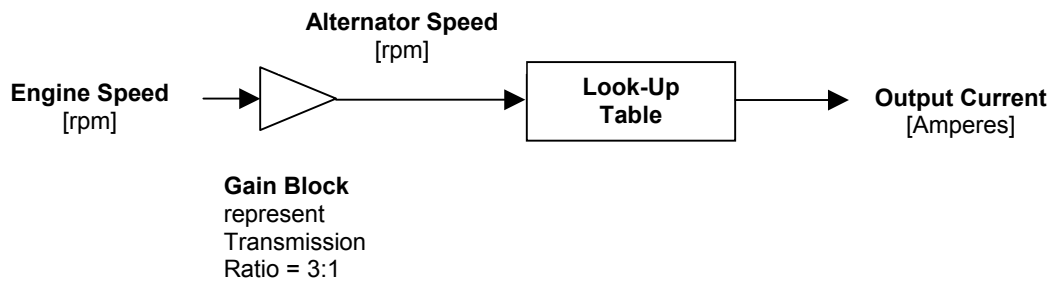


Figure 4-5: Block-diagram of alternator model in Simulink

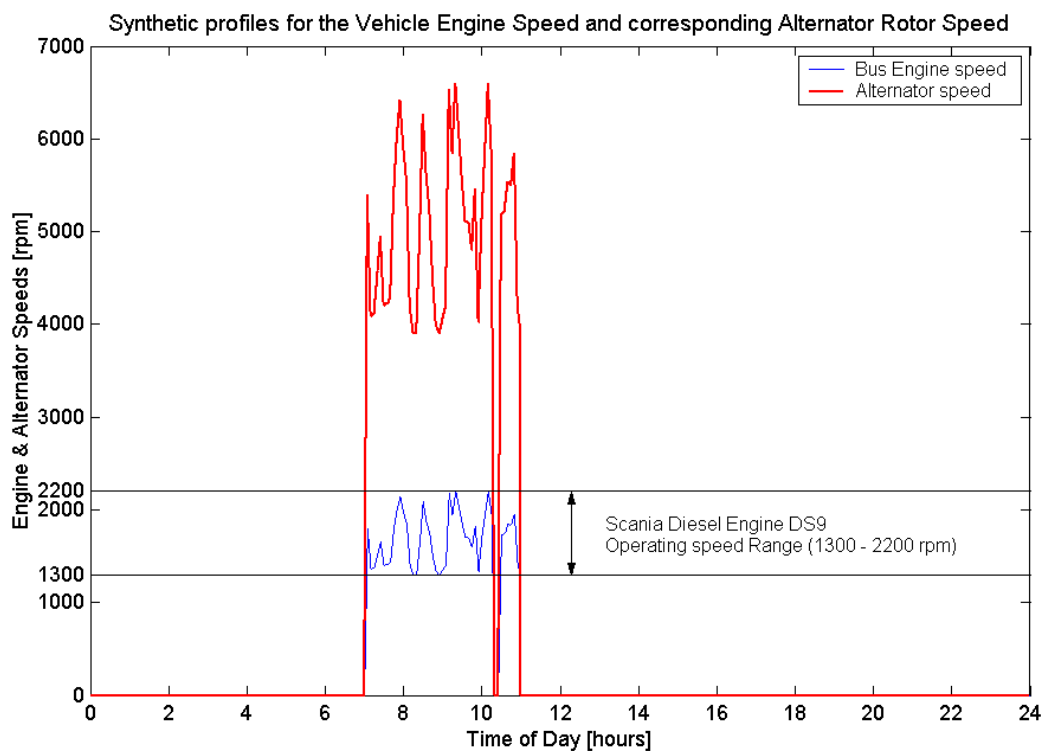


Figure 4-6: Synthetic engine and alternator speed profiles

4.4.2 Diesel DC Genset Model

The variable-speed diesel DC genset performance model is represented in Matlab/Simulink as shown in **Figure 4-7** below. A number of look-up tables are used in the simulation model, for example:

- Electrical machine performance is represented by maximum output electrical power (or current) as a function of rotational speed, that is, I_{out} (or P_{out}) versus Speed
- Automatic engine speed control is represented by engine speed as a function of power demand, that is, Speed versus P_{out}
- Diesel fuel consumption as a function of engine speed and load size

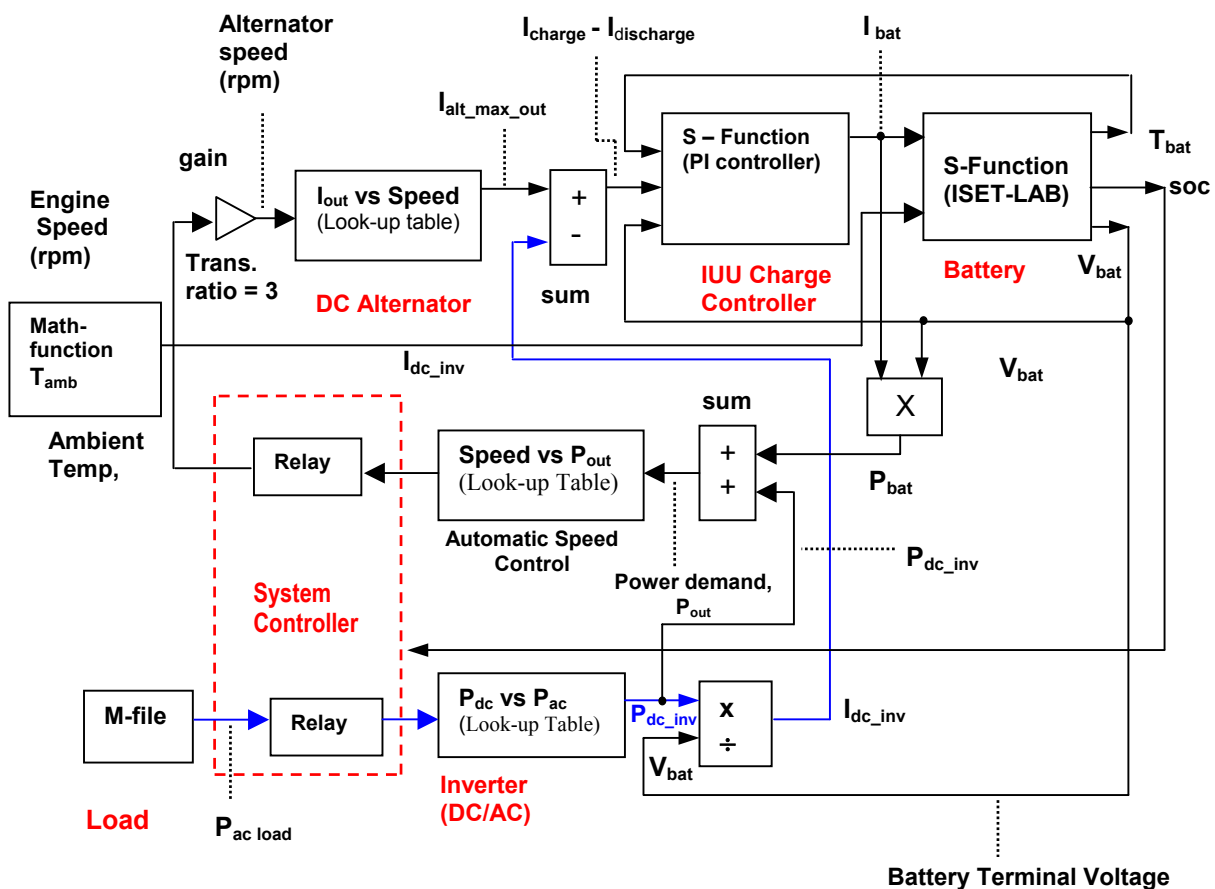


Figure 4-7 : Diesel DC genset performance model in Simulink

Automatic engine speed control

As a practical example, results reported in [Andriulli et al, 2002] and [Tolbert et al, 2001] of an advanced electronic variable-speed genset designed for mobile application and rated at 7.5kW at an altitude of 4000ft (1200m) above sea level, have

been used. It incorporates intelligent engine speed control techniques using a Digital Signal Processor (DSP) controller. An ‘Electrical Power Output as a function of Engine Speed’ map is first obtained empirically by plotting the thermal efficiency contours and then drawing a line through the highest efficiency region referred to as the ‘maximum efficiency line’ (orange line) in **Figure 4-7** below. To handle load transients without stalling the engine or reducing the transient power quality, the optimum operating line may have to trade off some thermal efficiency to allow for excess torque capacity needed for engine acceleration. A small offset is therefore added by increasing the engine speed beyond the maximum efficiency line e.g. by 200 rpm as shown in the figure so as to obtain the ‘operating line’. In this example, however, the value of 200 rpm was chosen intuitively and is therefore not optimised.

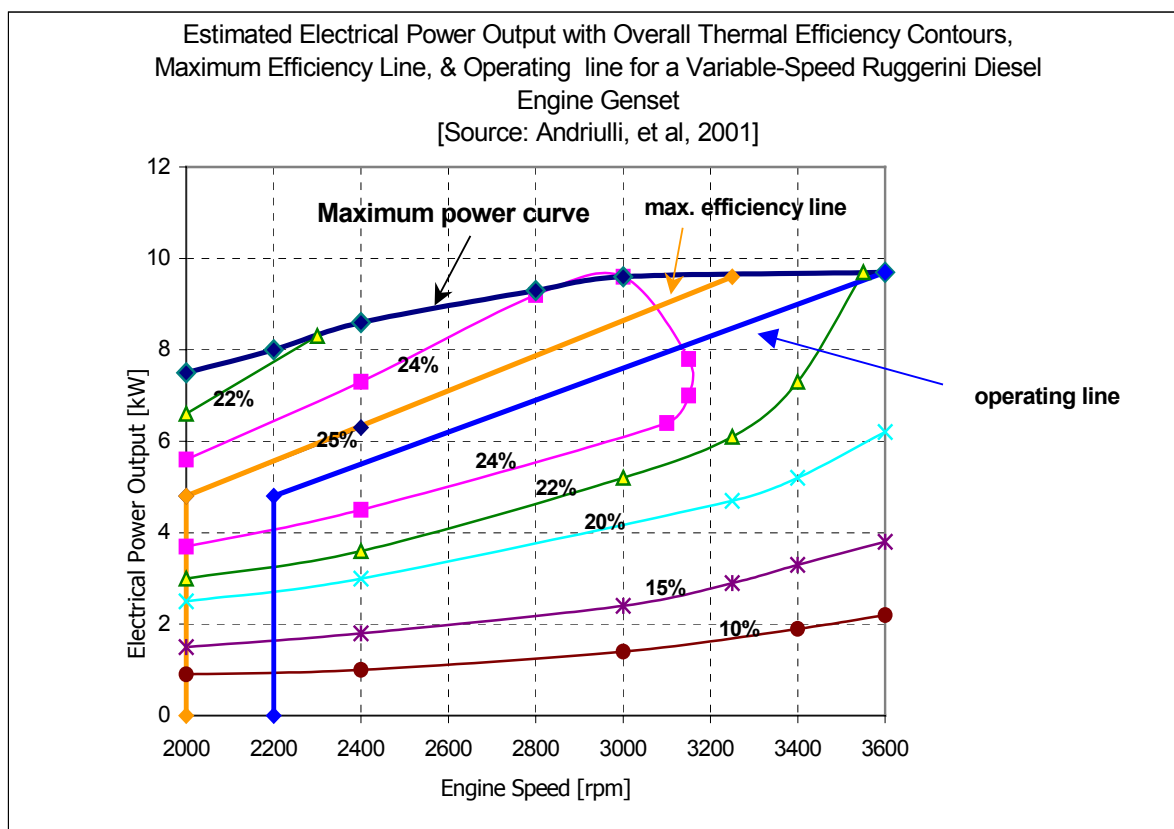


Figure 4-8: Estimated operating line in a variable-speed diesel genset

If the axes of the graph in **Figure 4-8** are switched, we obtain the graph of ‘Engine Speed as a function of Electrical Power Output (or demand)’ [see **Figure 4-9** below]. The associated look-up table is programmed into the DSP controller and is then used

for automatic genset speed control. This is modelled as a Look-up table in Simulink block.

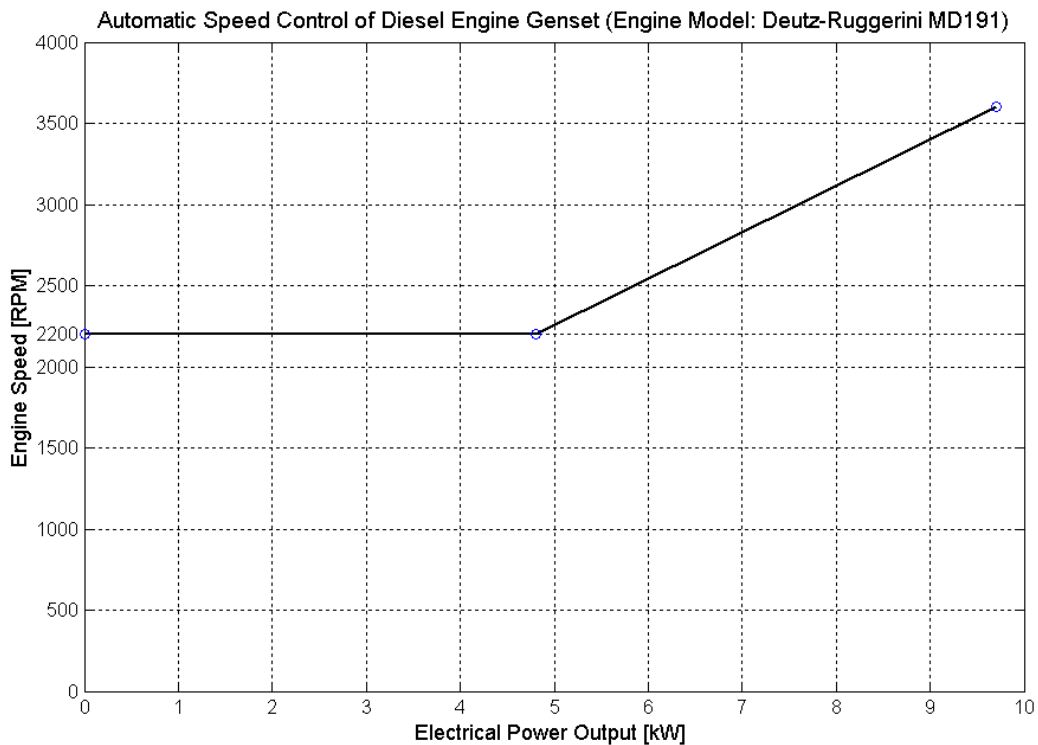


Figure 4-9: Engine speed as a function of output power

Empirical Look-up tables for the Deutz-Ruggerini engine in the reports by Andriulli and Tolbert were used for an AC genset version, but it is assumed here that the same could be used also for a DC genset version assuming the electrical converter losses are the same.

Estimation of diesel fuel consumption

The fuel consumption for a fixed-speed diesel genset may be estimated by using a linearized diesel fuel consumption curve as shown in **Figure 4-10** for a given engine speed, for instance, 3000 rpm.

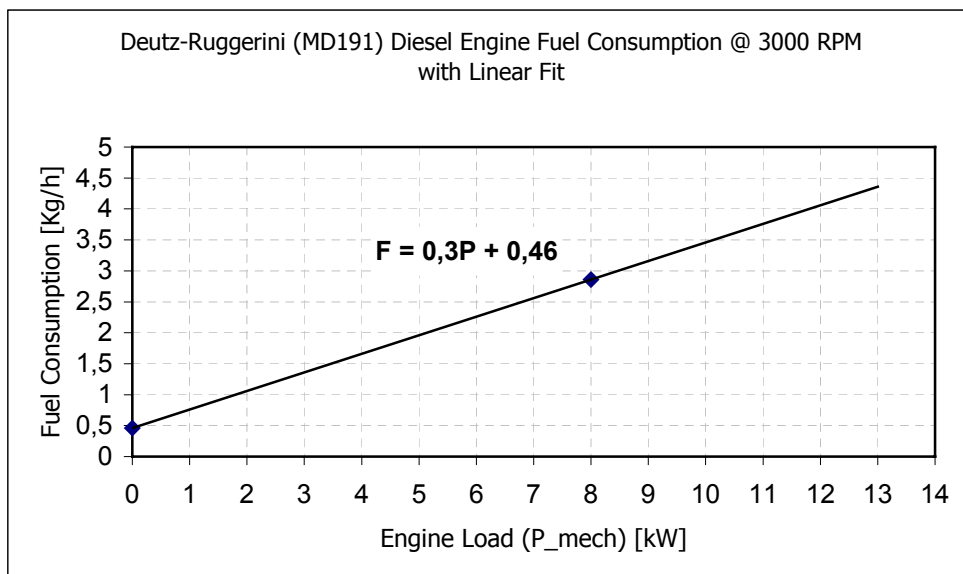


Figure 4-10: Linearized fuel consumption as a function of output power

For a variable-speed operation, the fuel consumption varies with operating speed as well as load size. This is evident from the specific fuel consumption curve with the characteristic U-shape as in **Figure 4-11**. When altitude de-rating is included, the specific fuel consumption curve shifts upwards for altitudes higher than the rated value.

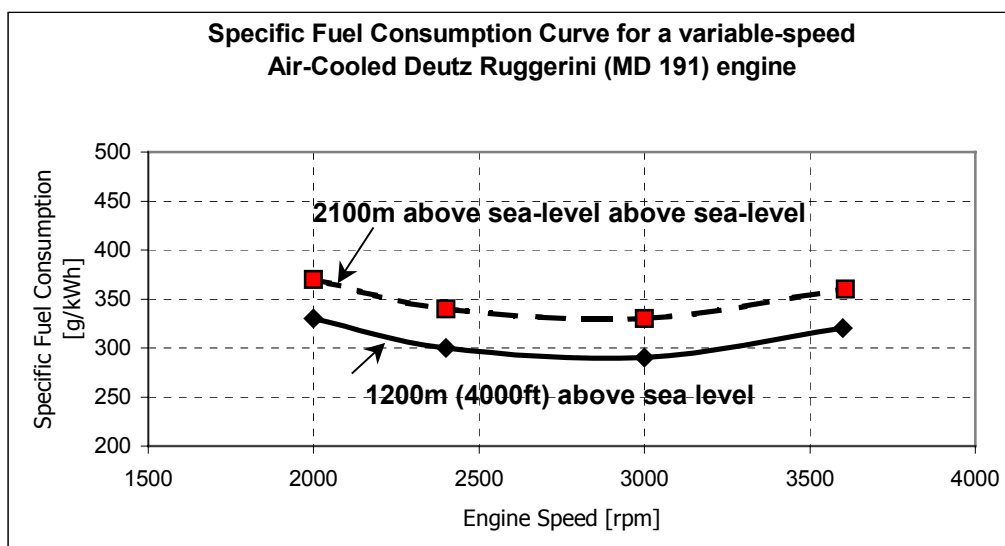


Figure 4-11: Estimated specific fuel consumption curve

4.4.3 Inverter model

Power electronic converters (i.e. inverters, DC/DC converters, and rectifiers) are modelled by their efficiency curves represented by Look-up tables in Simulink. Data from one commercial inverter (Solarix 900RI from Steca/Fronius GmbH) was used [Chapter 8, Appendix B, Table 8-1]. The efficiency curve is shown in **Figure 4-12** below.

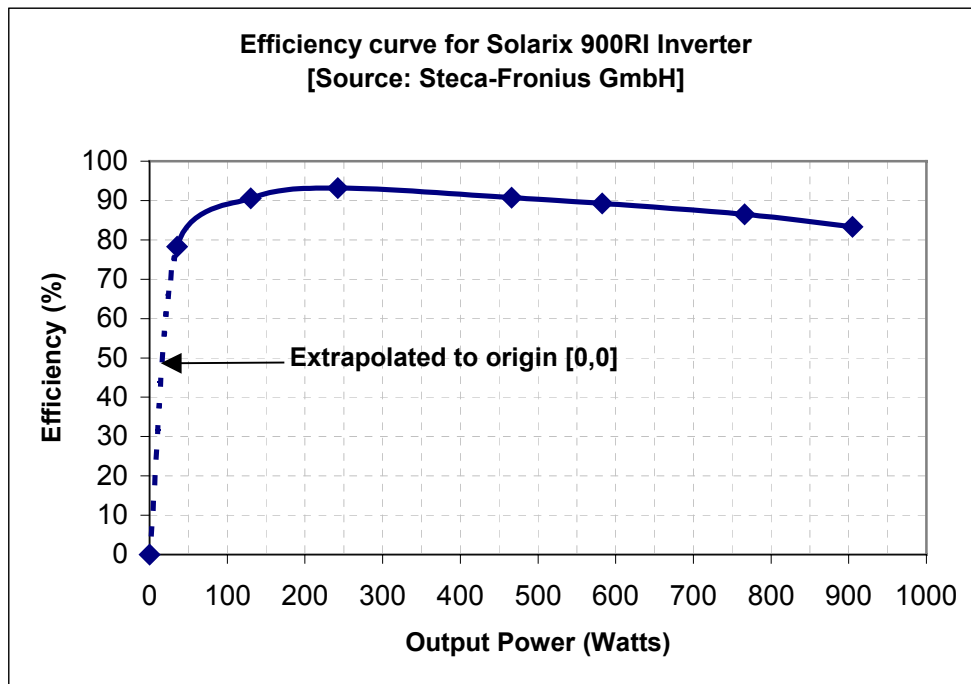


Figure 4-12: 24V/900W Inverter Efficiency Curve

4.4.4 ISET-LAB battery model

An accurate model of the battery is an important precondition for accurate modelling of the power balance of the hybrid system. Various battery models are available in literature with different capabilities to model real operating conditions. They can be broadly classified as those based on (a) equivalent electrical circuits, (b) neural networks, and (c) physical and electrochemical processes.

We used the ISET-LAB battery model developed at the Institut für Solare Energieversorgungstechnik (ISET), which is based on modelling physical and electrochemical processes. The ISET-LAB software model has been used to simulate lead-acid starter batteries and on-board electrical networks by some enterprises in the automotive industry [Caselitz et al, 1998]. This battery model has

the advantage that it needs no measurements for initialisation. The only data required to simulate individual batteries are geometrical dimensions, substance quantities, and porosity values. Some of the necessary information may be readily obtainable from manufacturers facts sheets but others are considered proprietary by the battery manufacturers and are therefore only accessible under very special conditions. The ISET-LAB battery model version used is considered by the model developers to be suitable for modelling flooded or wet lead-acid batteries. The model was programmed as an S-Function in Matlab/Simulink and has two inputs, which are current (with a positive sign for charging and negative sign for discharging) and ambient temperature profile. It has three outputs, which are battery voltage, state-of-charge, and battery temperature [see **Figure 4-13**]. However, the equations for calculating these quantities are considered proprietary by the model developers.

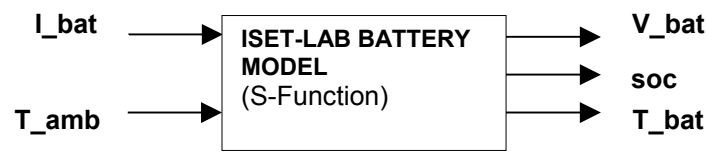


Figure 4-13 : Block diagram for ISET-LAB battery model in Simulink

4.4.5 Charge controller model

Charge controllers influence both the battery management and load management (i.e., load disconnect/reconnect). The functional behaviour of charge controllers, that is, the charging characteristics or algorithms, is modelled using a PI controller block. The high frequency switching behaviour (e.g. for PWM-type charge controllers) is not taken into account. Although, the real system may have a number of controllers with different charging characteristics, we have assumed the same IUU behaviour for all. Further, when more than one controller is present in the system, which more often have different settings (e.g. absorption and float voltages, absorption time setting, etc), some controller settings may contradict the settings of others. As a consequence, some settings are overridden. We avoided this in the simulation model by assuming a single central controller, which obviously differs from the

situation in a real system. The user-interface for the PI-controller based voltage regulator is shown in **Figure 4-14** below.

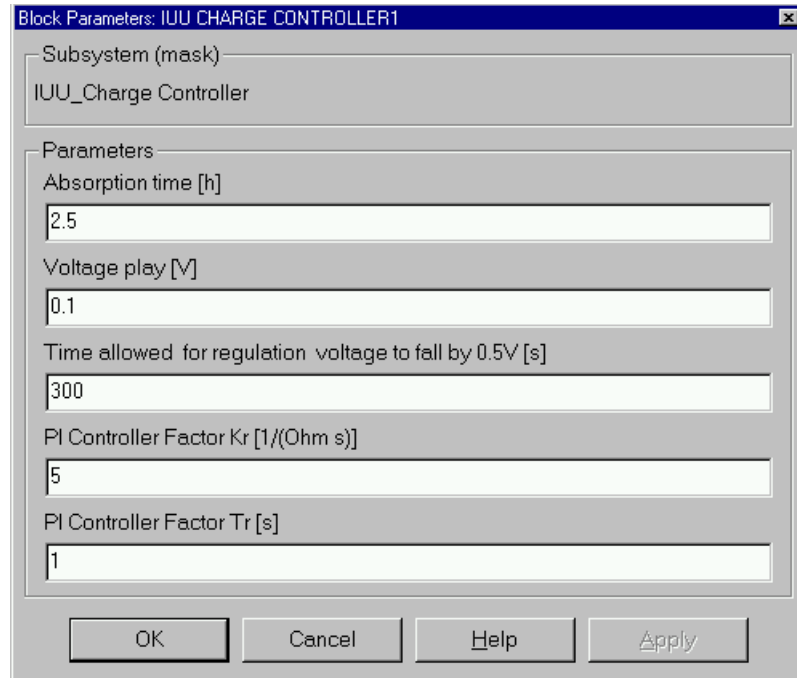


Figure 4-14: User-interface for the 'Alpha' IUU charge controller

4.4.6 System controller model

The system controller is modelled by in-built relay and switch blocks in Simulink. A supervisory controller may be an integral part of the system controller. A user-interface is shown in **Figure 4-15** below.

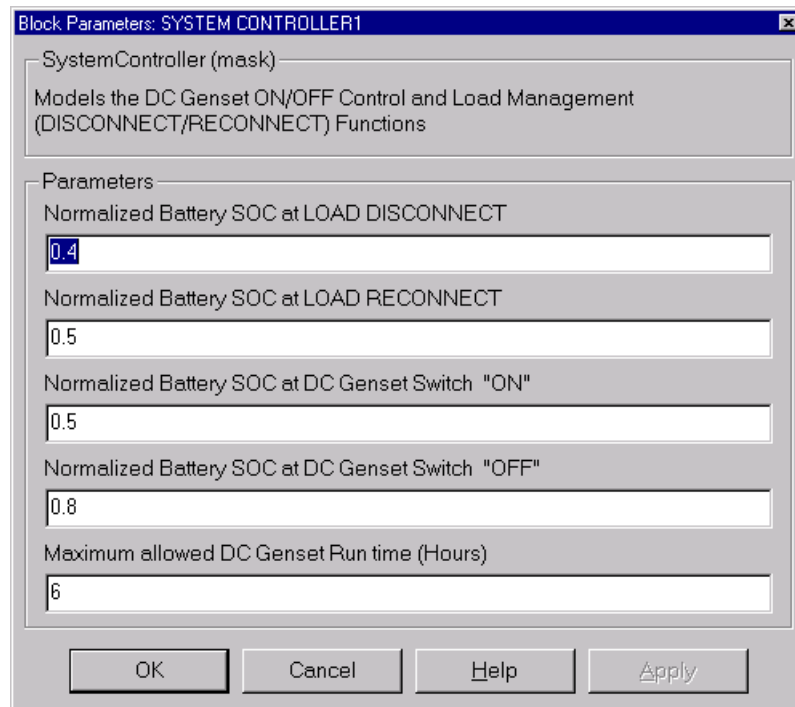


Figure 4-15: System controller user-interface

4.4.7 Photovoltaic (PV) Generator Performance Model

Studies of photovoltaic systems in outdoor conditions require precise knowledge of the details of the system. The goal is to construct a model where the interdependence between the electrical parameters of a PV module and the environmental parameters is established. With the help of the simulation model, the energy output of photovoltaic systems can be predicted in different weather conditions, different climates, and different seasons: the main goal being the characterisation of the PV module from which an estimate of the energy yield can be obtained through simulations.

Mathematical Modelling

The simplest equivalent circuit (also called 'ideal' model) of a solar cell consists of a current source in parallel with a diode. The output of the current source is directly proportional to the light falling on the cell. The diode determines the current-voltage (I-V) characteristics of the cell. Approximation accuracy of the solar cell model can be improved by adding whenever necessary [Walker, 2000]:

- Temperature dependence of the diode saturation current, I_0

- Temperature dependence of the photocurrent, I_{ph}
- Series resistance, R_s , which gives a more accurate shape between the maximum power point and the open circuit voltage, V_{oc}
- Shunt (or parallel) resistance, R_p , in parallel with the diode
- Either allowing the diode quality factor n to become a variable parameter (instead of being fixed at either 1 or 2) in what is referred to as the ‘one-diode’ model, or introducing 2 parallel diodes (one with $n = 1$, the other with $n = 2$) with independent set of saturation currents, I_{01} and I_{02} , respectively, to form the so-called ‘two-diode’ model (a diode quality factor of $n = 1$ represents an ideal diode behaviour). This is illustrated in **Figure 4-16** below.

In the commonly used one-diode model, $n \sim 1.0 - 1.5$ for mono- and multi-crystalline silicon (c-Si and mc-Si), silicon-film cells and cadmium telluride (CdTe) cells, $n \sim 1.5 - 1.8$ for copper-indium-diselenide (CIS), and $n \sim 3.0 - 3.8$ for the multi-junction amorphous cells (2-a-Si and 3-a-Si) [Sandia PV Module Database, available on Sandia National Laboratories website].

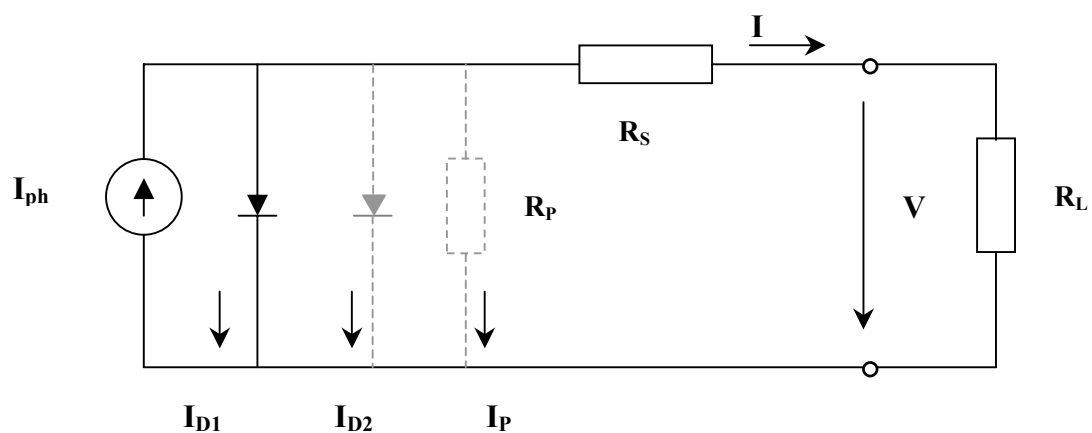


Figure 4-16: Equivalent circuit of a PV generator model

The One-Diode Model

The one-diode model is generally considered adequate for PV system-level design purposes and was therefore chosen for this work. The two-diode model is considered too elaborate for this purpose, because manipulation of its mathematical expressions is quite involving compared to the one-diode model case. Besides, its superior

accuracy is inconsistency with other assumptions made elsewhere in the system simulation model. The relationship between the current I and voltage V of the equivalent circuit in **Figure 4-16** is given below:

$$I = I_{ph} - I_D - I_{sh} = I_{ph} - I_0 \left\{ \exp \left[q \left(\frac{V + IR_s}{nkT_c} \right) \right] - 1 \right\} - \left(\frac{V + IR_s}{R_p} \right) \quad (4.1)$$

Where:

I_{ph} = photo-current

I_D = diode current

I_{sh} = shunt current

I_0 = diode reverse saturation current

I = operating or load current

V = operating voltage

R_s = series resistance

R_p = shunt (or parallel) resistance

k = Boltzmann's constant

n = diode quality factor

T_c = cell temperature

q = electron charge

Normally the shunt resistance, R_p , in most modern cells is very large; thus the last term in equation (4.1) can be neglected, and the expression simplifies to:

$$I = I_{ph} - I_0 \left\{ \exp \left[q \left(\frac{V + IR_s}{nkT_c} \right) \right] - 1 \right\} \quad (4.2)$$

Equation (4.2) has an implicit form and may be solved using numerical (iterative) techniques (e.g. Newton-Raphson method), which are generally more mathematically involved than analytical methods. Use of analytical methods is desirable, but demands that equation (4.2) be rewritten in an explicit form as in equation (4.3) below.

$$V(I) = \frac{nkT_c}{q} \ln \left[\frac{I_{ph} - I}{I_0} + 1 \right] - IR_s \quad (4.3)$$

Where $V(I)$ is the terminal voltage of a cell (or module or array). Generally, this equation can be used to represent an individual cell, a module consisting of several cells, or an array consisting of several modules.

An I-V curve plotted using equation (4.3) has four important points (i.e. characteristic parameters) on it, namely: the short circuit current, open circuit voltage, maximum power current and maximum power voltage conditions [i.e., I_{sc} , V_{oc} , I_{mp} , and V_{mp}]. These four values can be used to generate a curve that accurately represents the module's I-V characteristics at the operating conditions for which these values are given. Rauschenbach [Rauschenbach, 1980] developed a set of equations (4.4 – 4.6) that can be used with the four characteristic parameters to model the I-V characteristic of a module [read from Fitzpatrick, 2001].

$$I = I_{sc} \left\{ 1 - C_1 \left[\exp \left(\frac{V}{C_2 V_{oc}} \right) - 1 \right] \right\} \quad (4.4)$$

Where:

$$C_1 = \left(1 - \frac{I_{mp}}{I_{sc}} \right) \exp \left(- \frac{V_{mp}}{C_2 V_{oc}} \right) \quad (4.5)$$

$$C_2 = \left(\frac{V_{mp}}{V_{oc}} - 1 \right) / \ln \left(1 - \frac{I_{mp}}{I_{sc}} \right) \quad (4.6)$$

These equations can be extended to represent the I-V characteristics for a single module or an array with M modules in parallel and N modules in series. For a single module, M and N is both equal to 1.

$$I_{Array} = I_{sc, Module} \cdot M \cdot \left\{ 1 - C_1 \left[\exp \left(\frac{V_{Array}}{N \cdot C_2 V_{oc, Module}} \right) - 1 \right] \right\} \quad (4.7)$$

Where:

$$C_1 = \left(1 - \frac{I_{mp, Module}}{I_{sc, Module}} \right) \exp \left(- \frac{V_{mp, Module}}{C_2 V_{oc, Module}} \right) \quad (4.8)$$

$$C_2 = \left(\frac{V_{mp, Module}}{V_{oc, Module}} - 1 \right) / \ln \left(1 - \frac{I_{mp, Module}}{I_{sc, Module}} \right) \quad (4.9)$$

Photovoltaic Module and Array performance model for outdoor operating condition

Commercially available PV modules have module label ratings at Standard Reporting Conditions, SRC (also called Standard Testing Conditions, STC) given as $E_0 =$

1000W/m^2 , $T_c = 25^\circ\text{C}$, and $\text{AM} = 1.5$), where E_0 = Reference “1 sun” irradiance in the plane-of-array, (1000W/m^2), T_c = Temperature of cells inside modules, and AM = Air Mass. However, these conditions are rarely encountered in the field, for example, outdoor operating conditions commonly result in cell temperatures closer to 50°C [King, et al, 1997]. The power that a module produces at STC is a useful number for comparing the performance of modules under fixed conditions, but is not particularly helpful in describing how a module will perform under a range of actual conditions [Marion, 1999]. Module manufacturers may also provide label ratings at nominal operating cell temperature (NOCT), where the following meteorological conditions are given as: nominal irradiance, $E_{\text{nom}} = 800\text{W/m}^2$, air mass, $\text{AM} = 1.5$, cell temperature, $T_c = 20^\circ\text{C}$, wind speed, $\text{WS} = 1\text{m/s}$, and no load operation. If the PV generator is connected to load, this is referred to as installed nominal operating cell temperature (INOCT). Additionally, module data sheets may provide I-V curves for a few sets of operating conditions, and module’s voltage and current temperature coefficients (or correction factors).

The Sandia I-V curve Translation Procedure (Sandia Model)

It is known that different PV technologies have different temperature coefficients, irradiance spectral response characteristics, and angle-of-incidence effects that cause their performance to vary with changing conditions [King et al, 1997 / Holley et al, 2000 / Betts et al, 2001 / Gottschalg et al, 2001 / Jardine et al, 2002]. A method has been developed by Sandia National Laboratories (hereafter referred to simply as the ‘Sandia model’) to predict module output under all operating conditions [King et al, 1997], also called I-V curve translation procedure. The Sandia model compensates for the influences of irradiance, temperature, air mass, and angle-of-incidence on module performance. A fundamental premise of this performance model is that the I_{mp} , V_{oc} , and V_{mp} of a PV module can be described as functions of I_{sc} and the cell temperature T_c . In this method, the PV array or module performance for an arbitrary operating condition can be described by equations (4.10 – 4.15). The variables defining the operating condition are solar irradiance (effect of intensity and spectrum separately considered), cell temperature, absolute air mass (related to irradiance spectrum), and solar angle-of-incidence on the array. King et al have also determined that four separate temperature coefficients for the four characteristic

parameters $[I_{sc}, I_{mp}, V_{oc}, V_{mp}]$ are necessary to accurately model the effect of temperature on module I-V characteristic [King et al, 1998]. In the common practice, only two temperature coefficients for I_{sc} , and V_{oc} are indicated in the manufacturer's performance data sheets. Given a set of STC label ratings, operation at another set of operating conditions can be predicted by means I-V curve translation equations. The equations that represent the latest implementation of the Sandia model as reported in [Davis et al, 2002] are given in **Appendix D**.

In this work, we have assumed that the PV generator technology to be employed is the mono-crystalline silicon [e.g., Siemens SM55]. The effects of solar spectrum and angle-of-incidence are not very significant and may be ignored. The Sandia model equations therefore simplifies to the following:

$$I_{sc}(E_e, T_c) = I_{sc0} \cdot E_e \cdot [1 + \bar{\alpha}_{I_{sc}} \cdot (T_c - T_0)] \quad (4.10)$$

$$E_e = \frac{E}{E_0} = \frac{I_{sc}}{I_{sc0} \cdot [1 + \bar{\alpha}_{I_{sc}} \cdot (T_c - T_0)]} \quad (4.11)$$

$$I_{mp}(E_e, T_c) = I_{mp0} \cdot (C_0 E_e + C_1 \cdot E_e^2) \cdot [1 + \bar{\alpha}_{I_{mp}} \cdot (T_c - T_0)] \quad (4.12)$$

For the selected mono-crystalline silicon PV module [Siemens SM55], the following coefficients are given in a database compiled by Sandia National Laboratories: $C_0 = 1.02 \approx 1.0$ and $C_1 = -0.02 \approx 0.0$. Hence equation (4.12) may be simplified to,

$$I_{mp}(E_e, T_c) = I_{mp0} \cdot E_e \cdot [1 + \bar{\alpha}_{I_{mp}} \cdot (T_c - T_0)] \quad (4.12)$$

$$\delta(T_c) = \frac{n \cdot k \cdot (T_c + 273.15)}{q} \quad (4.13)$$

$$V_{oc}(E_e, T_c) = V_{oc0} \cdot [1 + \bar{\beta}_{V_{oc}} \cdot (T_c - T_0)] + N_s \cdot \delta(T_c) \cdot \ln(E_e) \quad (4.14)$$

$$V_{mp}(E_e, T_c) = V_{mp0} \cdot [1 + \bar{\beta}_{V_{mp}} \cdot (T_c - T_0)] + C_2 \cdot N_s \cdot \delta(T_c) \cdot \ln(E_e) + C_3 \cdot N_s \cdot \{\delta(T_c) \cdot \ln(E_e)\}^2 \quad (4.15)$$

Where:

$E = E_{POA}$ = Plane-of-array (POA) solar irradiance using broadband pyranometer measurement corrected for angle-of-incidence sensitivity, $[W/m^2]$

E_0 = Reference "1 sun" irradiance in the plane-of-array, $[1000W/m^2]$

E_e = "Effective" irradiance, [dimensionless, or "suns"]

E_{beam} = beam irradiance, $[W/m^2]$

E_{diff} = diffuse irradiance, $[W/m^2]$

I_{sc} = short-circuit current, [A]

$I_{sc0} = I_{sc} (E_e = 1, T_c = T_0)$, e.g. at STC [$E = 1000 \text{ W/m}^2$, $T_c = T_0 = 25^\circ\text{C}$ (or 50°C), $AM_a = 1.5$, and $AOI = 0^\circ$]

I_{mp} = maximum power current, [A]

$I_{mp0} = I_{mp} (E_e = 1, T_c = T_0)$, i.e. at STC

V_{oc} = open-circuit voltage, [V]

$V_{oc0} = V_{oc} (E_e = 1, T_c = T_0)$ at STC

V_{mp} = maximum power voltage, [V]

$V_{mp0} = V_{mp} (E_e = 1, T_c = T_0)$ at STC

T_c = Temperature of cells inside modules

T_0 = Reference temperature of cells inside modules, e.g., 25 or 50°C

$\bar{\alpha}_{I_{sc}}$ = short-circuit temperature coefficient normalized with respect to I_{sc0} , $1/^\circ\text{C}$

$\bar{\alpha}_{I_{mp}}$ = maximum-power temperature coefficient normalized with respect to I_{mp0} , $1/^\circ\text{C}$

$\bar{\beta}_{V_{oc}}$ = open-circuit temperature coefficient normalized with respect to V_{oc} , $1/^\circ\text{C}$

$\bar{\beta}_{V_{mp}}$ = maximum-power temperature coefficient normalized with respect to V_{mp} , $1/^\circ\text{C}$

$\delta(T_c)$ = "thermal voltage" as a function of temperature

C_0, C_1 = Empirically determined coefficients relating I_{mp} to irradiance

C_2, C_3 = Empirically determined coefficient relating V_{mp} to irradiance

N_s = number of cells in series in the module

N = empirical diode factor

k = Boltzmann's constant, $1.380 \times 10^{-23} [\text{J/K}\cdot\text{mol}]$

REMARK: The temperature coefficients have been normalized to $1/^\circ\text{C}$ by dividing by the value of the parameter at SRC. This simplifies the application of these coefficients to arrays of modules.

Estimating PV cell and module temperature

Cell temperature and solar irradiance determine a PV module's operational curve, and the coupling of PV modules and system components determines where a system will operate on the PV operational curve. Cell temperature is however not a directly

measurable quantity. In the Sandia model, a simple empirical model is used to estimate the module operating temperature from environmental parameters (ambient temperature, wind speed, and plane-of-array irradiance) and it is claimed to provide an accuracy of ($\pm 5^\circ\text{C}$) of module back surface temperature for typical flat-plate modules, near thermal equilibrium, mounted on in an open rack structure [King et al, 1997]. The Sandia developers have provided empirical coefficients (a and b), **Table 4.1**, for three typical module construction and application scenarios: glass-cell-tedlar module in open rack, glass-cell-glass module mounted flat on a roof, and a glass-cell-glass in an open rack.

$$T_m = T_a + E_{\text{POA}} \cdot \exp(a + b \cdot \text{WS}) \quad (4.18)$$

$$T_c = T_m + \frac{E_{\text{POA}}}{E_0} \cdot \Delta T \quad (4.19)$$

Where:

T_m = back-surface module temperature, $^\circ\text{C}$

T_a = ambient temperature, $^\circ\text{C}$

E = solar irradiance on module, W/m^2

E_0 = reference irradiance, $1000 \text{ W}/\text{m}^2$

WS = wind speed measured at standard 10m height, m/s

ΔT = temperature difference between back surface and the cell

a, b = empirical coefficients related to wind speed

Table 4-1 Empirical parameters for modelling PV cell temperature

Module Type	Mount	a	b	ΔT
Glass/Cell/Glass	Open Rack	-3.47	-0.059	2
Glass/Cell/Glass	Close Roof Mount	-2.98	-0.047	3
Glass/Cell/Tedlar	Open Rack	-3.56	-0.075	3

Remarks on Sandia Model

The Sandia Model is empirical in nature, and it requires a number of parameters that are not provided by manufacturers. Temperature coefficients for V_{mp} and I_{mp} , polynomial coefficients related to the effect of air mass and incident angles, empirical coefficients for the estimation of PV cell temperature, and an empirical diode quality factor are less-common parameters that a system designer or analyst would need. However, the model developers have provided these values in a large database of parameters for some popular commercially available PV modules (114 different

brands with the following technologies; c-Si, mc-Si, EFG mc-Si, Si-Film, 2-a-Si, 3-a-Si, CdTe, and CIS) which can be used for daily, monthly, or annual energy prediction of PV modules and arrays, needed for PV system design, performance analysis, and monitoring. However, for this work, the Sandia model was found to be cumbersome to use in practice because of the large number of empirical parameters needed for simulation initialisation.

A module or array I-V curve can be modelled at some desired cell temperature and irradiance by first determining the characteristic parameters [I_{sc} , I_{mp} , V_{oc} , V_{mp}] at the desired conditions using equations (4.10 – 4.15) and then calculating the modelled curve values using equations (4.7 – 4.9). **Figures 4-17 to 4-20** show the simulated (or predicted) PV array temperature and IV characteristics. The PV model user-interface is shown in **Figure 4-21**.

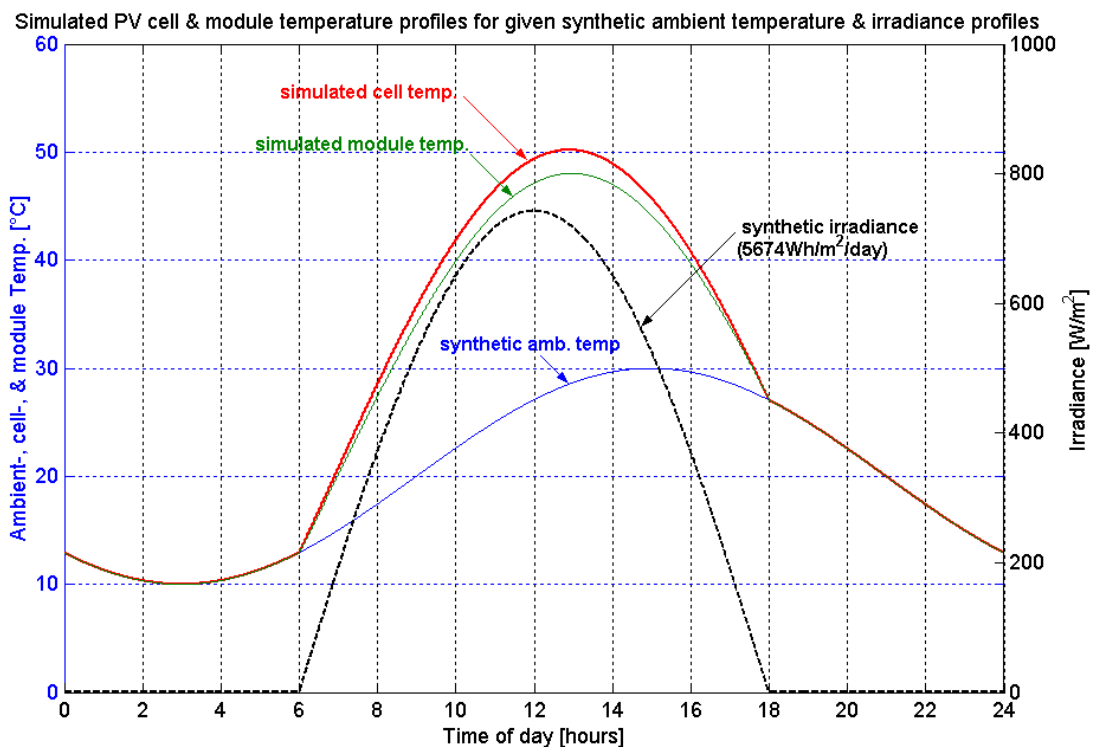


Figure 4-17: Simulated PV cell temperature

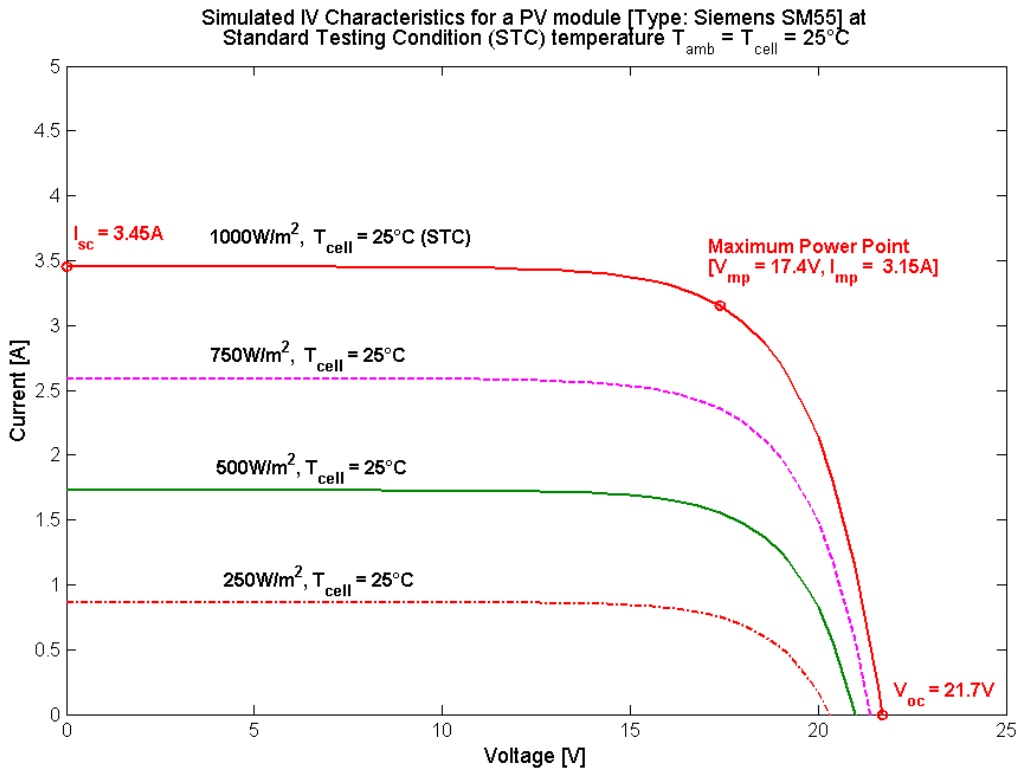


Figure 4-18: Simulated IV characteristics for the PV array at STC temperature (25°C)

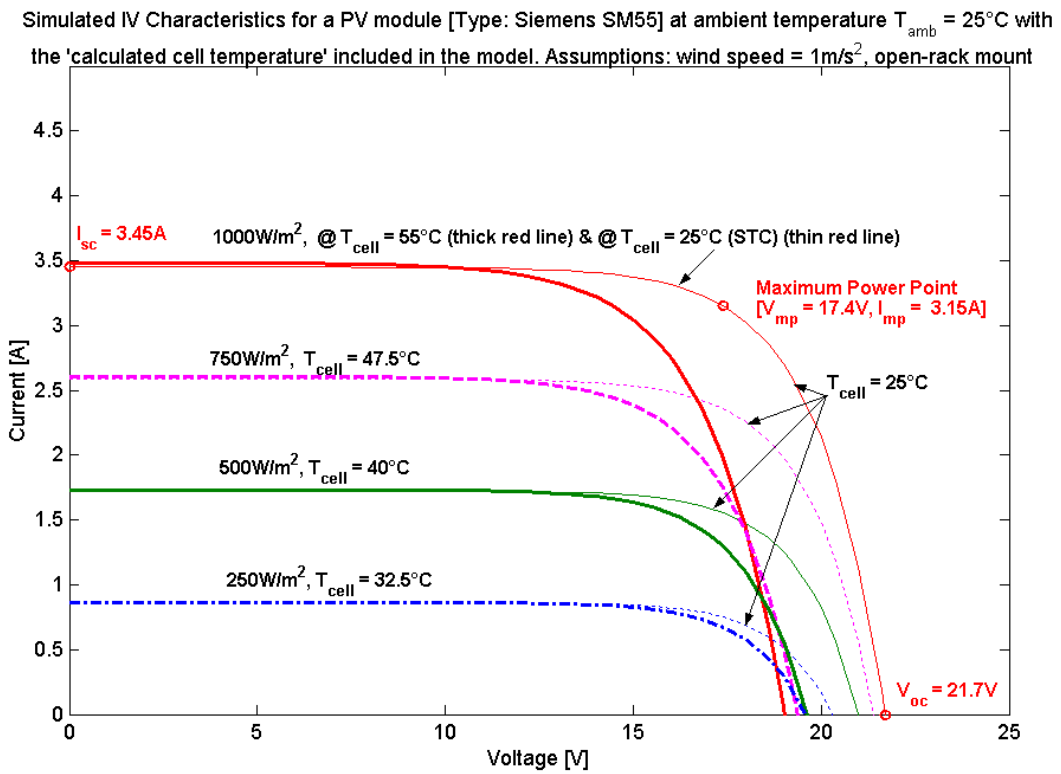


Figure 4-19: Simulated IV characteristics using calculated cell temperature

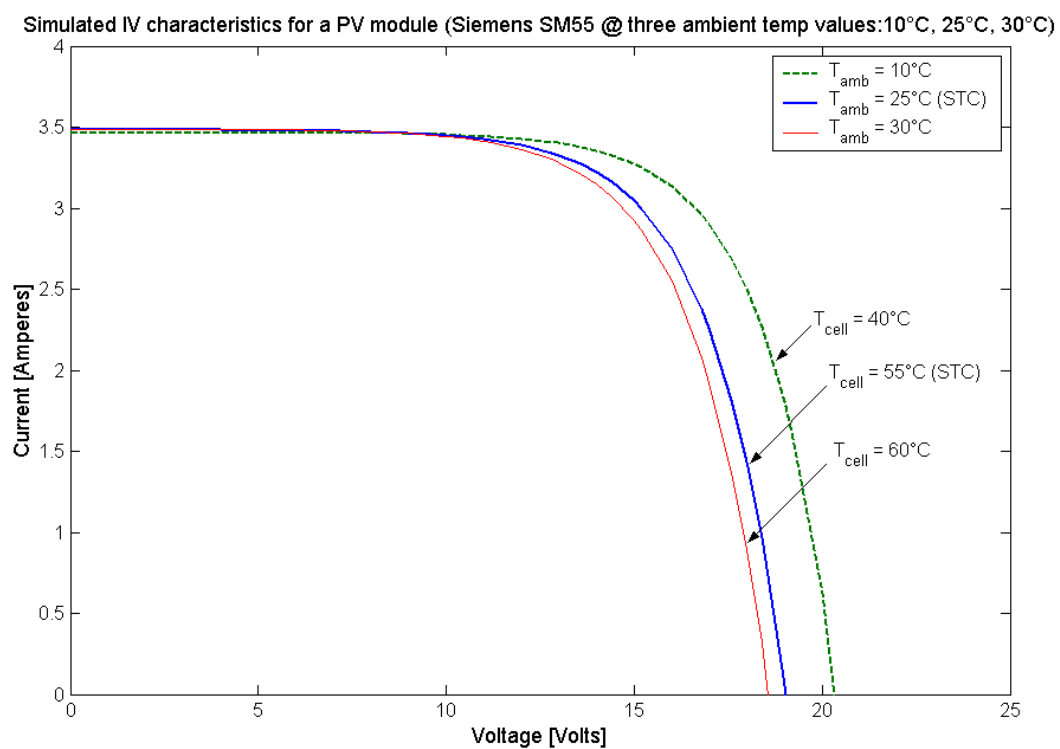


Figure 4-20: Simulated IV characteristics for different ambient temperatures

Block Parameters: PV MODULE

Subsystem (mask)

Parameters

No. of modules in series
2

No. of modules in parallel
5

Reference temperature at STC condition [°C]
25

Short circuit current (I_{sc}) at STC [A]
3.45

Open circuit voltage (V_{oc}) at STC [V]
21.7

Maximum power current (I_{mp}) [A]
3.15

Maximum power voltage (V_{mp}) at STC [V]
17.4

Normalized I_{sc} temperature coefficient [1/°C]
0.00032

Normalized I_{mp} temperature coefficient [1/°C]
-0.00031

Normalized V_{oc} temperature coefficient [1/°C]
-0.0041

Normalized V_{mp} temperature coefficient [1/°C]
-0.0053

OK Cancel Help Apply

Figure 4-21: User-interface for the PV array model

5 SIMULATION RESULTS AND DISCUSSIONS

The main results are presented in the form of dynamic simulations of power flow, battery current, battery voltage, battery state-of-charge (SOC), and battery temperature. These plots are used to visualize and analyse diesel genset management, load management, and battery management.

There are a number of possible scenarios depending on the vehicle speed profile, total distance travelled, the solar irradiance profile, and the load profile. Therefore, no single set of conditions can represent the operation of the system. In this regard, only some selected scenarios are considered in the simulation. Synthetic (fictitious) simulation input profiles are employed; examples of which are shown in **Figure 5-1**.

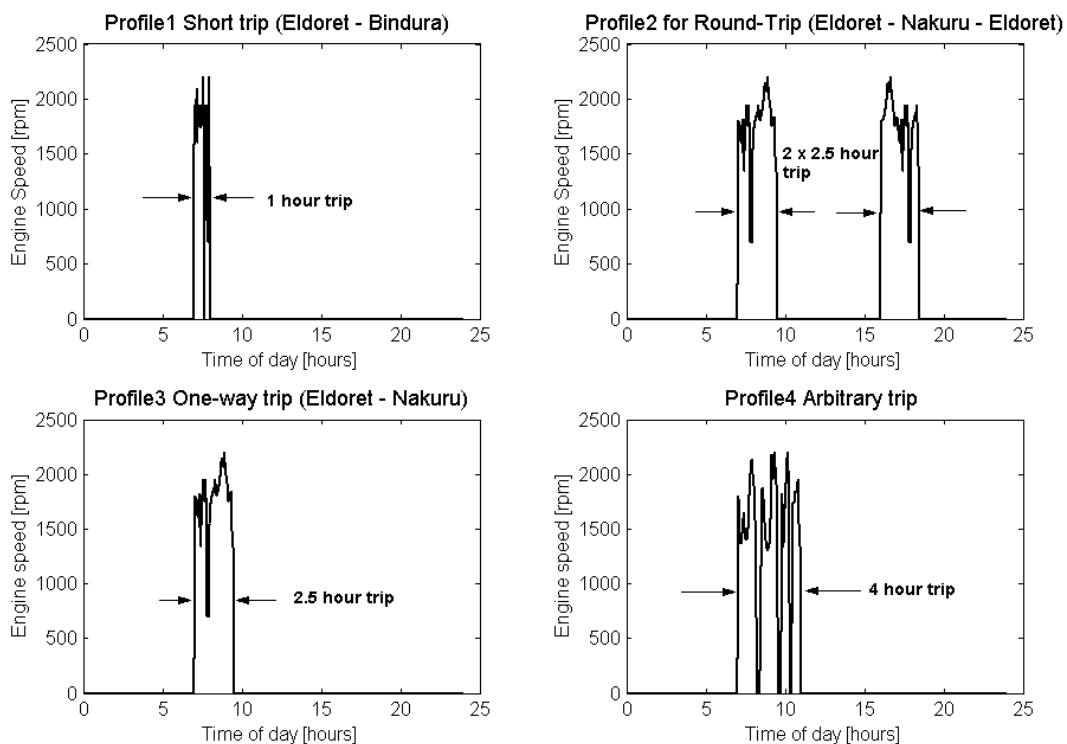


Figure 5-1: Synthetic engine speed profiles

A solar irradiance for worst-case monthly mean daily for Eldoret in the year 1997 was $5674 \text{Wh/m}^2/\text{day}$ as modelled by Heliosat II method [Rigollier, et al, 2001]. We can regenerate an irradiance profile having a half-sine wave form when the monthly

mean daily irradiation is known. Mathematically this is equal to the area under the curve formed by the function: $f(x) = -A \cdot \cos\left(\frac{\pi}{12} t\right)$ between the limits 6.00 and 18.00 hrs.

By integrating the function within the given limits, we can solve for the amplitude, A.

$$\int_6^{18} -A \cos\left(\frac{\pi}{12} t\right) dt = E_d, \quad (5.1)$$

where A is the amplitude, and E_d the daily irradiation in $Wh/m^2/day$. This works out as follows,

$$-A \cdot \frac{12}{\pi} \cdot \sin\left(\frac{\pi}{12} t\right) \Big|_6^{18} = E_d \quad (5.2)$$

$$-A \cdot \frac{12}{\pi} \sin\left(\frac{\pi}{12} \cdot 18 - \frac{\pi}{12} \cdot 6\right) = E_d \quad (5.3)$$

$$-A \cdot \frac{12}{\pi} \left[\sin\left(\frac{3\pi}{2}\right) - \sin\left(\frac{\pi}{2}\right) \right] = E_d \quad (5.4)$$

$$-A \cdot \frac{12}{\pi} (-1 - 1) = E_d \quad (5.5)$$

therefore $A = \frac{\pi}{24} E_d$, and hence the daily irradiation may be expressed as:

$$\int_6^{18} -\frac{\pi}{24} \cdot E_d \cdot \cos\left(\frac{\pi}{12} t\right) dt \quad (5.6)$$

This is shown graphically in **Figure 5-2** below.

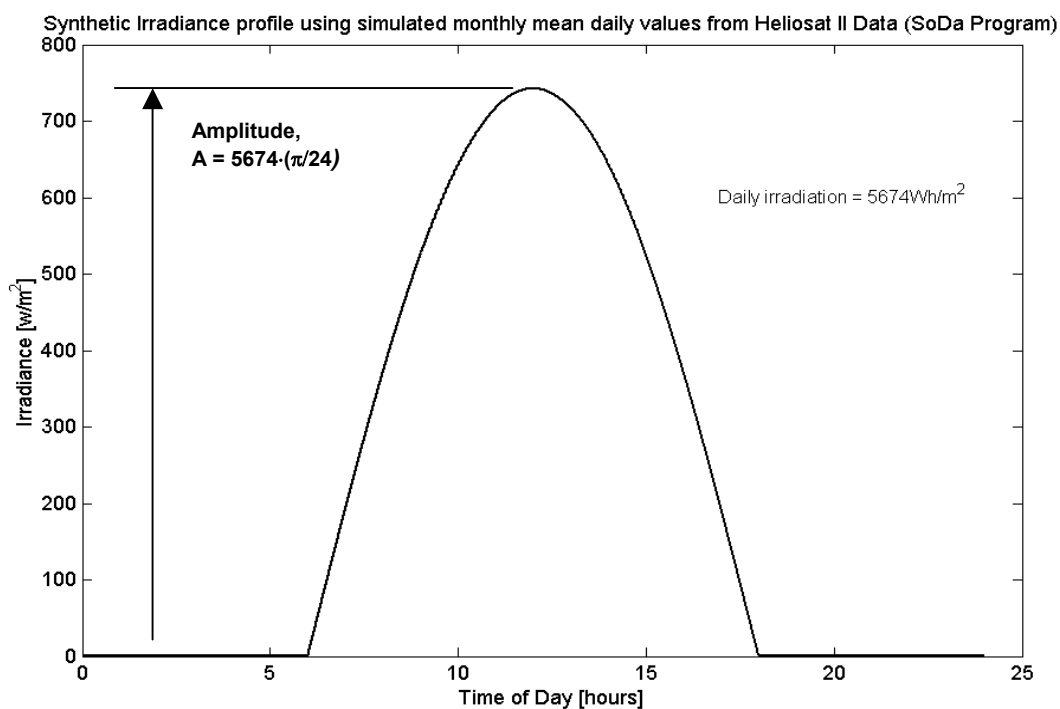


Figure 5-2: Synthetic monthly mean daily irradiance profile

5.1 Power flow simulations

Scenario 1

A scenario is considered, whereby the bus makes a round-trip between Eldoret and Nakuru towns which are 150km apart (referred to as 'Profile2' in **Figure 5-1** and redrawn for clarity in **Figure 5-4**). During the period between the trips, a medical operation is conducted. The return trip should hopefully replace the energy consumed during the operation. We have set the minimum allowable battery SOC to 0.4 for all cases. This is also taken as the initial battery status. In **Scenario 1**, we assumed an operation without a genset (in the simulation model this is accomplished by setting the allowed genset run time to 'zero'). We wish to investigate the power flow of the system, from which we determine whether the load is satisfied or there are periods of loss of load. A PV generator of 550W_p and a battery bank of 550Ah are assumed. The load profile is as shown earlier in **Figure 3-3**. In the first instance, the refrigerator is assumed to operate at 100% duty cycle.

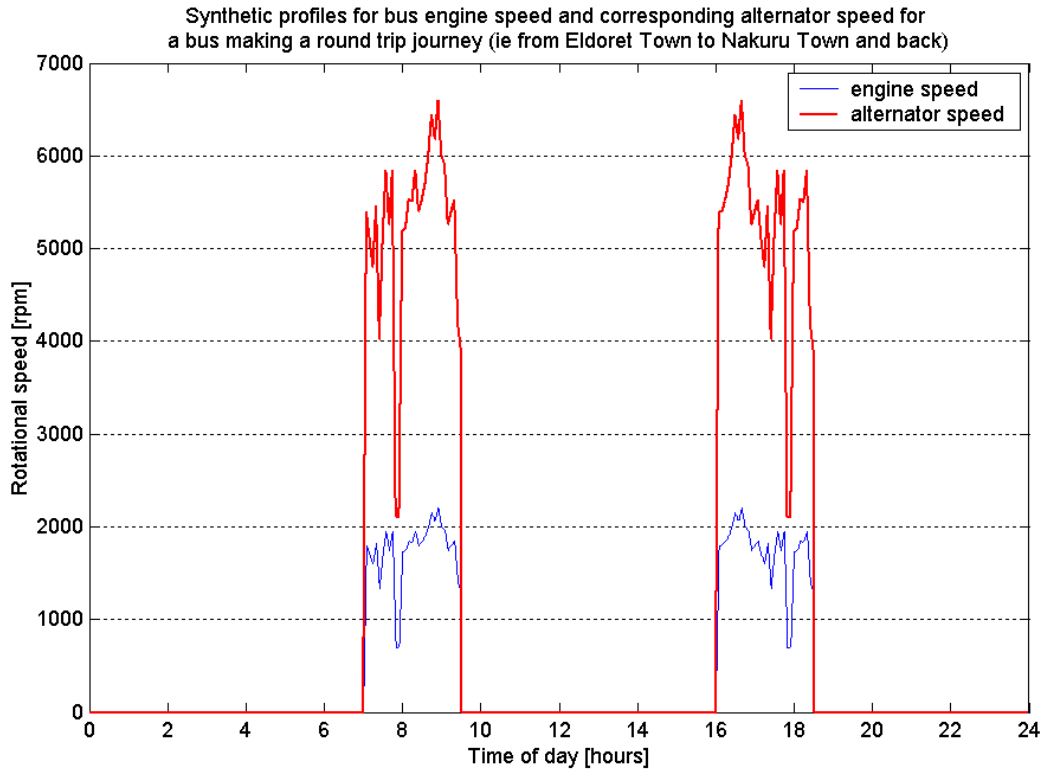


Figure 5-3: Speed profiles for round trip between Eldoret and Nakuru

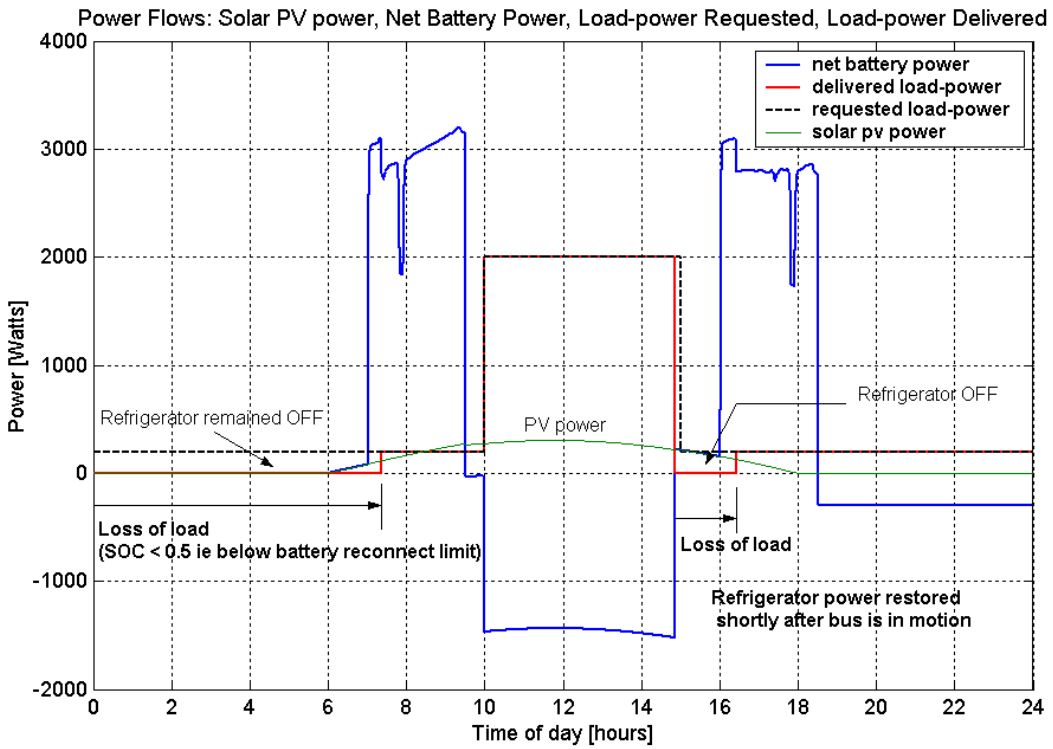


Figure 5-4 : Power flow simulation for operation without genset

Analysis of the power flow in **Figure 5-5** shows that the refrigerator was OFF between midnight and around 7.30 in the morning and again later in the afternoon between 15.00 and 16.30. However, the system was almost able to satisfy the load demand for the remainder of the day. Power availability, therefore cannot be assured unless the DC genset is started, and this may be critical when vaccines are involved.

Scenario 2

In **Scenario 2**, we consider a bus taking a single trip of the same distance as in **Scenario 1** to the site of the medical operation and not travelling back the same day. The PV generator, the battery bank size, and the initial SOC are as in **Scenario 1** (i.e. unchanged). However, a DC genset is now included.

The genset run time is found to be 6 hours with a corresponding diesel fuel consumption of 10.92Kg (~11.0Kg) as shown in **Figure 5-6**.

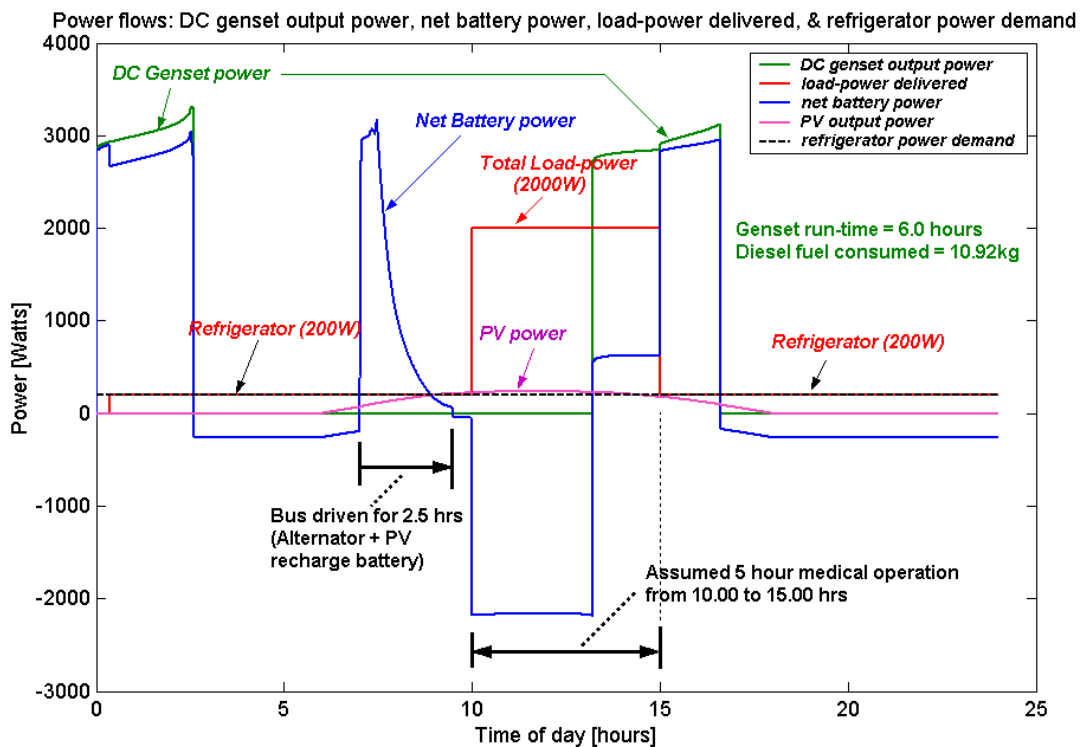


Figure 5-5: Power flow simulation for operation with genset

Effect of doubling the PV array size

When the PV generator size is increased to 1100 Watt, that is, doubled, the genset run time drops from 6.0 to 5.1 hours and correspondingly the fuel consumption drops from 10.92 to 9.44Kg. This is a fuel saving of about 1.5Kg (or 14%) as shown in **Figure 5-7** below. This does not seem to be a very significant improvement in performance. Therefore, if other component dimensions remain unchanged, it may not be economically worthy to increase the PV array size by a factor as large as 2. There is poor utilization of the 1100W array when the battery is almost fully charged (SOC ≥ 0.8) and the loads are not drawing much power. An increase in PV array size should be accompanied by an increase in battery size if energy generation and consumption do not coincide in order to avoid this. However, as mentioned earlier in section 3.3.2, the battery has weight limits in a mobile application.

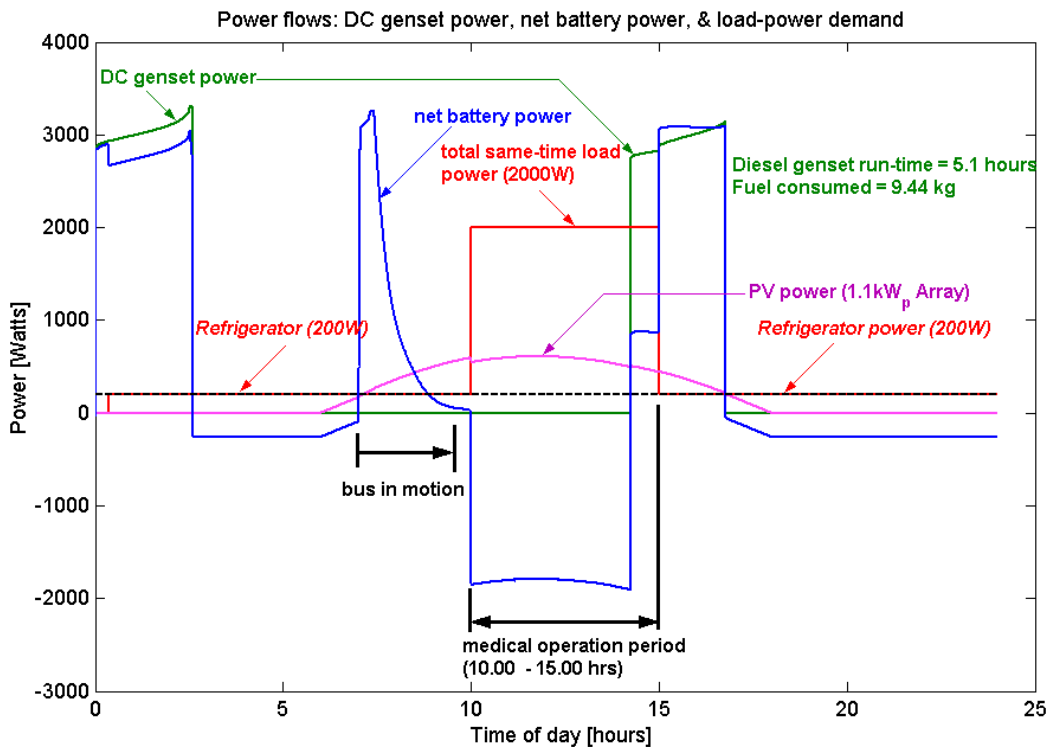


Figure 5-6: Power flow simulation for system with larger array size

Scenario 3

In the above scenarios the refrigerator duty cycle was taken as 100%. The duty cycle normally varies with the interior chamber temperature. However, the dynamic temperature changes in the chamber which govern to the compressor motor ON/OFF operation have not been modelled. If we assume a constant 50% duty cycle, the situation is as shown in **Figure 5-8** below. The diesel fuel consumption, which was 9.4Kg for the 100% duty cycle is now 7.4Kg (or 21% less). The effect of frequently opening the refrigerator door is ignored.

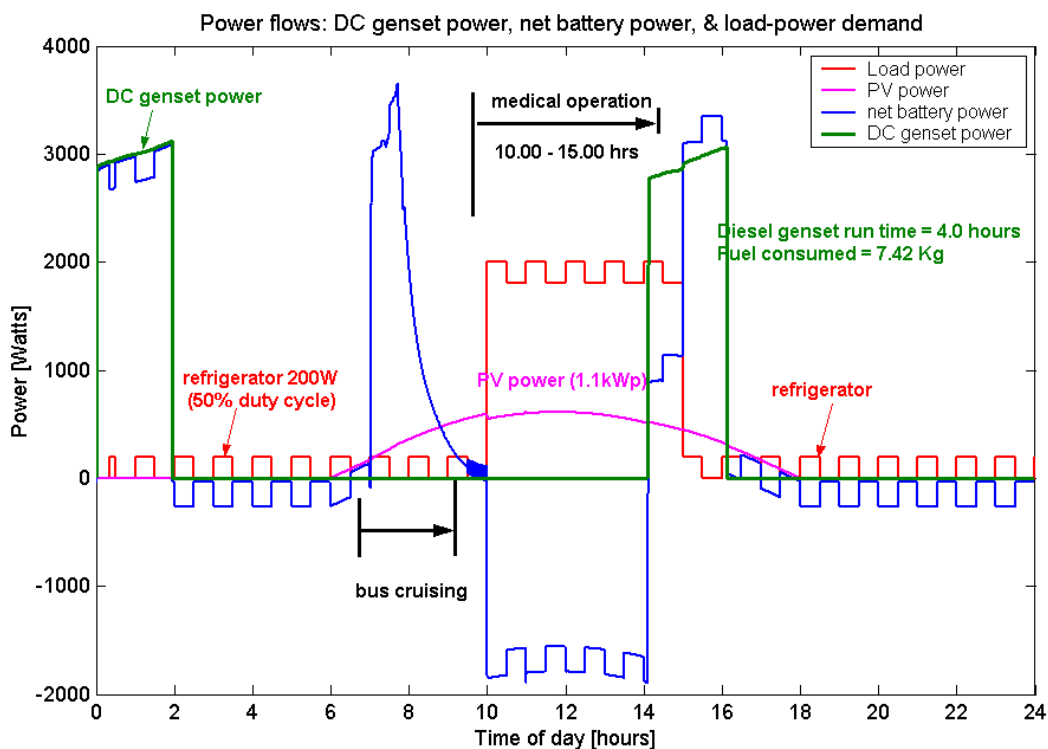


Figure 5-7: Power flow simulation for 50% duty cycle operation of refrigerator

5.2 Diesel and Load management

Visualization of diesel and load management is best done by means of battery SOC and power flow plots obtained by simulation.

5.2.1 Control set-points

An important factor in the diesel genset and load management is the selection of control set-points. Battery SOC is used as parameter for the ON/OFF control of genset and the disconnection/reconnection of the load. Here, it is assumed that the controllers have the means of estimating the SOC. The control set points for the load disconnection and reconnection are chosen as $SOC \leq 0.4$ and $SOC \geq 0.5$, respectively. The hysteresis is introduced in practice to avoid the chattering of the relays (i.e., rapid turning ON and OFF).

From a number of literature sources on the use of diesel gensets for lead-acid battery charging, it is claimed that the genset is economically utilized by turning it ON when SOC falls below 0.5 and OFF when the battery attains SOC somewhere between 0.8 and 0.9 [Barley, 1996]. We wish to investigate through simulation the influence of diesel genset the control set-point at turn OFF on the fuel consumption. Also the number of genset start-ups is of particular interest.

For the $SOC = 0.8$ setting, the simulated DC Genset run-time is 5 hours with a corresponding diesel fuel consumption of 9.08Kg, whereas for the $SOC = 0.9$ setting, the genset run-time is 6 hours with a diesel fuel consumption of 10.92Kg – a difference of about 2.0Kg. The number of start-ups is the same for both settings [see **Figure 5-3** below]. If the long term effects of partial charge on the battery is ignored, it may be economical (at least in terms of fuel consumption) to operate the diesel between $SOC = 0.5$ and 0.8, instead of $SOC = 0.5$ and 0.9. This conclusion is of course based on the given load profile assuming other parameters are held constant.

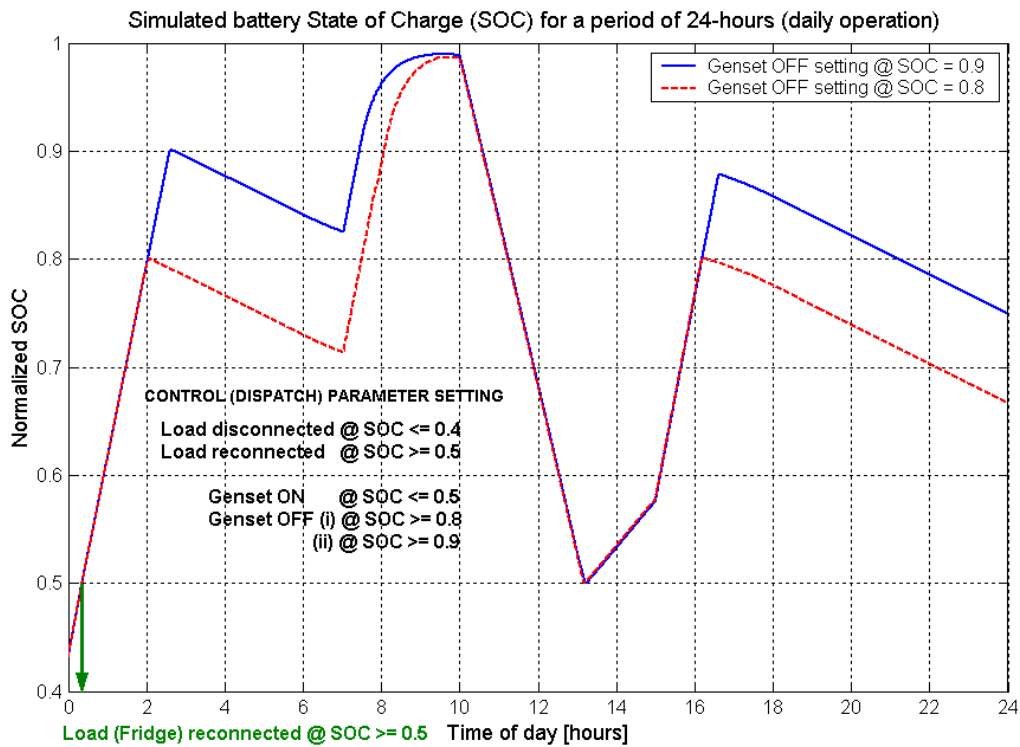


Figure 5-8 : Effect on simulated SOC profile by changing control set-points

5.3 Battery management

Battery management is visualized by means of simulating the current, the voltage, the temperature and the SOC of the battery over a daily cycle (a single day autonomy is assumed).

5.3.1 Battery charge/discharge cycle

Dynamic simulation of battery voltage and current as shown in **Figure 5-9** below is used to visualize the charge/discharge cycle of the battery and the operation of charge controllers.

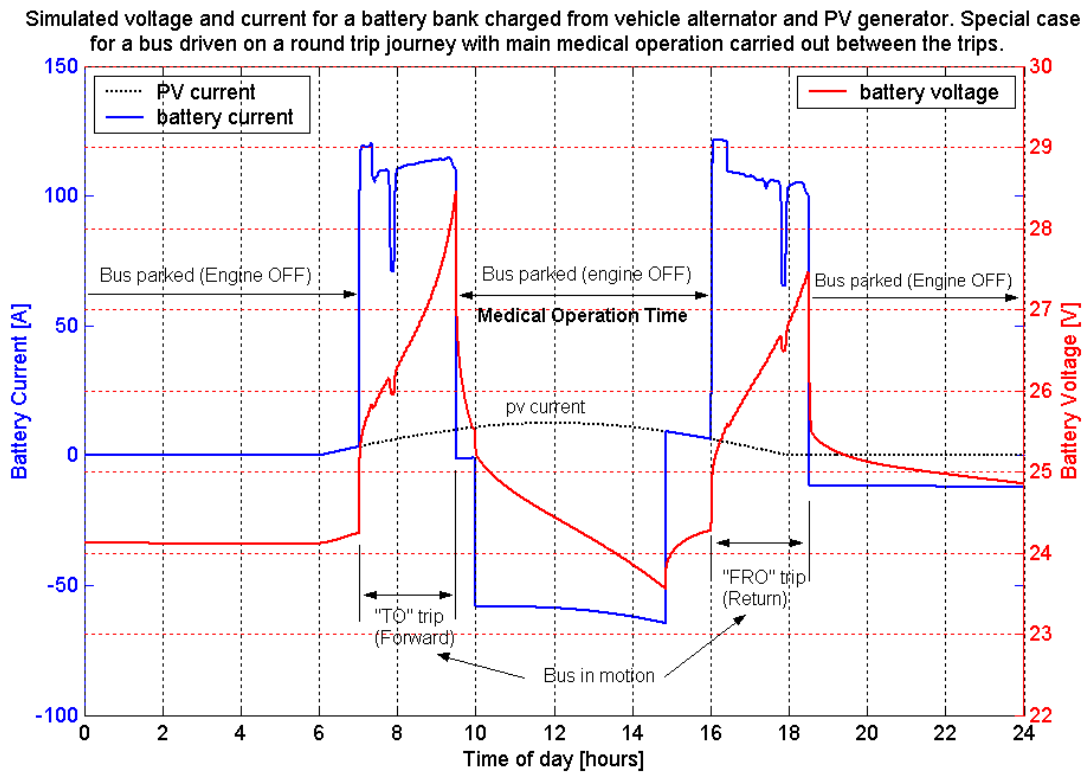


Figure 5-9: Simulated battery charge/discharge cycle

5.3.2 IUU controller functional behaviour

The functional behaviour of the IUU charge controller is visualized by simulating the dynamic battery voltage and current. The goal is to verify, the proper functioning of the controller in the simulation model. In particular, we wish to show that the timer function that sets the absorption time, T_a , chosen for example as 2.5 hours in the model initialisation stage, behaves as expected.

Assuming no load is connected and that only the PV array and alternator are charging the battery, the initial battery SOC status is set at 0.4. Using the engine speed profile denoted as 'Profile 3' in **Figure 5-1**, the charging behaviour is as shown in **Figure 5-10**.

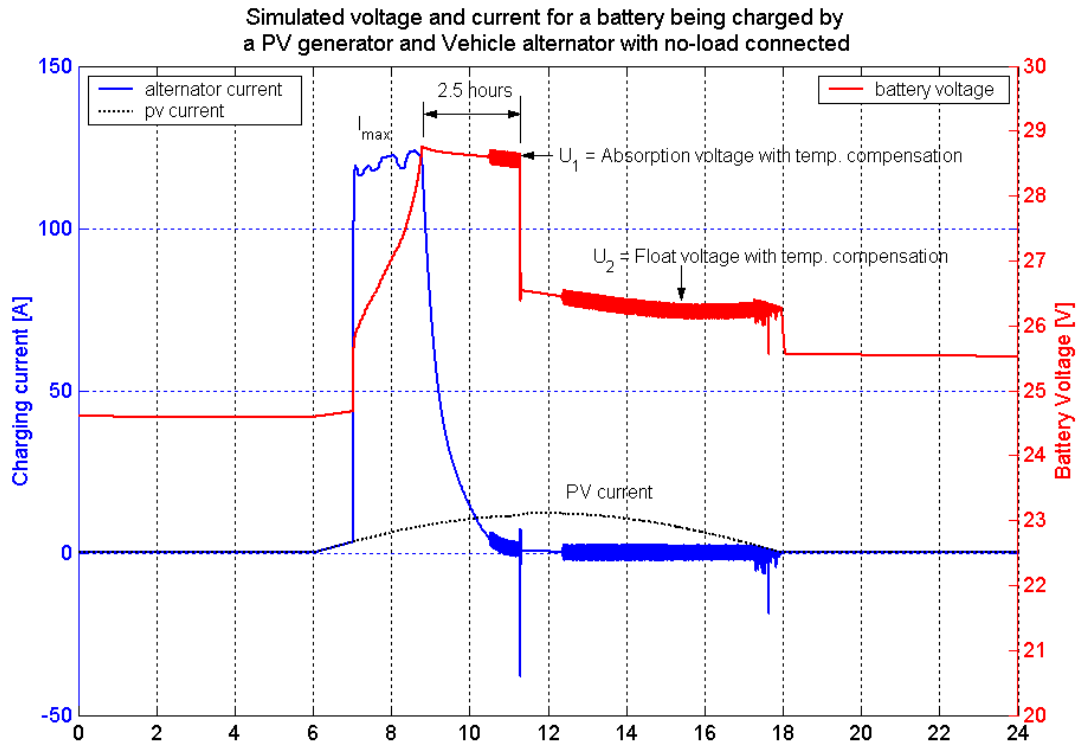


Figure 5-10: Simulated IUU charging characteristics

‘Alpha’ controller IUU algorithm

We consider the engine speed profile denoted as ‘Profile 4’ in **Figure 5-1** of section 5.1 . In this profile there are instances when the engine speed is zero (or engine ‘off’). Such a profile would give rise to interruptions in the charging process. According to the ‘Alpha’ charging algorithm, during the absorption phase the controller timer function stops and resets to ‘zero’ when there is no charging current. It resumes timing afresh as soon as the charging current is ‘non-zero’ once again as shown in **Figure 5-11** below. During the constant voltage charging (U stage), a voltage sag that drops by less than 0.5V is ignored if it lasts for less than 5 minutes, otherwise the controller goes into the bulk charge phase. We were able to model this functionality in Matlab/Simulink, and hence the simulation mimics a real controller. This means the simulation model can, in principle, be subjected to experimental validation.

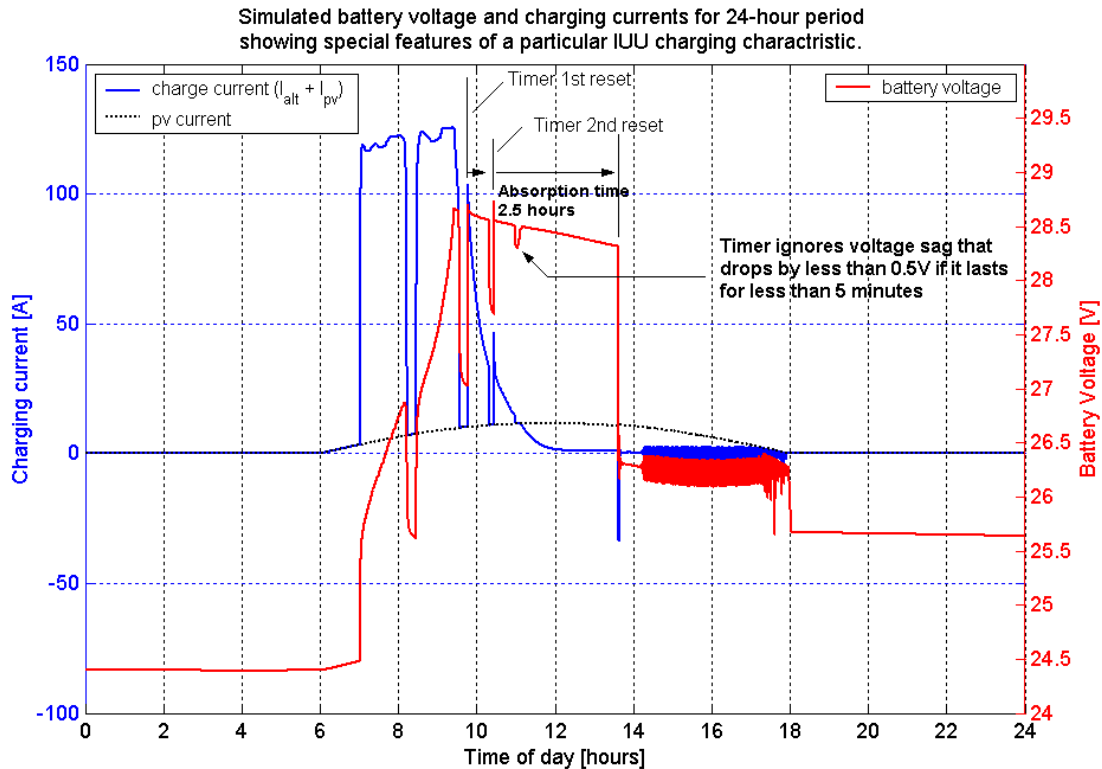


Figure 5-11: Two interruptions in the charging at the absorption phase

Remark: The ‘Alpha’ charge regulator has a classic 3-step (IUU) algorithm that has a fixed absorption time which is manually resettable, for example 2.5 hours in the above example. Charging a battery with a fixed absorption time works well as long as the battery has been, on average, substantially discharged before a recharge cycle is started. However, a battery that has been deeply discharged needs an absorption time of several hours, whereas a battery that is only slightly discharged requires a much shorter absorption period. In several applications a fixed absorption time can lead to either overcharging or prolonged partial charge, which will reduce service life either way. New versions charger controllers referred by some manufacturers as ‘adaptive chargers’ employ algorithms with variable absorption time.

5.3.3 Battery temperature

The dynamic battery temperature for the scenario corresponding to **Figure 5-9** is shown in **Figure 5-12**. This is modelled with the help of the ISET-LAB battery model and is a function of the ambient temperature and the battery current. The instances when the battery temperature significantly increases above ambient temperature correspond to the high charging rates and vice versa for the high discharging rates,

which is evident from the simulated profile. High battery temperatures will reduce the battery life by means of increased corrosion. Visualization allows to better implement strategies to manage battery temperature.

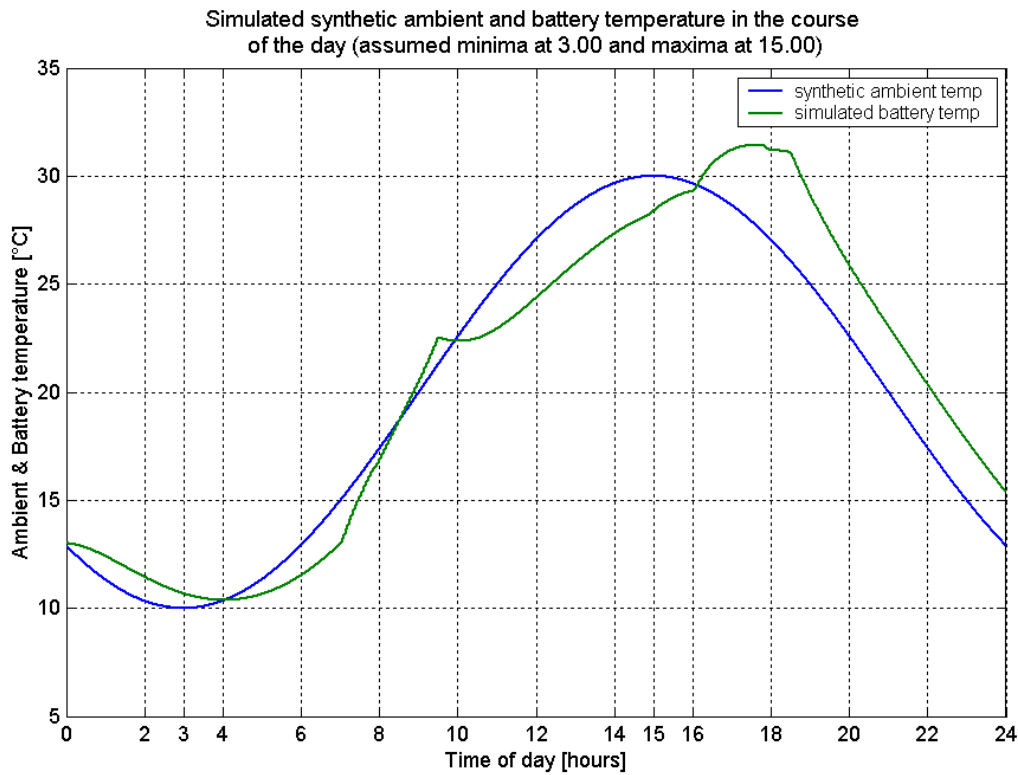


Figure 5-12: Simulated battery temperature and synthetic ambient temperature

6 CONCLUSIONS AND RECOMMENDATIONS

Modelling and simulation in Matlab/Simulink has been used to explore some of the possible scenarios in a mobile hybrid power system (MHPS) designed for a mobile medical clinic application. The aspect of visualization has been particularly emphasized in this work. By using synthetic profiles (e.g. the solar irradiance, ambient temperature profiles, etc) and component manufacturer's measured data for various components, virtual experiments that give graphical results similar to real tests can be carried out. In principle, the system simulation model could be subjected to experimental validation. Dynamic fuel consumption of the genset for changing load conditions can be estimated. We are able to visualize the charge controller functional behaviour (i.e. IUU algorithm), the operation of the diesel genset and battery management from the simulation. Hence, the operation of the system can be predicted before the actual hardware realization.

The following conclusion may be drawn from these results:

- With the given shape of the load profile, which has a relatively large power fluctuation (200W for 80% and 2000W for 20% of the time, respectively), a single inverter rated for peak power would not operate at high efficiency for all load conditions. It is therefore recommended that two inverters be used in the system, whereby a smaller inverter is used to run the low-power continuous loads (e.g. refrigerator and a few other low-power loads) and the bigger inverter only switched on when more loads are added. Alternatively, inverter losses may be avoided by using a DC refrigerator instead of the AC refrigerator.
- When the PV generator size is decreased from 1100 W_p to 550 W_p (50% decrease) while keeping all other dimensions and control set-points unchanged; the fuel consumption increases by only 17%. Therefore, there is no significant influence of PV generator size on diesel fuel consumption in the given range and hence a PV size of about 500 W_p can be optimal.
- The use of a variable-speed genset in combination with an inverter and a battery system, allows shorter run time since the genset engine can be turned off when the battery has enough energy storage and AC power is obtainable via the inverter.
- If the long term effects of partial charge on the battery is ignored, it may be economical (at least in terms of fuel consumption) to operate the diesel between

SOC = 0.5 and 0.8, instead of SOC = 0.5 and 0.9. In this regard, the PV generator is best sized to provide only the finishing or floating charge current and therefore its dimension need not be sized to always cover the total load. This minimizes the cost of purchasing modules.

6.1 Outlook and future work

The trend to provide mobile power with standard AC voltage on-board vehicles used for special applications such as ambulances, mobile clinics, emergency response, etc is expected to continue gaining popularity. In this regard, there appears to be an analogy in the trend in the developments of mobile power systems and mobile telecommunications. Other developments in automotive industry such as hybrid electric vehicles and new electrical network architecture will accelerate the developments of efficient electrical machines and power converters that are both relevant to vehicular (mobile) and residential (stationary) application. The development of simulation tools will be needed to cut down the cost of hardware prototyping, and one would expect more virtual prototyping in the future.

7 REFERENCES

Andriulli, J.B. et al (2001) "Development of Proof-of-Concept units for the Advanced Medium-Sized Mobile Power Sources (AMMPS) Program"

Barley, C.D. (1996) "Modelling and Optimisation of Dispatch Strategies for Remote Hybrid Power Systems," Ph.D. dissertation, Dept. of Mechanical Engineering, Colorado State University, 1996.

Bergeron, D. (2001) "Solar Powered Refrigeration for Transport Application. An Application Study".

Berndt, D. (1993) "Maintenance-Free Batteries". A Handbook of Battery Technology. Published by John Wiley & Sons

Betts, T.R. et al (2001) Progress towards modelling solar spectral radiation for optimisation of amorphous silicon photovoltaic systems (<http://www.lboro.ac.uk/crest/PDF>)

Bosch, R. (2000) "Alternators: Principles, construction, regulators, over-voltage protection, types of alternators and vehicle electrical systems, energy balance, vehicle operation". Published by Bentley Publishers.

Brooks, A. et al (2001) "Integration of Electric Drive Vehicles with the Electric Power Grid – a New Value System".

Brück, D. (2002) "Dymola for Multi-Engineering Modeling and Simulation". 2nd International Modelica Conference, Proceedings, pp. 55-1 to 55-8 held at Deutsches Zentrum für Luft und Raumfahrt e.V. (DLR), Oberpfaffenhofen, Germany.

Caselitz, P., et al. (1998) Computer Aided Design of Battery Management Systems for Automobiles – A Model for Lead Acid Battery, International Congress and Exposition, Detroit, Michigan, Feb. 23 – 26, 1998

Fernando, B.M., et al, (1998) "Generators for 60Hz 120/240Volt Power on Vehicles"

Fish, S., et al, 2001 Simulation-Based Optimal Sizing of Hybrid Electric Vehicle Components for Specific Combat Missions

Fitzpatrick, S., 2000 "A Method for Predicting PV Module and Array Performance at other than Standard Reporting Conditions"

Goldie, J.H., (2002) "SatCon's Hybrid PM/homopolar Generator offers Compact, Portable Power Generation"

Gottschalg, R. et al (2001) Influence of Environmental Conditions on Thin Film Photovoltaic Device Performance: (<http://www.lboro.ac.uk/crest/>. PDF)

Hofmann, M., 2001 Leistungssteigerung von Kfz-Generatoren durch stoßarme Wicklungsumschaltung mittels steuerbarer Halbleiter (Dissertation – Fakultät für Elektrotechnik der Universität der Bundeswehr München)

Holley, M.J. et al (2000) Modelling the performance of a-Si PV systems (<http://www.lboro.ac.uk/crest/>.PDF)

Kassakian, J. G., et al (1996) "Automotive Electrical Systems circa 2005," IEEE Spectrum, Aug. 1996, pp. 22- 27.

Kempton, et al (2001) "Electric Drive Vehicles (Battery, Hybrid, Fuel Cell) as resources for grid power in California" (<http://www.udel.edu/V2G/V2G-Cal-2001.pdf>)

King, et al, 1997 "Photovoltaic Module and Array Performance Characterization Methods for All System Operating Conditions" Proceedings of NREL/SNL Photovoltaics Program Review Meeting, November 1996. Press New York, 1997.

King, et al, 1997 "Temperature Coefficients for PV Modules and Arrays: Measurements, Methods, Difficulties and Results". Presented at the 26th IEEE Photovoltaic Specialist Conference, September 29 – October 3, 1997, Anaheim, California.

King, et al, 1997 Measuring Solar Spectral and Angle-of-Incidence Effects on Photovoltaic Modules and Solar Irradiance Sensors. Presented at the 26th IEEE Photovoltaic Specialist Conference, September 29 – October 3, 1997, Anaheim, California.

King, et al, 1998 "Field Experience with a new performance characterization Procedure for photovoltaic Arrays". Presented at the 2nd World Conference and Exhibition on Photovoltaic Solar Energy Conversion, 6-10 July 1998, Vienna, Austria.

Kininger, F. (2003) Photovoltaic System Technology. Course Lectures. University of Kassel, 2003. <http://www.re.e-technik.uni-kassel.de>

Linden, D. (1995) Handbook of Batteries. Second Edition. Published by McGraw-Hill Inc.

Lipman, T. et al (2002) "Economic Implication of Net Metering for Stationary and Motor Vehicle Fuel Cell Systems in California".

Lovelace, E. C. (1998) "An Interior PM Starter/Alternator for Automotive Applications"

Marion, B., et al. Validation of a Photovoltaic Module Energy Rating Procedure at NREL

Masrur, M.A., et al, (2001) "Electrical Power System Architecture for Military and Commercial Vehicular Applications

Miller, J.M., et al. (1998) "Making the Case for a Next Generation Automotive Electrical System". IEEE-SAE International Congress on Transportation Electronics (Convergence), Dearborn, MI, Oct. 1998.

Richert, et al. (2003) "Vergleich von Modelica[®] and Matlab[®] anhand der Modellbildung eines Dieselmotors" GMA-Kongress 2003, VDI-Berichte 1756, VDI-Verlag, Düsseldorf 2003. S.1049 – 1058.

Robert Bosch GmbH, (1992), "Automotive Electric/Electronic Systems", Published by Robert Bosch GmbH.

Schmid, J. (1999), "Photovoltaik – Strom aus der Sonne", Technologie, Wirtschaftlichkeit, und Marketentwicklung, 1999, Published by C.F. Müller Verlag.

Tiller, M. (2001) "An Introduction to Physical Modeling with Modelica". Book. Kluwer Academic Publishers.

Tolbert, L.M., et al, 2001 "Electronic Power Conversion for an Advanced Mobile Generator Set"

Turcotte, 2001 Photovoltaic Hybrid System Sizing and Simulation Tools: Status and Needs

Walker, G., 2000 Evaluating MPPT Converter Topologies using a MATLAB PV Model. http://www.cs.uq.edu.au/~walkerg/publications/pvmodel_00.pdf

8 APPENDICES

8.1 Appendix A: Vehicle Engine driven Alternators

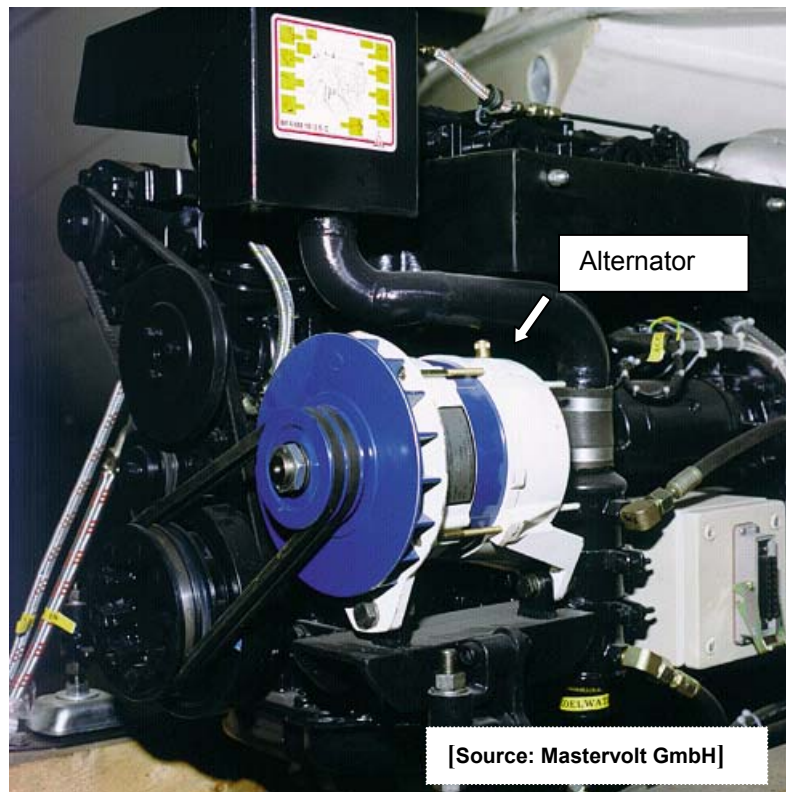


Figure 8-1: Belt-drive mounting arrangement for 3kW DC alternator

8.2 Appendix B: Inverter Efficiency Curve

The measured values of a 24Volt, 900Watt inverter (Solarix 900RI from Steca-Fronius) is given in Table 8-1.

Table 8-1: Measured values for inverter efficiency [Source: Steca GmbH]

INPUT VALUES (BATTERY-SIDE)			OUTPUT VALUES (LOAD-SIDE)			
DC Voltage [V]	DC Current [A]	DC Power [W]	AC Voltage [V]	AC Current [A]	AC Power [W]	Efficiency [%]
26.30	2.1	45	228.90	0.15	35.25	78.3
27.00	6.4	144	225.60	0.58	130.40	90.6
25.44	12.5	260	221.30	1.10	242.32	93.2
25.60	24.7	514	216.40	2.15	466.13	90.7
26.34	30.5	652	218.00	2.67	582.50	89.3
24.06	45.7	886	217.60	3.52	765.95	86.5

8.3 Appendix C: Relationship between battery measured parameters

Table 8-2 Specific Gravity of Lead-Acid Battery Electrolyte at Different States of Charge* [Source: Linden, 1995]

State of Charge (%)	Specific Gravity [g/cm ³]			
	A	B	C	D
100 (full charge)	1.330	1.280	1.265	1.225
75	1.300	1.250	1.225	1.185
50	1.270	1.220	1.190	1.150
25	1.240	1.190	1.155	1.115
0 (discharged)	1.210	1.160	1.120	1.080

*Assumed flooded cell design

A – Electric Vehicle Battery


B – Traction Battery

C – Starter Battery

D – Stationary Battery

Table 8-4: Voltages versus Depth of Discharge

V (V)	12.8	10.5	11.4	11.7	11.9	12.1	12.2	12.4	12.5	12.7	12.9
SOC (%)	90	0	10	20	30	40	50	60	70	80	99



Identity

Control File:
Battery:
Type of Battery:

Structure

Segmentation of Battery Regions

Positive: Glassmat: Electrolyte: Separator: Negative:

Double Layer Capacity

Positive Negative

Initial State

Degree of Discharge

Positive: Negative:

Temperature: C


Terminal Voltage: V Deviation Potential: mV Acid Density: kg/l

Source and Destination Files

Initial State:
 Final State:
 Stop when U < V
 Output

[Source: ISET e.V.]

Figure 8-2: User-interface for initialisation of ISET-LAB model

Starter-Batterie Typ 61042				
B61042.PA3				
Rated Values				
Capacity [Ah]	Discharge Time [h]	Density [kg/l]		
110.0	20.0	1.28		
Cells				
Positive				Negative
10	Number of Plates			10
101.8	Active Mass [g]			88.9
56.0	Grid Mass [g]			51.5
11.45	Height [cm]			11.45
14.7	Width [cm]			14.7
Thickness [cm]				
0.09	0.045	0.05	0.025	0.075
Porosity in full charged state				
0.5	1.0	1.0	0.6	0.6
Positive	Separator	Separator	Separator	Negative
Container				
38.9	Length [cm]	6	Number of Cells	
17.5	Width [cm]	953.0	Acid Volume [ccm]	
19.0	Height [cm]	2.0	Plate - Wall [cm]	
0.2	Thickness [cm]			
Aggregate				
OK	Cancel	Apply		

[Source: ISET e.V.]

Figure 8-3: User-interface for ISET-LAB model for entering battery geometrical dimensions

8.4 Appendix D: The Sandia I-V curve Translation Procedure

The Sandia model has been implemented in some commercial software PV simulators such as 'IV Curve Tracer' and 'PV-Design Pro' developed jointly by Sandia National Laboratories (SNL) and Maui Solar Software Corporation.

The equations given below represent the latest implementation of the Sandia model as reported in [Davis et al, 2002]:

$$I_{sc}(E_e, T_c, AM_a, AOI) = I_{sc0} \cdot f_1(AM_a) \cdot \left\{ \frac{E_{beam} \cdot f_2(AOI) + f_d \cdot E_{diff}}{E_0} \right\} \cdot [1 + \bar{\alpha}_{Isc} \cdot (T_c - T_0)] \quad (8.1)$$

$$E_e = \frac{E}{E_0} = f_1(AM_a) \cdot \left\{ \frac{E_{\text{beam}} \cdot f_2(\text{AOI}) + f_d \cdot E_{\text{diff}}}{E_0} \right\} = \frac{I_{\text{sc}}}{I_{\text{sc0}} \cdot [1 + \bar{\alpha}_{\text{Isc}} \cdot (T_c - T_0)]} \quad (8.2)$$

$$I_{\text{mp}}(E_e, T_c) = I_{\text{mp0}} \cdot (C_0 E_e + C_1 \cdot E_e^2) \cdot [1 + \bar{\alpha}_{\text{Imp}} \cdot (T_c - T_0)] \quad (8.3)$$

$$\delta(T_c) = \frac{n \cdot k \cdot (T_c + 273.15)}{q} \quad (8.4)$$

$$V_{\text{oc}}(E_e, T_c) = V_{\text{oc0}} \cdot [1 + \bar{\beta}_{\text{Voc}} \cdot (T_c - T_0)] + N_s \cdot \delta(T_c) \cdot \ln(E_e) \quad (8.5)$$

$$V_{\text{mp}}(E_e, T_c) = V_{\text{mp0}} \cdot [1 + \bar{\beta}_{\text{Vmp}} \cdot (T_c - T_0)] + C_2 \cdot N_s \cdot \delta(T_c) \cdot \ln(E_e) + C_3 \cdot N_s \cdot \{\delta(T_c) \cdot \ln(E_e)\}^2 \quad (8.6)$$

$$f_1(AM_a) = A_0 + A_1 \cdot (AM_a) + A_2 \cdot (AM_a)^2 + A_3 \cdot (AM_a)^3 + A_4 \cdot (AM_a)^4 \quad (8.7)$$

$$f_2(\text{AOI}) = B_0 + B_1 \cdot (\text{AOI}) + B_2 \cdot (\text{AOI})^2 + B_3 \cdot (\text{AOI})^3 + B_4 \cdot (\text{AOI})^4 + B_5 \cdot (\text{AOI})^5 \quad (8.8)$$

Where:

E_{beam} = beam irradiance, [W/m²]

E_{diff} = diffuse irradiance, [W/m²]

f_d = fraction of diffuse irradiance used by module, $f_d = 1$ for non-concentrating modules

$f_1(AM_a)$ = Empirically determined “ AM_a function” (a 4th order polynomial) describing solar spectral influence on I_{sc}

$f_2(\text{AOI})$ = Empirically determined “AOI function” (a 5th order polynomial) describing angle-of-incidence influence on I_{sc}

AM_a = Absolute Air Mass

AOI = Solar angle-of-incidence on module, degrees

$A_0 - A_4$ = polynomial coefficients for air-mass function, $f_1(AM_a)$

$B_0 - B_5$ = polynomial coefficients for incident angle function, $f_2(\text{AOI})$

Other terms and coefficients are as previously defined in Chapter 4

Compensation for the time-of-day dependent solar spectrum influence is achieved using an empirically determined function, $f_1(AM_a)$. This function relates solar spectral influence on I_{sc} to the absolute air mass (AM_a), which is the air mass (AM) adjusted for the altitude of the site. AM_a is readily calculated knowing the sun’s zenith angle (θ_z) and the site altitude using empirical relations (3.15 – 3.17) [King et al, 1998]:

$$AM = [\cos(\theta_z) + 0.5057 \cdot (96.080 - \theta_z)]^{-1} \quad (8.9)$$

$$AM_a = (P/P_0) \cdot AM \quad (8.10)$$

$$P/P_0 \approx \exp(-0.0001184 \cdot h) \quad (8.11)$$

Where:

AM = atmospheric optical air mass

AM_a = absolute (pressure corrected) air mass

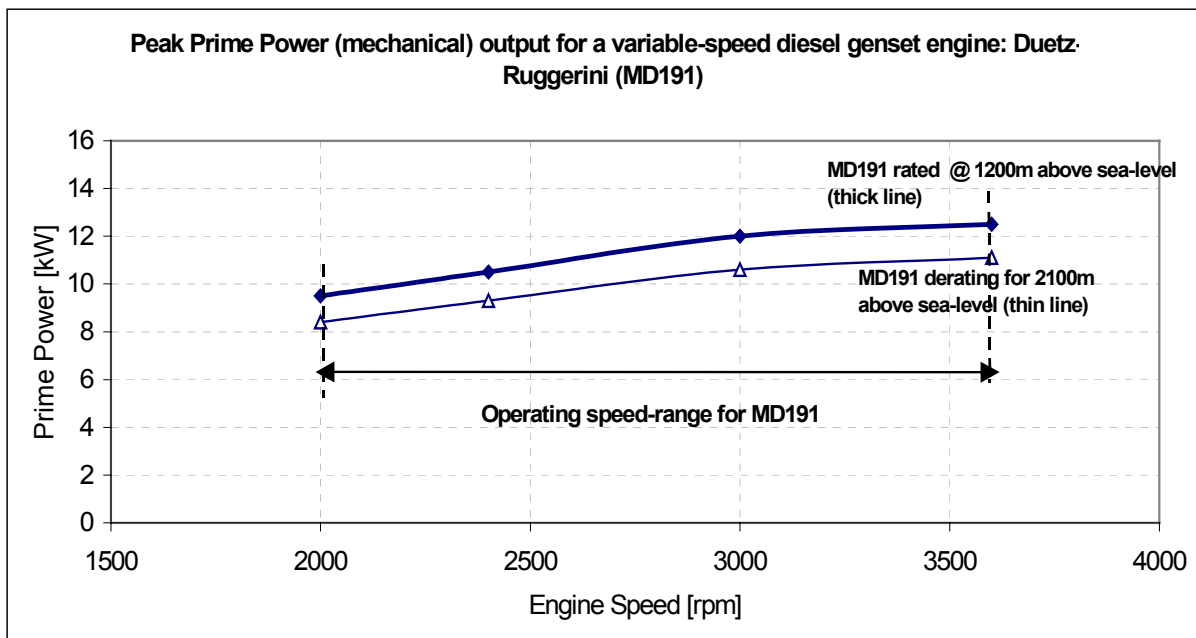
θ_z = zenith angle of the sun

P = local atmospheric pressure, mmHg

P₀ = standard pressure at sea level, 760mmHg

h = site altitude, m

8.5 Appendix E: Genset Rating and De-rating



The following standards are quoted for Diesel Engines [Source: Lister-Petter]

Rating: Standards [BS5514 /ISO3046 /DIN6271 /SAE1995]

The output ratings apply only to fully run engines without radiator, fan, or power absorbing accessories

De-rating: Standards [BS5514 /ISO3046 /DIN6271 /SAE1995]

Altitude – Approximately 4% for every 300m (1000ft) higher than 100m (330ft) above sea level.

Temperature – Approximately 2% for every 5°C above 25°C.